Sterne

# SANDIA REPORT

SAND89—0869 • UC—721
Unlimited Release
Printed December 1991

WIPP Library

# Interpretations of Single-Well Hydraulic Tests of the Rustler Formation Conducted in the Vicinity of the Waste Isolation Pilot Plant Site, 1988-1989

Richard L. Beauheim, Timothy F. Dale, John F. Pickens

**Prepared by**
**Sandia National Laboratories**
**Albuquerque, New Mexico 87185 and Livermore, California 94550**
**for the United States Department of Energy**
**under Contract DE-AC04-76DP00789**

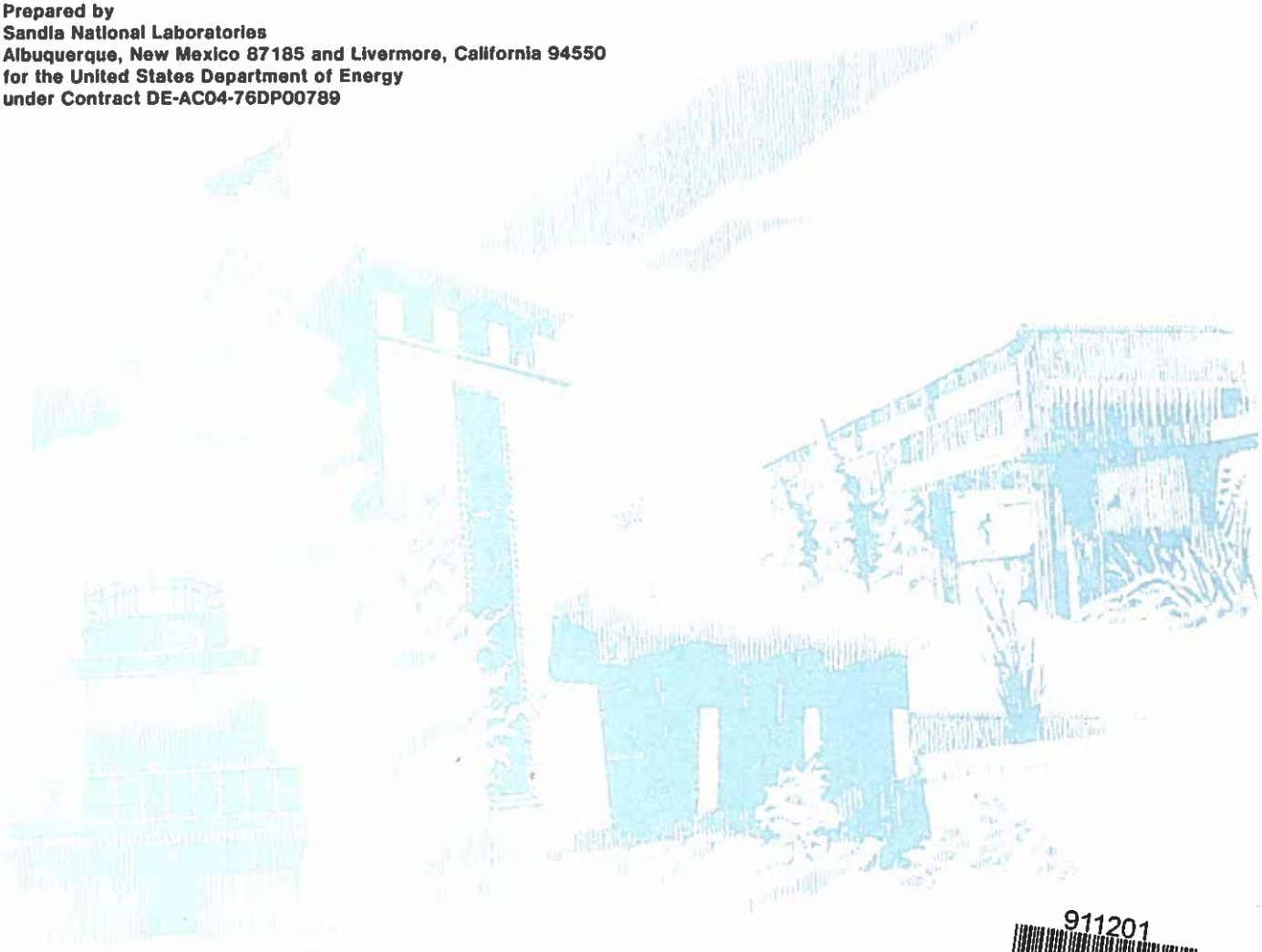

911201

Issued by Sandia National Laboratories, operated for the United States Department of Energy by Sandia Corporation.

**NOTICE:** This report was prepared as an account of work sponsored by an agency of the United States Government. Neither the United States Government nor any agency thereof, nor any of their employees, nor any of their contractors, subcontractors, or their employees, makes any warranty, express or implied, or assumes any legal liability or responsibility for the accuracy, completeness, or usefulness of any information, apparatus, product, or process disclosed, or represents that its use would not infringe privately owned rights. Reference herein to any specific commercial product, process, or service by trade name, trademark, manufacturer, or otherwise, does not necessarily constitute or imply its endorsement, recommendation, or favoring by the United States Government, any agency thereof or any of their contractors or subcontractors. The views and opinions expressed herein do not necessarily state or reflect those of the United States Government, any agency thereof or any of their contractors.

Printed in the United States of America. This report has been reproduced directly from the best available copy.

Available to DOE and DOE contractors from
Office of Scientific and Technical Information
PO Box 62
Oak Ridge, TN 37831

Prices available from (615) 576-8401, FTS 626-8401

Available to the public from
National Technical Information Service
US Department of Commerce
5285 Port Royal Rd
Springfield, VA 22161

NTIS price codes
Printed copy: A04
Microfiche copy: A01

SAND89-0869
Unlimited Release
Printed December 1991

Distribution
Category UC-721

# INTERPRETATIONS OF SINGLE-WELL HYDRAULIC TESTS OF THE RUSTLER FORMATION CONDUCTED IN THE VICINITY OF THE WASTE ISOLATION PILOT PLANT SITE, 1988-1989

Richard L. Beauheim
Sandia National Laboratories
Fluid Flow and Transport Division
Albuquerque, NM 87185

Timothy F. Dale and John F. Pickens
INTERA Inc.
6850 Austin Center Blvd, Suite 300
Austin, TX 78731

## ABSTRACT

In 1988 and 1989, hydraulic tests were conducted in seven wells to provide data on the transmissivities of four members of the Rustler Formation. These data will be used in modeling of groundwater flow through the Rustler Formation. Pressure-pulse, slug, and pumping tests were performed. The pressure-pulse and slug tests were simulated using the computer code GTFM to obtain estimates of transmissivity and the radius of influence of the testing. The pressure-pulse tests proved difficult to interpret because no measurements of test-zone compressibility were made. Slug tests at two of the wells were also interpreted using type curves based on an analytical solution for slug tests. The type-curve results differed by 35 percent or less from the transmissivities determined using GTFM. The pumping test was interpreted using the computer code Interpret/2. The slug-test interpretations provided estimates of transmissivity as follows: $2.1 \times 10^{-4}$ to $3.0 \times 10^{-4}$ $ft^2$/day for the siltstone within the unnamed lower member of the Rustler at well H-16; 0.16 to 0.20 $ft^2$/day and 1.9 to 2.5 $ft^2$/day for the Culebra dolomite at wells AEC-7 and D-268, respectively; $2.1 \times 10^{-3}$ to $2.7 \times 10^{-3}$ $ft^2$/day and 0.14 to 0.18 $ft^2$/day for the Magenta dolomite at wells H-2b1 and H-3b1, respectively; and $3.5 \times 10^{-3}$ to $4.5 \times 10^{-3}$ $ft^2$/day for the Forty-niner claystone at well H-3d. The calculated radii of influence of the tests ranged from about 50 to 300 ft. Interpretations of the pumping test of the Culebra dolomite at well H-18 are ambiguous in that the test responses are equally representative of a single-porosity medium having a transmissivity of 2.0 $ft^2$/day and a no-flow boundary 58 ft from H-18, and of a double-porosity medium with a transmissivity of 1.0 $ft^2$/day and no apparent boundaries.

# ACKNOWLEDGEMENTS

The authors are indebted to George Saulnier, Wayne Stensrud, Jeff Palmer, Michael Bame, and Kent Lantz for their efforts in fielding the tests discussed in this report. Tom Corbet, Peter Swift, and Elaine Gorham provided helpful review comments. Jo Ann Quintana's preparation of the camera-ready manuscript is especially appreciated.

# TABLE OF CONTENTS


1. INTRODUCTION . . . . . 1

2. SITE HYDROGEOLOGY . . . . . 3

3. TEST WELLS . . . . . 5
   - 3.1 AEC-7 . . . . . 5
   - 3.2 D-268 . . . . . 5
   - 3.3 H-2b1 . . . . . 6
   - 3.4 H-3b1 . . . . . 7
   - 3.5 H-3d . . . . . 7
   - 3.6 H-16 . . . . . 7
   - 3.7 H-18 . . . . . 8

4. TEST METHODS . . . . . 9
   - 4.1 Slug Tests . . . . . 9
   - 4.2 Pressure-Pulse Tests . . . . . 9
   - 4.3 Pumping Tests . . . . . 10
   - 4.4 Isolation Verification . . . . . 10

5. TEST OBJECTIVES AND INTERPRETATIONS . . . . . 11
   - 5.1 Unnamed Lower Member at Well H-16 . . . . . 11
   - 5.2 Culebra Dolomite Member . . . . . 16
     - 5.2.1 Well AEC-7 . . . . . 16
     - 5.2.2 Well D-268 . . . . . 23
     - 5.2.3 Well H-18 . . . . . 27
   - 5.3 Magenta Dolomite Member . . . . . 33
     - 5.3.1 Well H-2b1 . . . . . 33
     - 5.3.2 Well H-3b1 . . . . . 38
   - 5.4 Forty-niner Member at Well H-3d . . . . . 43

6. SUMMARY AND CONCLUSIONS . . . . . 51

NOTATION . . . . . 52

REFERENCES . . . . . 53

APPENDIX A: Analysis and Interpretation of Hydraulic-Test Data Using the Well-Test-Simulation Model GTFM . . . . . 55

DISTRIBUTION . . . . . 59

# FIGURES


1-1 Location of the WIPP Site . . . . . 1

2-1 WIPP Area Stratigraphic Column . . . . . 3

2-2 Locations of Wells Near the WIPP Site . . . . . 4

3-1 Well Configuration for AEC-7 Tests . . . . . 5

3-2 Well Configuration for D-268 Tests . . . . . 6

3-3 Well Configuration for H-2b1 Tests . . . . . 6

3-4 Well Configuration for H-3b1 Tests . . . . . 7

3-5 Well Configuration for H-3d Tests . . . . . 8

3-6 Well Configuration for H-16 Test . . . . . 8

3-7 Well Configuration for H-18 Test . . . . . 8

5-1 Linear-Linear Sequence Plot of Pressure Data from the Slug-Withdrawal Test of the Unnamed Lower Member Siltstone at Well H-16 . . . . . 12

5-2 Linear-Linear Plot of GTFM Simulation of the Slug-Withdrawal Test of the Unnamed Lower Member Siltstone at Well H-16 . . . . . 13

5-3 Semilog Plot of GTFM Simulation of the Slug-Withdrawal Test of the Unnamed Lower Member Siltstone at Well H-16 . . . . . 13

5-4 Semilog Plot of GTFM Simulations of the Slug-Withdrawal Test of the Unnamed Lower Member Siltstone at Well H-16 Using Different Values for Storativity . . . . . 14

5-5 Simulated Pore Pressures at Selected Radial Distances from Well H-16 During the Slug-Withdrawal Test of the Unnamed Lower Member Siltstone . . . . . 16

5-6 Linear-Linear Sequence Plot of Pressure Data from the Slug Tests of the Culebra Dolomite at Well AEC-7 . . . . . 17

5-7 Linear-Linear Plot of GTFM Simulation of the Slug Tests of the Culebra Dolomite at Well AEC-7 . . . . . 18

5-8 Semilog Plot of GTFM Simulation of the Slug-Withdrawal Test of the Culebra Dolomite at Well AEC-7 . . . . . 18

5-9 Semilog Plot of GTFM Simulation of the First Slug-Injection Test of the Culebra Dolomite at Well AEC-7 . . . . . 19

5-10 Semilog Plot of GTFM Simulation of the Second Slug-Injection Test of the Culebra Dolomite at Well AEC-7 . . . . . 19

5-11 Semilog Plot of GTFM Simulations of the First Slug-Injection Test of the Culebra Dolomite at Well AEC-7 Using Different Values for Storativity . . . . . 20

5-12 Simulated Pore Pressures at Selected Radial Distances from Well AEC-7 During the Slug Tests of the Culebra Dolomite . . . . . 20

5-13 Semilog Analytical-Solution Type-Curve Match to the Slug-Withdrawal Test of the Culebra Dolomite at Well AEC-7 . . . . . 21

5-14 Semilog Analytical-Solution Type-Curve Match to the First Slug-Injection Test of the Culebra Dolomite at Well AEC-7 . . . . . 22

5-15 Linear-Linear Sequence Plot of Pressure Data from the Slug Tests of the Culebra Dolomite at Well D-268 . . . . . 23

5-16 Linear-Linear Plot of GTFM Simulation of the Slug Tests of the Culebra Dolomite at Well D-268 . . . . . 24

5-17 Semilog Plot of GTFM Simulations of the First Slug-Injection Test of the Culebra Dolomite at Well D-268 . . . . . 24

5-18 Semilog Plot of GTFM Simulations of the Second Slug-Injection Test of the Culebra Dolomite at Well D-268 . . . . . 25

5-19 Semilog Plot of GTFM Simulations of the Second Slug-Injection Test of the Culebra Dolomite at Well D-268 Using Different Values for Storativity . . . . . 26

5-20 Simulated Pore Pressures at Selected Radial Distances from Well D-268 During the Slug Tests of the Culebra Dolomite . . . . . 26

5-21 Semilog Analytical-Solution Type-Curve Match to the First Slug-Injection Test of the Culebra Dolomite at Well D-268 . . . . . 27

5-22 Flow Rates During the Pumping Test of the Culebra Dolomite at Well H-18 . . . . . 28

5-23 Linear-Linear Sequence Plot of Pressure Data from the Pumping Test of the Culebra Dolomite at Well H-18 . . . . . 28

5-24 Log-Log Plot of Interpret/2 Simulation of the Recovery from the Pumping Test of the Culebra Dolomite at Well H-18 Assuming Bounded Single-Porosity Conditions . . . . . 29

5-25 Horner Plot of Interpret/2 Simulation of the Recovery from the Pumping Test of the Culebra Dolomite at Well H-18 Assuming Bounded Single-Porosity Conditions . . . . . 30

5-26 Linear-Linear Plot of Interpret/2 Simulation of the Pumping Test of the Culebra Dolomite at Well H-18 Assuming Bounded Single-Porosity Conditions . . . . . 31

5-27 Log-Log Plot of Interpret/2 Simulation of the Recovery from the Pumping Test of the Culebra Dolomite at Well H-18 Assuming Double-Porosity Conditions . . . . . 31

5-28 Horner Plot of Interpret/2 Simulation of the Recovery from the Pumping Test of the Culebra Dolomite at Well H-18 Assuming Double-Porosity Conditions . . . . . 32

5-29 Linear-Linear Plot of Interpret/2 Simulation of the Pumping Test of the Culebra Dolomite at Well H-18 Assuming Double-Porosity Conditions . . . . . 32

5-30 Linear-Linear Sequence Plot of Pressure Data from the Slug-Withdrawal and Pulse-Injection Tests of the Magenta Dolomite at Well H-2b1 . . . . . 34

5-31 Linear-Linear Sequence Plot of Water-Level Data from the Slug-Injection Test of the Magenta Dolomite at Well H-2b1 . . . . . 34

5-32 Linear-Linear Plot of GTFM Simulation of the Slug-Withdrawal and Pulse-Injection Tests of the Magenta Dolomite at Well H-2b1 . . . . . 35

5-33 Semilog Plot of GTFM Simulation of the Slug-Withdrawal Test of the Magenta Dolomite at Well H-2b1 . . . . . 36

5-34 Semilog Plot of GTFM Simulation of the Pulse-Injection Test of the Magenta Dolomite at Well H-2b1 . . . . . 36

5-35 Linear-Linear Plot of GTFM Simulation of the Slug-injection Test of the Magenta Dolomite at Well H-2b1 . . . . . 37

5-36 Semilog Plot of GTFM Simulation of the Slug-Injection Test of the Magenta Dolomite at Well H-2b1 . . . . . 37

5-37 Semilog Plot of GTFM Simulations of the Slug-Injection Test of the Magenta Dolomite at Well H-2b1 Using Different Values for Storativity . . . . . 38

5-38 Simulated Pore Pressures at Selected Radial Distances from Well H-2b1 During the Slug-Withdrawal and Pulse-Injection Tests of the Magenta Dolomite . . . . . 39

5-39 Simulated Hydraulic-Head Changes at Selected Radial Distances from Well H-2b1 During the Slug-Injection Test of the Magenta Dolomite . . . . . 39

5-40 Linear-Linear Sequence Plot of Pressure Data from the Pulse and Slug Tests of the Magenta Dolomite at Well H-3b1 . . . . . 40

5-41 Linear-Linear Plot of GTFM Simulation of the Pulse and Slug Tests of the Magenta Dolomite at Well H-3b1 . . . . . 41

5-42 Semilog Plot of GTFM Simulation of the Pulse-Withdrawal Test of the Magenta Dolomite at Well H-3b1 . . . . . 41

5-43 Semilog Plot of GTFM Simulation of the Slug-Withdrawal Test of the Magenta Dolomite at Well H-3b1 . . . . . 42

5-44 Semilog Plot of GTFM Simulation of the Slug-Injection Test of the Magenta Dolomite at Well H-3b1 . . . . . 42

5-45 Semilog Plot of GTFM Simulations of the Slug-Injection Test of the Magenta Dolomite at Well H-3b1 Using Different Values for Storativity . . . . . 43

5-46 Simulated Pore Pressures at Selected Radial Distances from Well H-3b1 During the Pulse and Slug Tests of the Magenta Dolomite . . . . . 44

5-47 Linear-Linear Sequence Plot of Pressure Data from the Pulse Tests of the Forty-niner Claystone at Well H-3d . . . . . 45

5-48 Linear-Linear Sequence Plot of Water-Level Data from the Slug-Withdrawal Test of the Forty-niner Claystone at Well H-3d . . . . . 45

5-49 Linear-Linear Plot of GTFM Simulation of the Slug-Withdrawal Test of the Forty-niner Claystone at Well H-3d . . . . . 46

5-50 Semilog Plot of GTFM Simulation of the Slug-Withdrawal Test of the Forty-niner Claystone at Well H-3d . . . . . 46

5-51 Semilog Plot of GTFM Simulations of the Slug-Withdrawal Test of the Forty-niner Claystone at Well H-3d Using Different Values for Storativity . . . . . 47

5-52 Linear-Linear Plot of GTFM Simulations of the Pulse-Withdrawal Test of the Forty-niner Claystone at Well H-3d . . . . . 48

5-53 Semilog Plot of GTFM Simulations of the Pulse-Withdrawal Test of the Forty-niner Claystone at Well H-3d . . . . . 48

5-54 Simulated Hydraulic-Head Changes at Selected Radial Distances from Well H-3d During the Slug-Withdrawal Test of the Forty-niner Claystone . . . . . 49

A-1 Verification of GTFM by Comparison to Theis (1935) Analytic Solution for Pumping Tests . . . . . 56

A-2 Verification of GTFM by Comparison to Cooper et al. (1967) Analytic Solution for Slug Tests . . . . . 57

A-3 Verification of GTFM by Comparison to Bredehoeft and Papadopulos (1980) Analytic Solution for Pulse Tests . . . . . 58

# TABLES

5-1 Summary of Single-Well Test Results . . . . . 15

5-2 Comparison of Analytical and GTFM Results . . . . . 22

# 1. INTRODUCTION

This report presents the results of single-well hydraulic tests performed in seven wells in the vicinity of the Waste Isolation Pilot Plant (WIPP) site in southeastern New Mexico (Figure 1-1) in 1988 and 1989. The WIPP is a U.S. Department of Energy research and development facility designed to demonstrate safe disposal of transuranic radioactive wastes from the nation's defense programs. The WIPP facility lies in bedded halite in the lower Salado Formation. The tests reported herein were conducted in the Rustler Formation, which overlies the Salado Formation. These tests were performed by INTERA Inc. under the technical direction of Sandia National Laboratories, Albuquerque, New Mexico.

The tests discussed in this report were performed in four of the five members of the Rustler Formation. The tests include: a slug-withdrawal test of the unnamed lower member of the Rustler at well H-16; slug-withdrawal and slug-injection tests of the Culebra Dolomite Member at well AEC-7; slug-injection tests of the Culebra at well D-268; a pumping test of the Culebra at well H-18; pulse-injection, slug-injection, and slug-withdrawal tests of the Magenta Dolomite Member at well H-2b1; pulse-withdrawal, slug-withdrawal, and slug-injection tests of the Magenta at well H-3b1; and pulse-withdrawal and slug-withdrawal tests of the Forty-niner Member at well H-3d. The tests were intended to provide data on the transmissivities of the Rustler members for use in regional-scale modeling of groundwater flow through the Rustler.

This report supplements an earlier report on single-well testing (Beauheim, 1987c), and completes reporting of all single-well testing performed by Sandia National Laboratories during the site-characterization phase of the WIPP project.

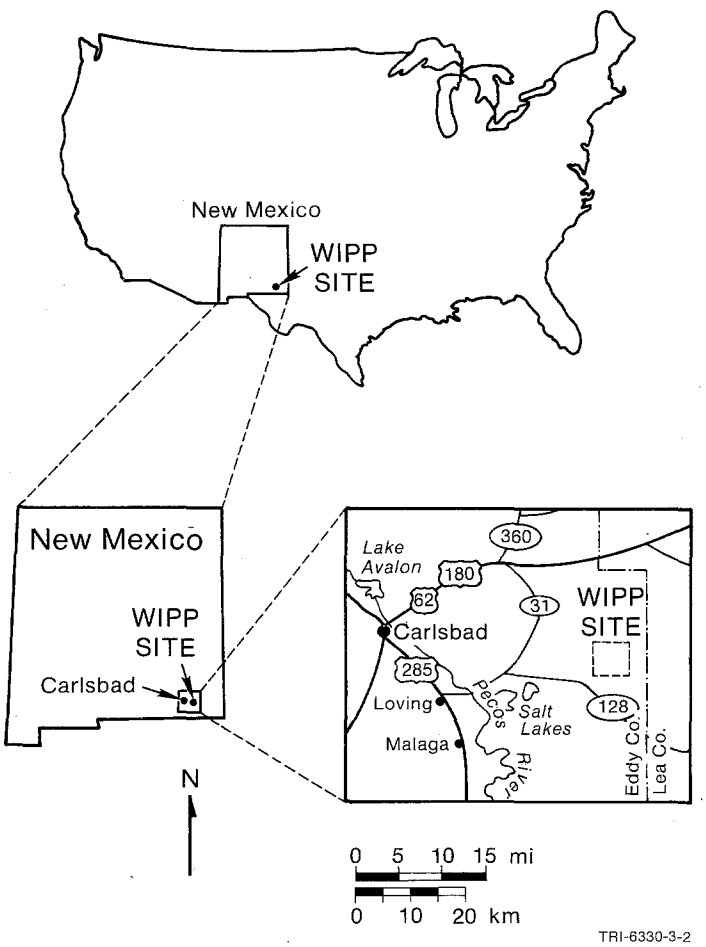


Figure 1-1 Location of the WIPP Site

# 2. RUSTLER HYDROGEOLOGY AND PREVIOUS TESTING

The WIPP site is located in the northern part of the Delaware Basin in southeastern New Mexico. Geologic investigations for the WIPP have concentrated on the upper seven formations typically found in that part of the Delaware Basin. These are, in ascending order, the Bell Canyon Formation, the Castile Formation, the Salado Formation, the Rustler Formation, the Dewey Lake Red Beds, the Dockum Group, and the Gatuña Formation (Figure 2-1). All of these formations are of Permian age, except for the Dockum Group, which is of Triassic age, and the Gatuña, which is a Quaternary deposit. The Bell Canyon and the Rustler contain the most transmissive of the regionally continuous and saturated intervals in these seven formations.

Sixty-seven wells on 42 drilling pads in the vicinity of the WIPP site are completed to one or more members of the Rustler Formation (Figure 2-2). At the locations of the tests discussed in this report, the top of the Rustler Formation lies from 187 (D-268) to 663 ft (AEC-7) below ground surface, and its bottom lies from 494 (D-268) to 988 ft (AEC-7) deep. At these locations, the Rustler consists of five mappable members (in ascending order): an unnamed lower member, the Culebra Dolomite Member, the Tamarisk Member, the Magenta Dolomite Member, and the Forty-niner Member. All of the Rustler members are fully saturated at all locations tested within the WIPP site boundary.

| SYSTEM | SERIES | GROUP | FORMATION | MEMBER |
|---|---|---|---|---|
| RECENT | RECENT | | SURFICIAL DEPOSITS | |
| QUATERNARY | PLEISTOCENE | | MESCALERO CALICHE | |
| | | | GATUÑA | |
| TRIASSIC | | DOCKUM | UNDIVIDED | |
| PERMIAN | OCHOAN | DELAWARE MOUNTAIN | DEWEY LAKE RED BEDS | |
| | | | RUSTLER | Forty-niner |
| | | | | Magenta Dolomite |
| | | | | Tamarisk |
| | | | | Culebra Dolomite |
| | | | | unnamed |
| | | | SALADO | |
| | | | CASTILE | |
| | GUADALUPIAN | | BELL CANYON | |
| | | | CHERRY CANYON | |
| | | | BRUSHY CANYON | |

TRI-6330-89-0

Figure 2-1 WIPP Area Stratigraphic Column

The unnamed lower member is composed of a layered sequence of clayey siltstone, anhydrite, and halite (absent on the western side of the WIPP site) ranging from 100 (AEC-7) to 126 ft (H-3b1) thick. West of the WIPP site in Nash Draw, some evaporite beds within the Rustler and upper Salado Formation have been dissolved, creating a transmissive zone at the Rustler-Salado contact referred to as a "brine aquifer" by Robinson and Lang (1938). Portions of the unnamed lower member, including the contact between the Rustler and Salado Formations, have been tested at 21 locations (Mercer, 1983; Beauheim, 1987c). Transmissivities of the tested intervals range from $3 \times 10^{-5}$ to 8 $ft^2$/day (Mercer, 1983). The brine aquifer is not present at the WIPP site, and the transmissivity of the unnamed lower member there ranges from $3 \times 10^{-5}$ to $3 \times 10^{-3}$ $ft^2$/day (Mercer, 1983).

The Culebra Dolomite Member is a light olive-gray, fine-grained, vuggy, silty dolomite, 18 (H-2b1) to 28 ft (AEC-7) thick. The Culebra is the most transmissive member of the Rustler, and is considered to be the most important potential groundwater-transport pathway for radionuclides which may escape from the WIPP facility to reach the accessible environment. Hence, the vast majority of hydrologic tests performed at the WIPP site have examined the hydraulic properties of the Culebra. Measured transmissivities of the Culebra at 58 wells range from about $4 \times 10^{-3}$ $ft^2$/day east of the WIPP site at P-18 (Beauheim, 1987c) to greater than $1 \times 10^3$ $ft^2$/day in Nash Draw west of the WIPP site at wells such as H-7, WIPP-26, and WIPP-29 (Mercer, 1983).

The Tamarisk Member is composed of two anhydrite and/or gypsum units separated by a silty-claystone interbed which contains halite along the southern and central portions of the eastern boundary of the WIPP site. The Tamarisk has a total thickness of 84 (H-2b1) to 105 ft (AEC-7). Testing of the claystone unit within the Tamarisk Member has been attempted at DOE-2 (Beauheim, 1986), H-3b3 (unpublished field notes), H-14 (Beauheim, 1987c), and H-16 (Beauheim, 1987c).

In all cases, the transmissivity of the unit is too low to measure with the equipment and techniques employed.

The Magenta Dolomite Member consists of a silty, gypsiferous, laminated dolomite, 20 (D-268) to 34 ft (AEC-7) thick. The Magenta is generally considered to be the second-most transmissive Rustler member, and has been tested at 16 locations by the U.S. Geological Survey (Mercer, 1983) and Sandia National Laboratories (Beauheim, 1986, 1987c). Magenta transmissivities range from about 1 x $10^{-3}$ $ft^2$/day at DOE-2 (Beauheim, 1986) to 3.7 x $10^2$ $ft^2$/day at WIPP-25 in Nash Draw (Mercer, 1983).

The Forty-niner Member consists of two anhydrite/gypsum units separated by a silty-claystone interbed which contains halite east of the WIPP site. The aggregate thickness of the Forty-niner varies between 58 (AEC-7, H-2b1, H-3b1, and H-16) and 68 ft (D-268). The medial claystone in the Forty-niner has been tested only at wells DOE-2, H-14, and H-16, where it was found to have transmissivities ranging from 2.5 x $10^{-3}$ to 7.1 x $10^{-2}$ $ft^2$/day (Beauheim, 1986, 1987c). Testing of a Forty-niner anhydrite/gypsum unit was attempted at H-14 (Beauheim, 1987c), but the transmissivity of the unit is below the limit of resolution of the measurement techniques and/or equipment.

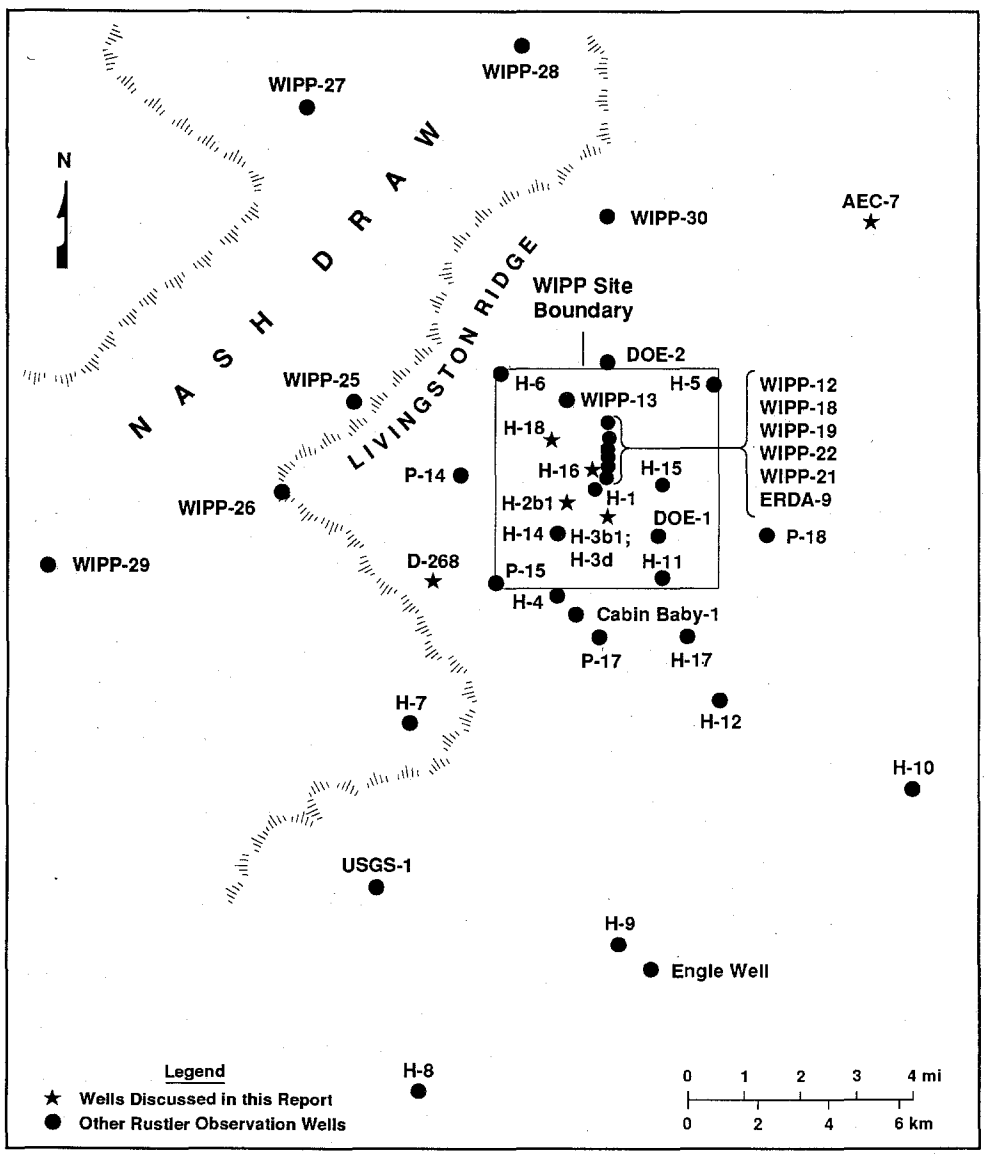


Figure 2-2 Locations of Wells Near the WIPP Site

# 3. TEST WELLS

The wells discussed in this report were drilled between 1974 and 1987 for a variety of purposes. Some of them have been recompleted one or more times since the original drilling. Three of the wells are open holes through the strata tested, while the others are cased and perforated to the tested intervals. The following sections contain brief histories of the wells, along with descriptions of their configurations at the times of testing. Unless otherwise indicated, all depths listed below are from ground surface.

## 3.1 AEC-7

Well AEC-7 was drilled under the direction of Oak Ridge National Laboratory in 1974 to provide lithologic and stratigraphic information on the evaporite sequence at a potential radioactive-waste repository site (Sandia and D'Appolonia, 1983). A 12.25-inch hole was drilled to the Upper Salado Formation (1004 ft) and cased with 8.625-inch casing. The well was then deepened to 3906 ft at a 7.875-inch diameter and left uncased and filled with brine. In 1979, Sandia National Laboratories (SNL) deepened AEC-7 to a total depth of 4722 ft to allow testing of borehole-plugging concepts and to measure formation pressures in the Bell Canyon Formation (Christensen and Peterson, 1981). Following those tests, AEC-7 was grouted from 4455 to 4483 ft to seal off the pressure and upward flow from the lower Bell Canyon Formation.

In 1988, AEC-7 was converted into a Culebra dolomite observation well (Stensrud et al., 1990). A retrievable bridge plug was installed at approximately 950 ft, after which the Culebra interval was shot-perforated with four shots/ft from 859 to 890 ft. A production-injection packer (PIP) was then installed from 840.5 to 842.2 ft for well-development operations. Before testing began, the interval was shut-in with a 1.5-inch-diameter packer ("minipacker") from 799.95 to 801.65 ft and anomalously high pressure readings were observed. This pressure is believed to have leaked past the bridge plug from either the Salado or the Bell Canyon Formation. All packers and plugs were removed, and the bridge plug was reset from 953.7 to 955.4 ft, ending the anomalous pressure readings. After well-development pumping, the PIP was reset at 840.96 to 842.66 ft and a 1.5-inch minipacker was used to conduct a series of hydraulic slug tests on the Culebra dolomite. The configuration of well AEC-7 during the testing period is shown in Figure 3-1.

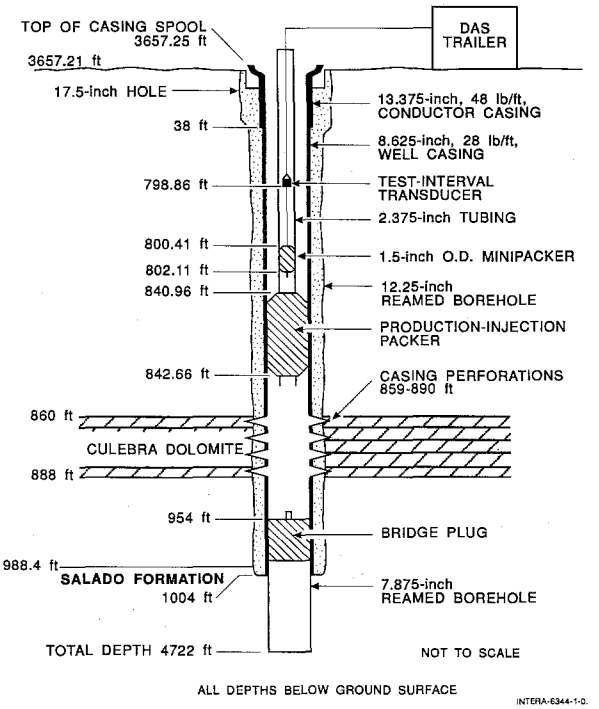


Figure 3-1 Well Configuration for AEC-7 Tests

## 3.2 D-268

Well D-268 was drilled as a potash exploration hole by the Duval Mining Company in 1984. Under an agreement with SNL, the hole was to be turned into a Culebra monitoring well after completion (Stensrud et al., 1990). The hole was drilled through the Rustler Formation and approximately 35 ft into the Salado Formation to a depth of 529 ft. A 4.5-inch casing was set to a depth of 528 ft. Due to the lack of cement returns at the surface during the cementing of the casing, an unknown percentage of the cement was presumed to have been lost to a permeable formation. Drilling fluid was lost as the Culebra interval was drilled, leading to speculation that the cement loss may also have occurred in the Culebra. However, no direct evidence for the location of the cement loss is available. The well was deepened to a total depth of 1411 ft and then cemented up to the casing just below the Rustler/Salado contact.

Because of uncertainty as to how well the casing was cemented, SNL decided to abandon the well. The casing was cut at 220 ft in order to retrieve the upper portion of the casing. The casing could not be retrieved from 220 ft, suggesting that the cement may

have reached that level, so the casing was cut again at 145 ft, with this section being successfully retrieved. SNL then decided to retain D-268 and the casing was replaced into the well with a 5.5-inch swedge coupling to provide an overshot to seat on the casing still in the hole.

In April 1988, D-268 was configured to develop and monitor the Culebra dolomite. The Culebra interval was shot-perforated with four shots/ft between 368 and 398 ft. Due to the possibility of water leaking into the casing from the two cuts at 145 and 220 ft, a PIP was installed from 340.64 to 344.94 ft. The Culebra water level and the water level in the annulus above the PIP were monitored to check the integrity of the packer seal. D-268 was developed by pumping in November 1988 and reconfigured for a series of hydraulic tests. A 1.5-inch minipacker was set into the 2.375-inch PIP tubing at a depth of 323.74 to 325.54 ft in order to conduct the hydraulic slug tests. The configuration of D-268 during the testing period is shown in Figure 3-2.

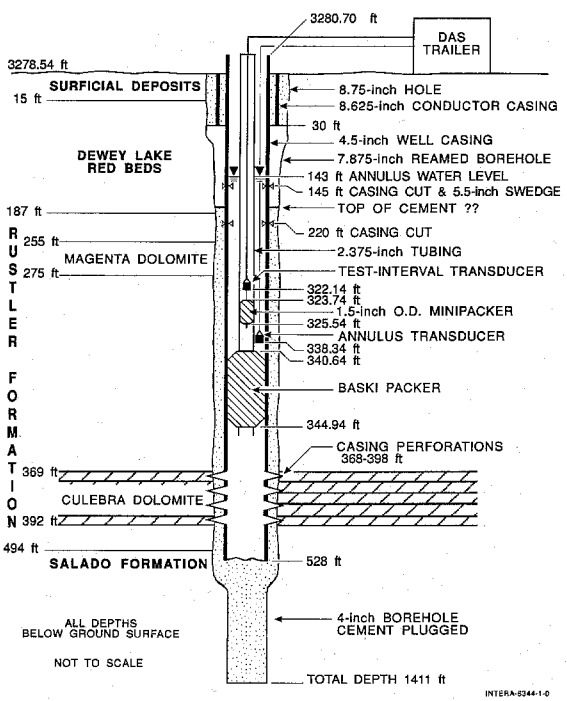


Figure 3-2 Well Configuration for D-268 Tests

## 3.3 H-2b1

Well H-2b1 (previously known as H-2b) was drilled in February 1977 as part of the initial hydrogeologic characterization of the WIPP site (Mercer and Orr, 1979). An 8.75-inch hole was rotary drilled, with air mist as the drilling fluid, through the Magenta dolomite to a depth of 611 ft (Figure 3-3). A 6.625-inch casing was cemented from the ground surface to a depth of 609 ft. A 4.75-inch hole was then cored through the Culebra to a depth of 661 ft. Following hydraulic tests of the Culebra, a retrievable bridge plug was installed below the Magenta interval to seal off the Culebra. The Magenta interval was then shot-perforated with three shots/ft from 510 to 538 ft and tested by bailing. Following those tests, the bridge plug below the Magenta was replaced with a PIP on 2.375-inch tubing. This configuration allowed monitoring of Culebra water levels in the tubing, and of Magenta water levels in the annulus between the well casing and the tubing.

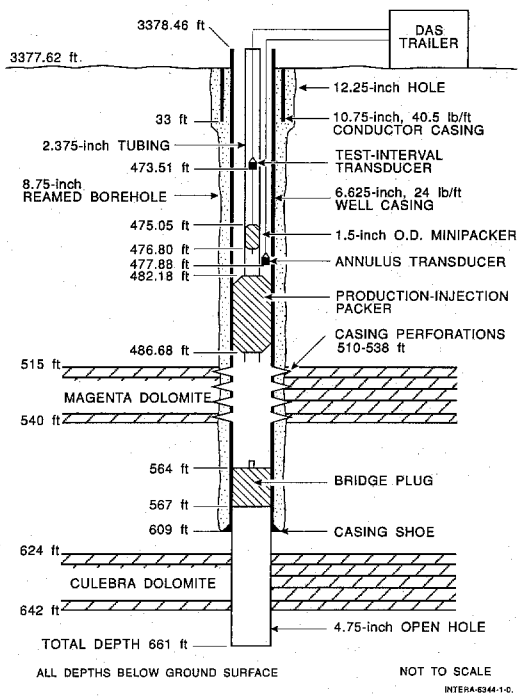


Figure 3-3 Well Configuration for H-2b1 Tests

The well was reconfigured on April 20, 1989 (Calendar Day 110) for hydraulic testing of the Magenta by replacing the PIP with a bridge plug, and setting a PIP on 2.375-inch tubing above the Magenta. Before setting the PIP, about 350 gallons of water were bailed from the well to clean and develop the well. The PIP was set from 482.18 to 486.68 ft and a 1.5-inch inflatable minipacker was set inside the tubing from 475.05 to 476.80 ft to facilitate the hydraulic testing. Figure 3-3 shows the configuration of the well at the time of the hydraulic testing. After testing was completed, the PIP was removed from the well.

## 3.4 H-3b1

Well H-3b1 (previously known as H-3) was drilled during July and August 1976 as part of the initial characterization of the hydrogeology of the WIPP site by the U.S. Geological Survey (Mercer and Orr, 1979). An 8.75-inch hole was rotary drilled, with air mist as the drilling fluid, into the upper Salado Formation to a total depth of 894 ft. After total depth was reached, a series of drillstem tests was performed with the use of an inflatable double-packer testing tool. The tests were conducted on the contact zone between the Rustler and Salado Formations, an argillaceous zone in the unnamed lower member of the Rustler, an interval that included most of the Culebra dolomite, and the Magenta dolomite interval. The well was then filled with brine to conduct geophysical logging and to set and cement 6.625-inch casing to a depth of 891 ft.

In 1977, the Rustler/Salado contact (813 to 837 ft) was shot-perforated and bailed. A retrievable bridge plug was then set at 795 ft, after which the Culebra interval from 675 to 703 ft was shot-perforated and bailed. A retrievable PIP was then set above the Culebra interval and the Magenta interval was shot-perforated using three shots/ft from 564 to 592 ft. The tubing was reattached to the PIP and well H-3b1 was used to monitor the water levels in both the Culebra and Magenta intervals. The PIP was replaced by a retrievable bridge plug in 1987 to convert H-3b1 into a water-level and water-quality-monitoring well for the Magenta.

On July 14, 1989, a 4.25-inch PIP was set above the Magenta interval from 549.02 to 553.50 ft on 2.375-inch tubing. A series of hydraulic tests was conducted with the use of a 1.5-inch inflatable minipacker placed inside the 2.375-inch tubing from 529.28 to 531.08 ft. The configuration of well H-3b1 during the testing is shown in Figure 3-4. Following the hydraulic testing, the PIP was removed.

## 3.5 H-3d

Well H-3d was drilled in April 1987 to obtain additional hydrologic data on the Dewey Lake Red Beds and the Forty-niner claystone of the Rustler Formation in the south-central region of the WIPP site (Stensrud et al., 1990). After cementing 8.625-inch surface casing to a depth of 39 ft, H-3d was rotary drilled at a diameter of 7.875 inches to a total depth of 553.9 ft, within the lower anhydrite of the Forty-niner Member. Brine was used as the drilling fluid, and the hole was left uncased. A 5.625-inch PIP was installed on 2.375-inch

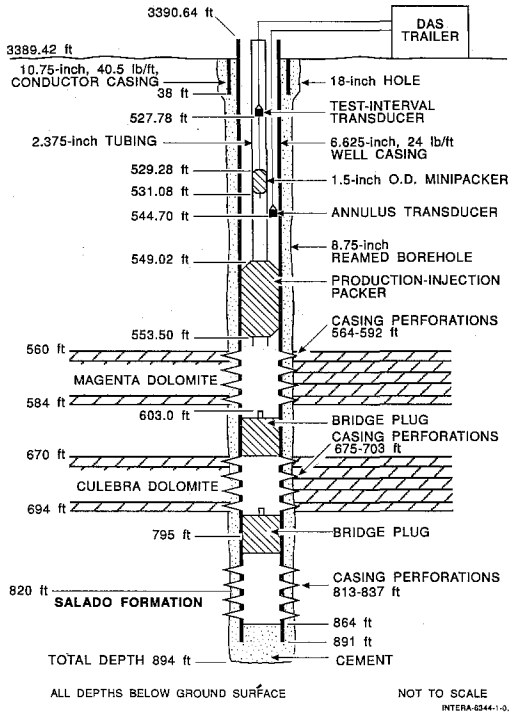


Figure 3-4 Well Configuration for H-3b1 Tests

tubing in the upper anhydrite of the Forty-niner Member at a depth of 515.60 to 517.98 ft. Three-quarter-inch polyvinyl chloride (PVC) tubing was also installed to a depth of 419 ft for water-level-sounder access to the annulus. Pulse and slug testing were performed on the Forty-niner claystone with the use of a 1.5-inch minipacker installed at a depth of 512.40 to 514.15 ft inside the 2.375-inch tubing. The configuration of well H-3d during the testing period is shown in Figure 3-5.

## 3.6 H-16

Well H-16 was drilled in July and August 1987 to monitor the hydraulic responses of the Rustler Formation during construction of the Air-Intake Shaft (AIS) at the WIPP site (Mercer and Snyder, 1990a). H-16, located 50 ft to the northwest of the AIS, was rotary drilled and reamed to a 9.625-inch diameter to a depth of 470 ft, just above the Rustler Formation. A 7.0-inch casing was set and cemented to a depth of 469 ft. Each member of the Rustler Formation was then cored and reamed to a 4.75-inch diameter. A series of hydraulic tests was conducted on each member before the next underlying member was penetrated. The hole was completed by reaming to a diameter of 6.125 inches to a total depth of 850.9 ft.

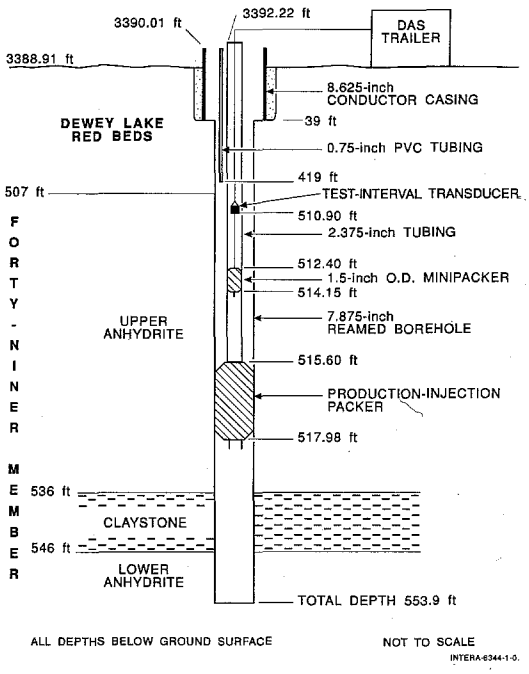


Figure 3-5 Well Configuration for H-3d Tests

A five-packer test tool was then installed to allow monitoring of fluid pressures in each Rustler member during and after construction of the AIS. Stratigraphic depths of the formations encountered in the hole, and the five-packer completion of the well are shown in Figure 3-6.

## 3.7 H-18

Well H-18 was drilled in October and November 1987 to investigate an area in the northwest portion of the WIPP site where large changes in Culebra transmissivity and water quality occur (Mercer and Snyder, 1990b). A 9.625-inch hole was cored and reamed to a depth of 674 ft, about 15 ft above the top of the Culebra, and 7-inch casing was set and cemented from 673 ft to the surface. The hole was then cored and reamed through the Culebra to about 714 ft to a diameter of 4.75 inches. Following drillstem and slug testing of the Culebra, the hole was cored to 830.5 ft for stratigraphic information, reamed and drilled at a 6.125-inch diameter to 840 ft for geophysical logging, and then plugged back to 766 ft with cement. In February 1988, a 5.625-inch sliding-end packer was set from 679.35 to 683.55 ft with a 1.5-horsepower pump installed at 688.15 ft (Stensrud et al., 1988). Stratigraphic depths of the formations encountered in H-18 and the configuration of the well at the time of the pumping test are shown in Figure 3-7.

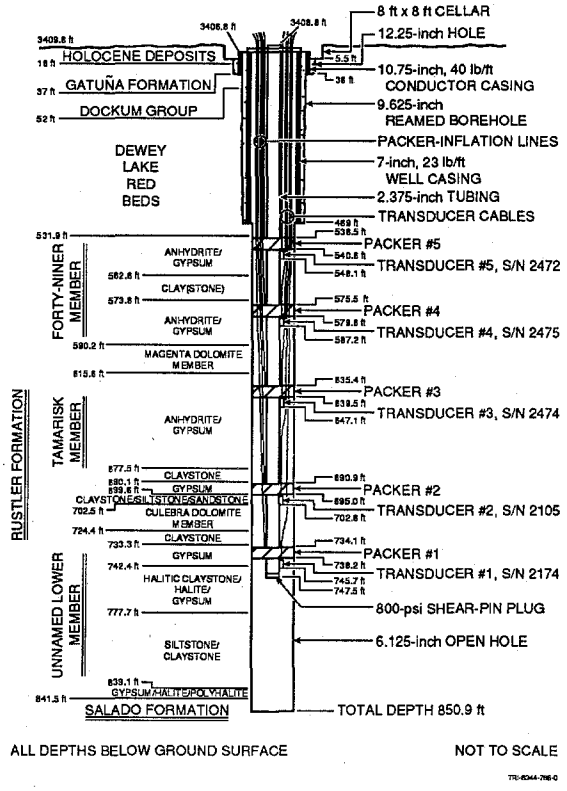


Figure 3-6 Well Configuration for H-16 Test

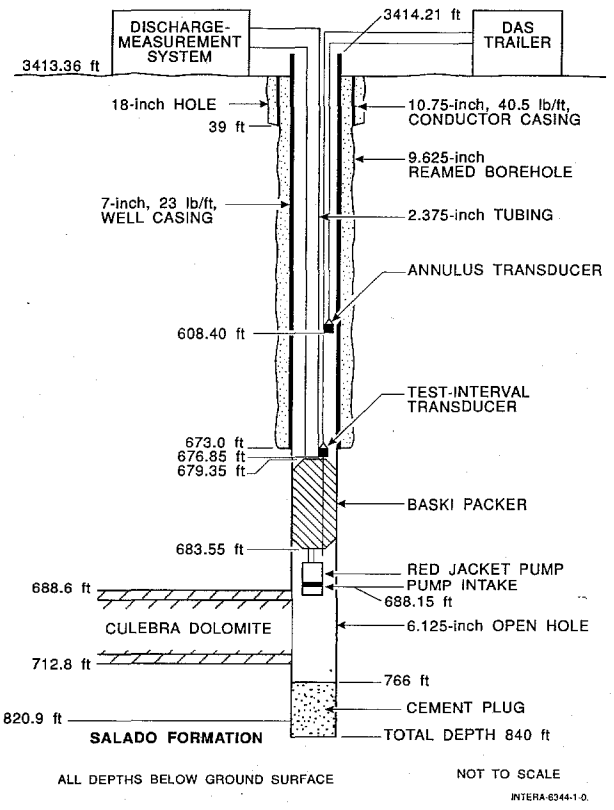


Figure 3-7 Well Configuration for H-18 Test

# 4. TEST METHODS

A variety of testing methods was employed for single-well tests at the WIPP site because of the wide range of transmissivities encountered and because of the different types of well completions. Slug-withdrawal (rising-head) tests, slug-injection (falling-head) tests, pulse-withdrawal tests, pulse-injection tests, and pumping tests were all employed in these investigations. Generalized procedures for each type of test are presented below. The techniques used to interpret the data from these tests are discussed in detail in Appendix A and by Beauheim (1987c).

## 4.1 Slug Tests

Slug-withdrawal or slug-injection tests, as described by Cooper et al. (1967), are commonly performed in wells that do not produce enough water to sustain a pumping test. At the WIPP, slug-withdrawal tests are typically performed with a PIP set in a well on a tubing string. Water is swabbed from the tubing, and a 1.5-inch-diameter minipacker is quickly lowered into the tubing on a wireline and inflated a short distance below the level of the water remaining in the tubing. A transducer wired to a data-acquisition system monitors the pressure below the minipacker. When the pressure stabilizes, the minipacker is deflated rapidly, stimulating flow from the formation into the relatively under-pressurized tubing. The water-level or fluid-pressure rise in the tubing is monitored to provide the data needed to analyze the test. Ideally, the slug test should continue until the initial pressure differential has decreased by ninety percent or more. However, forty percent recovery generally provides adequate data for analysis, particularly if log-log plotting techniques are used (Ramey et al., 1975). Slug-withdrawal tests were performed in the unnamed lower member at well H-16; in the Culebra at well AEC-7; in the Magenta at wells H-2b1 and H-3b1; and in the Forty-niner claystone at well H-3d.

To prepare for a slug-injection test, a packer is lowered into the well (or into tubing if a PIP is being used to isolate the test zone from other water-producing zones) below the water surface and inflated. Additional water is then added to the well (or tubing) above the packer. After pressures above and below the packer stabilize, the packer is deflated as rapidly as possible. This connects the overlying slug of water with the formation below, marking the beginning of the test. As with a slug-withdrawal test, a slug-injection test should be continued until the pressure change caused by the added slug of water dissipates to ten percent or less of its initial magnitude. Slug-injection tests were performed in the Culebra at wells AEC-7 and D-268, and in the Magenta at wells H-2b1 and H-3b1.

## 4.2 Pressure-Pulse Tests

Pressure-pulse tests are a more rapid method of hydraulic testing in water-bearing units with transmissivities that are so low (i.e., < 0.01 $ft^2$/day) that slug tests would take days to months to complete. Pressure-pulse tests proceed more rapidly than slug tests because they are performed under shut-in conditions. That is, the test intervals are isolated with one or more packers so that pressure changes are caused by the compression/expansion of water rather than by the filling/draining of a volume of tubing or casing. The theory of pressure-pulse testing was described by Bredehoeft and Papadopulos (1980) and Neuzil (1982), who referred to the tests as modified slug tests.

For the pressure-pulse tests discussed in this report, a testing technique was devised that required only the equipment that was already on site for slug tests. Both pulse-withdrawal and pulse-injection tests were performed using a minipacker inside a tubing string attached to a PIP isolating the test interval. The tubing string was either evacuated before inserting and inflating the minipacker for a pulse-withdrawal test, or filled above the inflated packer to some height above the expected static water level for a pulse-injection test. In either case, the test-interval pressure below the inflated packer was allowed to stabilize before testing proceeded. Once the test-interval pressure stabilized, the minipacker was deflated only long enough for the underpressure (pulse withdrawal) or overpressure (pulse injection) to be transmitted to the test zone, and then the minipacker was reinflated. The time required to deflate the minipacker, verify over several pressure readings that the pressure pulse had been transmitted, and reinflate the minipacker was typically about one minute. The dissipation of the resultant pressure difference between the test zone and the formation was then monitored for the actual test. Pressure-pulse tests were performed in the Magenta dolomite at wells H-2b1 and H-3b1, and in the Forty-niner claystone at well H-3d.

## 4.3 Pumping Tests

The only pumping test discussed in this report was performed on the Culebra dolomite at well H-18. This test was performed by lowering a pump mounted below a packer into the well, isolating the Culebra with the packer, and pumping water from the formation at a nominally constant rate while monitoring the decline in pressure in the isolated interval of the well. The pumping period lasted for 72 hr, with an average pumping rate of about 0.94 gallons per minute (gpm). Following the pumping period, the recovery (rise) of the pressure in the well was monitored for 116.5 hr.

## 4.4 Isolation Verification

Pressures or water levels in the wellbores above the tested intervals were monitored during all tests except for those at AEC-7 to detect leakage around packers (Stensrud et al., 1988, 1990). No leakage was detected during any of the tests.

# 5. TEST OBJECTIVES AND INTERPRETATIONS

The principal objective of each of the single-well hydraulic tests discussed in this report was to determine the transmissivity of a member of the Rustler Formation. Specific tests also had other objectives such as determination of the presence or absence of double-porosity conditions within the Culebra dolomite. The data and interpretations obtained from the tests are to be used in characterization and modeling of the groundwater-flow regime of the Rustler Formation. Descriptions of the testing instrumentation and data-acquisition systems and procedures, as well as tabulations and plots of the raw data for each test conducted, are contained in the Hydrologic Data Reports prepared for the WIPP hydrology program (Stensrud et al., 1988, 1990). Unless otherwise indicated, all depths listed below are referenced to ground surface.

Interpretations of the slug and pressure-pulse tests were performed with the well-test-simulation model GTFM (Pickens et al., 1987). For comparison purposes, several of the slug tests were also analyzed using graphical type-curve-fitting techniques based on analytical solutions. The H-18 pumping test was analyzed with the well-test-interpretation code Interpret/2, which uses an analytical-solution approach. Details on the theory and interpretation approaches are presented in Beauheim (1987c) for Interpret/2 and the analytical-solution techniques, and in Appendix A for the GTFM well-test-simulation model.

Interpretations using GTFM assume a one-dimensional radial-flow regime. The formation was discretized radially with 150 to 250 nodes, and the external boundary was assigned a fixed pressure equal to the estimated static formation pressure. The distance to the external boundary was chosen to be sufficiently large so as to have no effect on the calculated fluid-pressure or water-level response in the borehole. The formation thickness for simulation purposes is assumed to represent the most permeable hydro-stratigraphic unit (i.e., unnamed lower member siltstone, Culebra dolomite, Magenta dolomite, and Forty-niner claystone) within the test interval. This assumption is reasonable considering the lower permeability of the anhydrite/gypsum units immediately overlying and underlying each of these units. The discretization did not include a skin zone with different properties adjacent to the well. Interpreting the single-well hydraulic tests required selecting different combinations of transmissivity and static formation pressure (or water level). The parameter combination that yielded the simulated response that most closely matched the observed fluid-pressure or water-level response was considered to be representative of the actual formation parameters.

The procedures and interpretations for tests of the unnamed lower member at H-16, the Culebra dolomite at AEC-7, D-268, and H-18, the Magenta dolomite at H-2b1 and H-3b1, and the Forty-niner claystone at H-3d are presented below. Any pretest history (time-varying pressures/heads) was combined with the hydraulic tests performed into one continuous test sequence, when possible, for analysis using the GTFM model. This continuous test sequence is presented as a linear-linear plot of pressure versus time for the simulation. By combining several hydraulic tests within a sequence, single values of transmissivity were determined that best fit all tests simulated. Each of the simulated hydraulic tests is also presented as a semilog plot with normalized pressure (linear axis) versus elapsed time (log axis). A semilog plot provides a better indication of the fit between the simulation and the observed data at early time than a linear-linear plot. If the fits on the semilog plots were not acceptable, the parameters were adjusted to obtain an adequate match for both linear-linear and semilog presentations.

For those analyses performed using GTFM, radial-pressure plots are also presented showing the calculated pressure or hydraulic-head responses versus time within the tested interval at selected radial distances from the well. These plots can be used to determine whether the pressure had recovered completely from an individual test before the initiation of further testing or if the earlier test(s) had an effect on subsequent tests. Also, the radial-pressure plots allow an estimation of the radial extent of the rock stressed during the hydraulic tests.

## 5.1 Unnamed Lower Member at Well H-16

The unnamed lower member of the Rustler Formation was tested in well H-16. At well H-16, this member is composed of a siltstone layer bounded on top and bottom by beds of gypsum and/or halite (Figure 3-6). The interval tested extended from 738.2 to 850.9 ft below ground surface, with the siltstone bed occupying

the interval from 777.7 to 839.1 ft. For the test interpretations, a storativity of $1.0 \times 10^{-4}$ was initially assumed to maintain consistency with previous interpretations of hydraulic tests of the unnamed lower member (Beauheim, 1987c).

Well H-16 was installed to monitor the pressure responses of the different members of the Rustler Formation during the construction of the Air-Intake Shaft. During shaft construction, pressures responded in each member of the Rustler at H-16 except for the unnamed lower member siltstone (Avis and Saulnier, 1990). On October 8, 1988 (Calendar Day 282) a slug-withdrawal test was initiated on the unnamed lower member at well H-16 by bailing fluid from the tubing and then knocking the shear pin out of the bottom packer. The purposes of this test were twofold: first, to verify that the transducer monitoring the pressure of the unnamed lower member was functioning properly; and second, to provide data with which to evaluate the transmissivity of the unnamed lower member. Descriptions of the testing instrumentation and the data for this test were reported by Stensrud et al. (1990).

The measured pressures of the unnamed lower member from February 4, 1988 to April 13, 1990 are shown plotted in Figure 5-1. Immediately before the slug test began, the pressure from the unnamed lower member was 197 psi. During the recovery period after the slug withdrawal, the pressure rose to 204 psi before dropping back to 203 psi. The cause of this disparity between the pre- and post-test pressures is unknown. For the GTFM simulations of the test, the value of the static formation pressure that best fit the observed recovery data was assumed to be representative of conditions existing before the slug withdrawal.

The GTFM simulation that best fit the slug-test data is presented in Figure 5-2. This simulation was generated using a transmissivity of $3.0 \times 10^{-4}$ $ft^2$/day and a static formation pressure (at the depth of the transducer) of 204.5 psi. The best-fit GTFM simulation is also presented in semilog form as normalized pressure versus elapsed time (Figure 5-3). The simulated and observed pressure responses are in good agreement for both the linear-linear and semilog presentations.

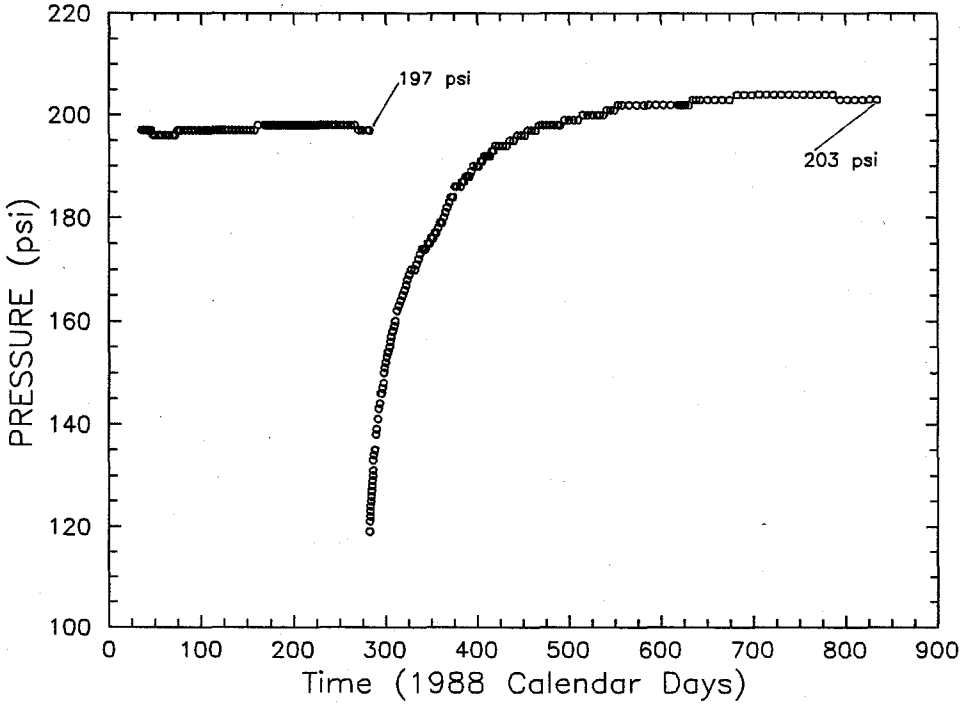


Figure 5-1 Linear-Linear Sequence Plot of Pressure Data from the Slug-Withdrawal Test of the Unnamed Lower Member Siltstone at Well H-16

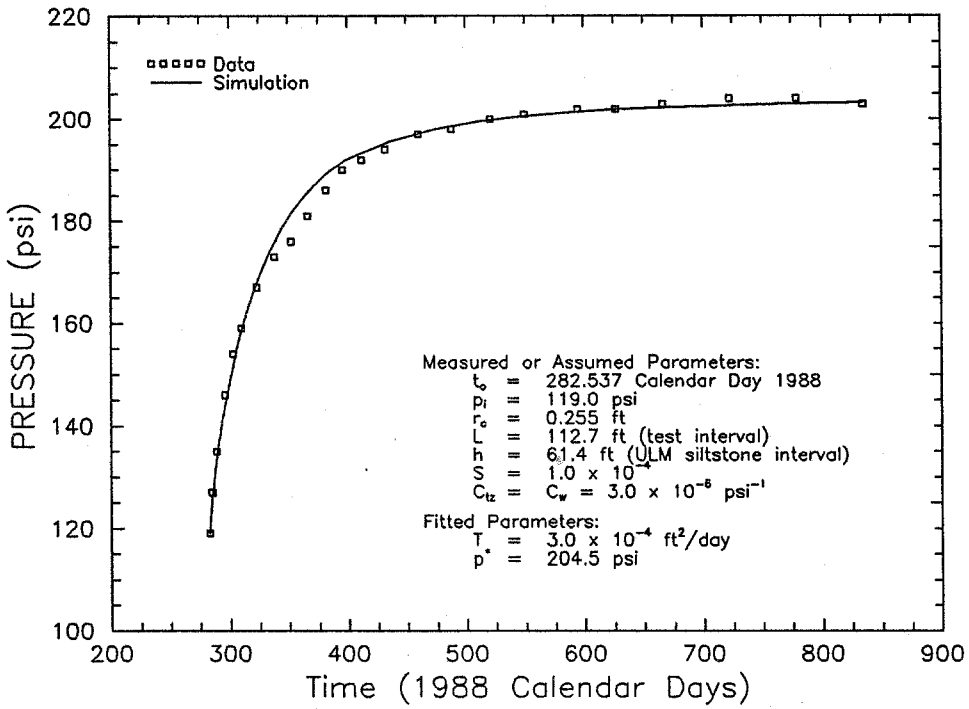


Figure 5-2 Linear-Linear Plot of GTFM Simulation of the Slug-Withdrawal Test of the Unnamed Lower Member Siltstone at Well H-16

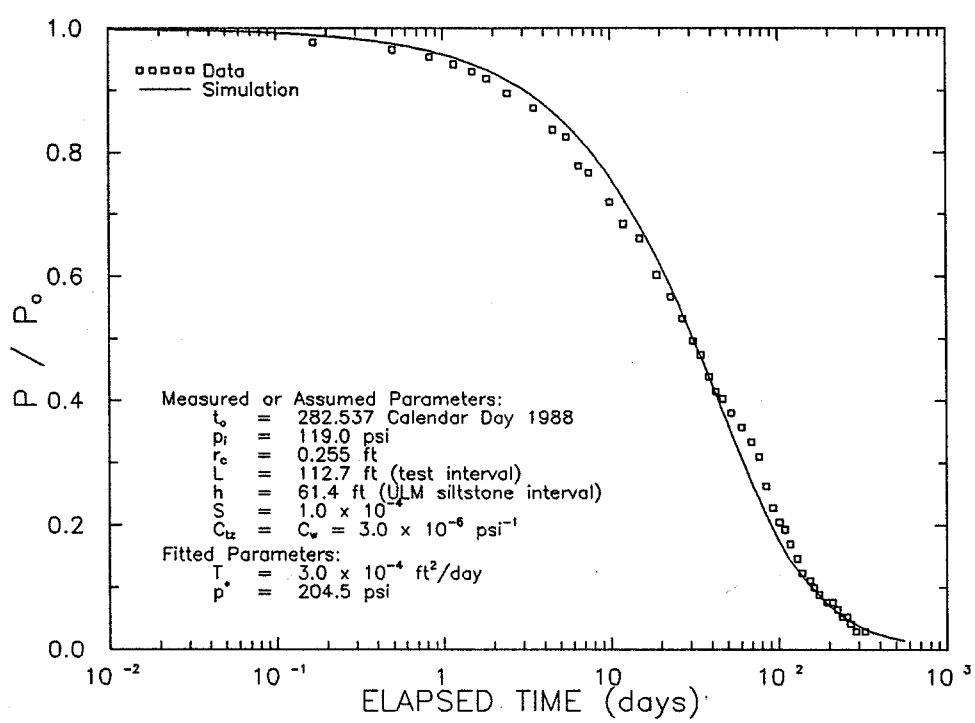


Figure 5-3 Semilog Plot of GTFM Simulation of the Slug-Withdrawal Test of the Unnamed Lower Member Siltstone at Well H-16

To evaluate the sensitivity of the interpreted transmissivity to the assumed ("base case") value of storativity of $1 \times 10^{-4}$, simulations were fit to the observed data using storativity values an order of magnitude higher and lower. These simulations are shown in semilog format in Figure 5-4. The best-fit simulation obtained assuming a storativity of $1 \times 10^{-3}$ used a transmissivity of $2.1 \times 10^{-4}$ $ft^2$/day. The best-fit simulation obtained assuming a storativity of $1 \times 10^{-5}$ used a transmissivity of $3.9 \times 10^{-4}$ $ft^2$/day. The simulation with the higher storativity appears to fit the observed data better over the first 50 percent of recovery than do either of the other two simulations, while the simulation with the base-case value of storativity fits the data best during the last 50 percent of recovery. The simulation using a lower value of storativity provides the poorest match to the observed data. Therefore, the actual storativity of the unnamed lower member siltstone around H-16 probably lies between $1 \times 10^{-4}$ and $1 \times 10^{-3}$, while the transmissivity is probably between $2.1 \times 10^{-4}$ and $3.0 \times 10^{-4}$ $ft^2$/day (Table 5-1). This range encompasses the results of Beauheim (1987c), who calculated transmissivity values of $2.2 \times 10^{-4}$ and $2.7 \times 10^{-4}$ $ft^2$/day from two drillstem tests of the unnamed lower member siltstone at H-16.

GTFM was also used to simulate the propagation of the pressure transient created within the unnamed lower member by the slug test. Figure 5-5 presents the calculated pressure responses at radial distances of 1, 10, and 50 ft from H-16 assuming a storativity of $1 \times 10^{-4}$. A pressure change of about 0.8 psi was calculated to have occurred at a radial distance of 50 ft. The pressure had recovered to within 1 psi of the static level by the end of the simulation period at all radii examined. If the storativity of the unnamed lower member siltstone is greater than $10^{-4}$, the radius of influence of the test would have been less, whereas if the storativity is less than $10^{-4}$, the radius of influence would have been greater. For example, GTFM simulations show that the maximum drawdowns occurring at radial distances of 1, 10, and 50 ft assuming a storativity of $1 \times 10^{-4}$ would occur at radial distances of 0.6, 3.6, and 16 ft if the storativity were $1 \times 10^{-3}$, and at 1.75, 27.5, and 155 ft if the storativity were $1 \times 10^{-5}$.

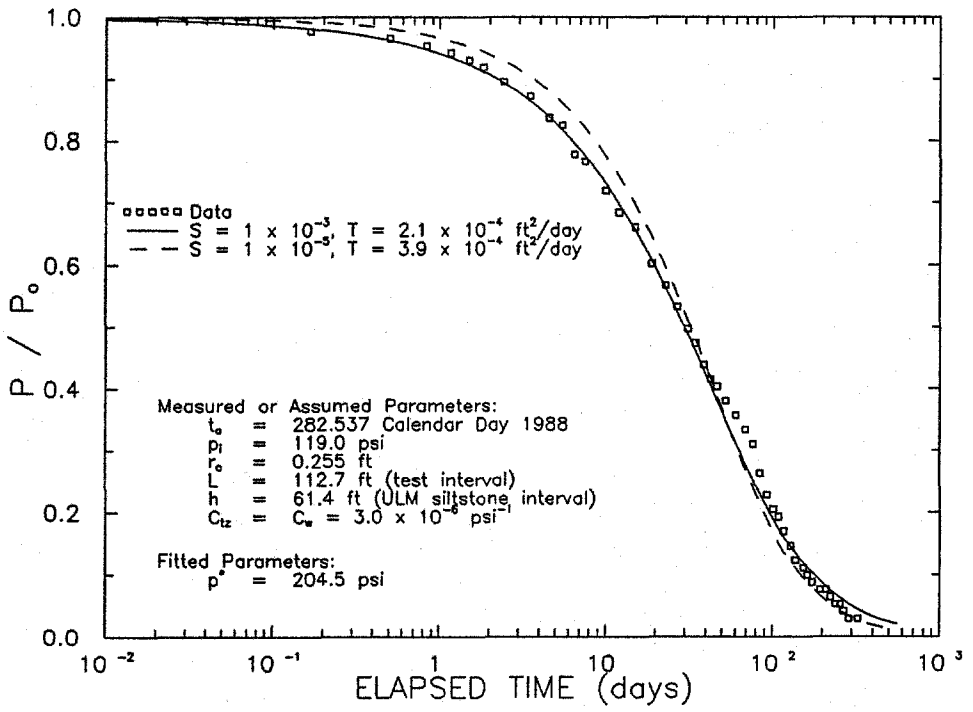


Figure 5-4 Semilog Plot of GTFM Simulations of the Slug-Withdrawal Test of the Unnamed Lower Member Siltstone at Well H-16 Using Different Values for Storativity

## Table 5-1

## Summary of Single-Well Test Results

| WELL | ZONE NAME | ZONE DEPTH INTERVAL (ft) | DEPTH INTERVAL TESTED (ft) | TEST TYPE | TRANSMISSIVITY* ($ft^2$/day) |
|---|---|---|---|---|---|
| H-16 | unnamed lower member siltstone | 778-839 | 738-851 | SLUG | $2.1 \times 10^{-4}$ to $3.0 \times 10^{-4}$ |
| AEC-7 | Culebra dolomite | 860-888 | 859-890 | SLUG(3) | 0.16 to 0.20 |
| D-268 | Culebra dolomite | 369-392 | 368-398 | SLUG(2) | 1.9 to 2.5 |
| H-18 | Culebra dolomite | 689-713 | 683-766 | PUMPING (RECOVERY) | 2.0 (single-porosity)<br>1.0 (double-porosity) |
| H-2b1 | Magenta dolomite | 515-540 | 510-538 | a) SLUG/PULSE<br>b) SLUG | $2.6 \times 10^{-3}$<br>$2.1 \times 10^{-3}$ to $2.7 \times 10^{-3}$ |
| H-3b1 | Magenta dolomite | 560-584 | 564-592 | PULSE/ SLUG(2) | 0.14 to 0.18 |
| H-3d | Forty-niner claystone | 536-546 | 518-554 | a) PULSE<br>b) SLUG | $4.0 \times 10^{-3}$ (?)<br>$3.5 \times 10^{-3}$ to $4.5 \times 10^{-3}$ |

* Range in transmissivity reflects uncertainty in storativity
( ) Number of tests
(?) Uncertain result
Note: All interpretations assume single-porosity medium except as noted

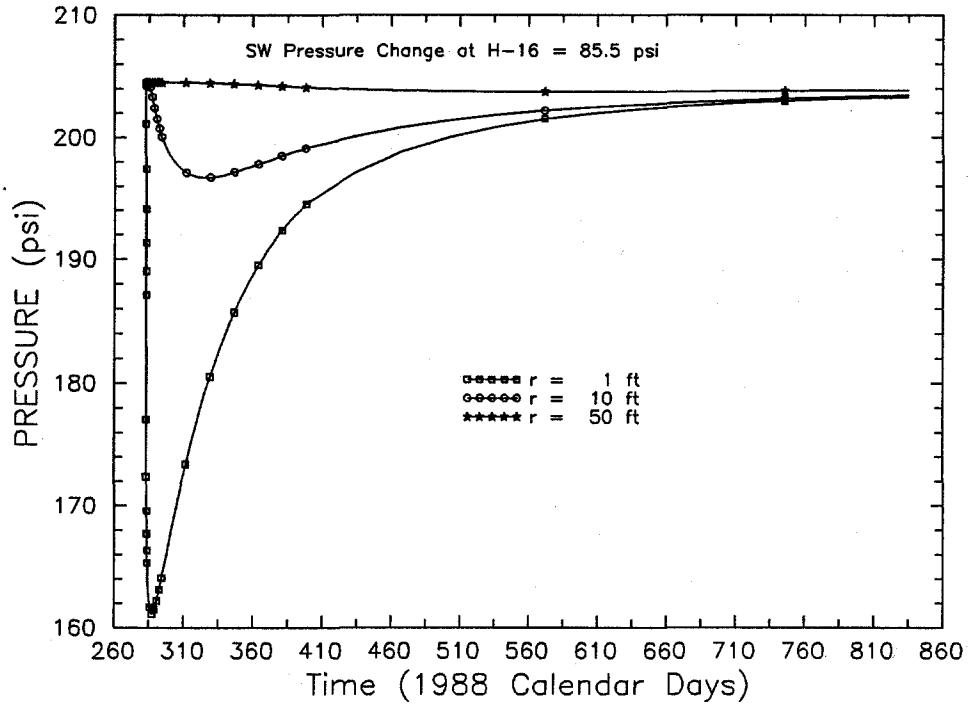


Figure 5-5 Simulated Pore Pressures at Selected Radial Distances from Well H-16 During the Slug-Withdrawal Test of the Unnamed Lower Member Siltstone

## 5.2 Culebra Dolomite Member

The Culebra dolomite was tested at wells AEC-7, D-268, and H-18. The testing was performed to determine the transmissivity of the Culebra at each of these locations and also to determine whether the Culebra behaved hydraulically as a single-porosity medium or as a double-porosity medium at each location. The storativity of the Culebra was initially assumed to be $1.0 \times 10^{-5}$ for the test interpretations, based on data reported by Gonzalez (1983).

**5.2.1 Well AEC-7.** A series of hydraulic tests was conducted on the Culebra dolomite at well AEC-7 from September 27 to October 13, 1988 (Calendar Days 271 to 287). The well casing is perforated from 859 to 890 ft below ground surface to provide hydraulic communication with the Culebra, which lies between 860 and 888 ft deep. The testing at well AEC-7 consisted of a slug-withdrawal test followed by two slug-injection tests. Descriptions of the testing instrumentation and the raw test data are presented in Stensrud et al. (1990).

Following well-development activities, AEC-7 was shut-in on day 271 to allow the Culebra pressure to build up to near the static formation pressure (Figure 5-6). During the shut-in period, the pressure increased to 79.6 psi and then decreased to 78.7 psi before the start of the slug-withdrawal test on day 277. During the slug-withdrawal test, the pressure recovered to a high of 78.1 psi and decreased to 77.9 on day 279, at which time the well was shut-in.

The pressure then decreased to 77.5 psi just before the start of the first slug-injection test on day 281. This behavior indicates that a pressure transient, probably caused by the anomalously high pressures observed the first time the Culebra interval was shut-in (see Section 3.1), was still dissipating through the Culebra when testing began. By the start of the second slug-injection test on day 286, the pressure had recovered to 77.5 psi. The second slug-injection test was terminated after approximately one day, with the last pressure measurement of 78.5 psi taken before full recovery was achieved. The pressure transient did not appear to affect either of the slug-injection tests. Therefore, the static formation pressure chosen for the GTFM simulation was based on the late-time pressure data from the first slug-injection test.

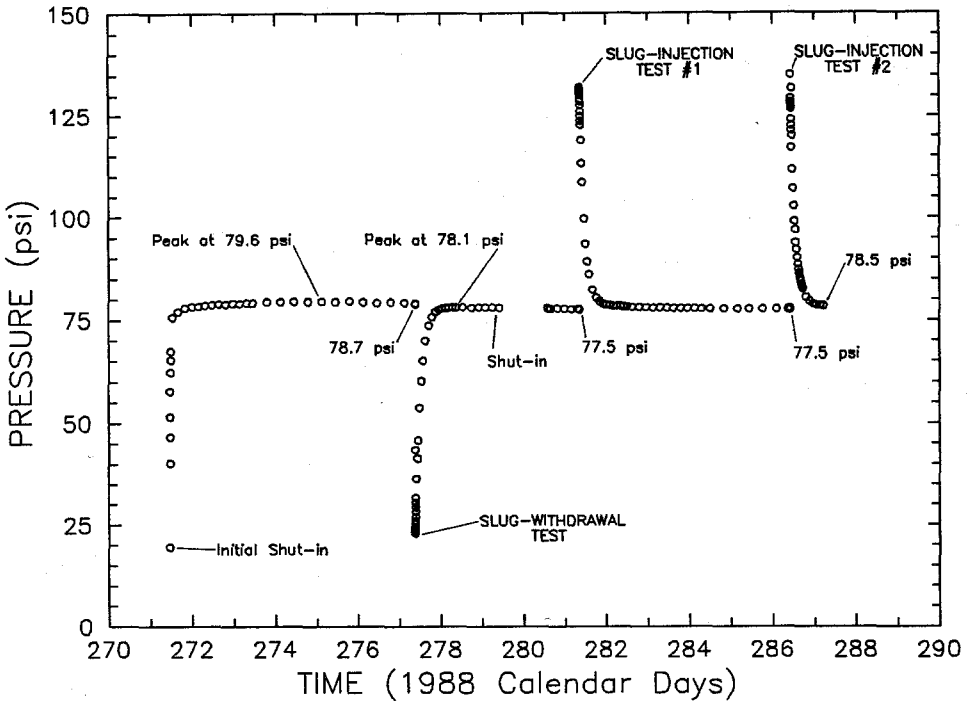


Figure 5-6 Linear-Linear Sequence Plot of Pressure Data from the Slug Tests of the Culebra Dolomite at Well AEC-7

The pressure data for the three slug tests presented in Figure 5-6 were combined into one simulation for analysis. Pretest well history for the period from day 271 to day 277 was included in the simulations. The GTFM simulation that best fit all three slug tests together (Figure 5-7) was generated using a transmissivity of 0.16 $ft^2$/day and a static formation pressure (at the depth of the transducer) of 77.5 psi. This simulation, along with the test data, was separated into the individual slug tests for semilog format presentation. Figures 5-8, 5-9, and 5-10 are semilog plots of normalized pressure versus elapsed time for the slug-withdrawal test, the first slug-injection test, and the second slug-injection test, respectively. The simulation fits the data from the two slug-injection tests better than it fits the data from the slug-withdrawal test. The deviation between the observed and simulated responses to the slug-withdrawal test is probably related to the pre-existing pressure transient that affected the observed response. This transient was not included in the simulation because it could not be well defined.

To evaluate the sensitivity of the interpreted transmissivity to the assumed value of storativity of 1 x $10^{-5}$, simulations were fit to the observed data from the first slug-injection test using storativity values an order of magnitude higher and lower. These simulations are shown in semilog format in Figure 5-11. The best-fit simulation obtained assuming a storativity of 1 x $10^{-4}$ used a transmissivity of 0.11 $ft^2$/day. The best-fit simulation obtained assuming a storativity of 1 x $10^{-6}$ used a transmissivity of 0.20 $ft^2$/day. The simulation assuming a storativity of 1 x $10^{-6}$ may match the observed data slightly better than does the simulation with the base-case value of storativity, whereas the simulation assuming a storativity of 1 x $10^{-4}$ provides the poorest match to the data. Therefore, the storativity of the Culebra dolomite at well AEC-7 is probably less than 1 x $10^{-5}$, and the transmissivity is probably between 0.16 and 0.20 $ft^2$/day (Table 5-1).

The propagation of the pressure transients created within the Culebra dolomite during the pretest history and testing periods was simulated by GTFM. Figure 5-12 presents the pressure responses calculated at radial distances of 10, 100, and 300 ft from AEC-7 assuming a storativity of 1 x $10^{-5}$. Pressure changes on the order of a few tenths of a psi are calculated to have occurred at a radial distance of 300 ft in response to the testing at AEC-7. The pressure recovered to

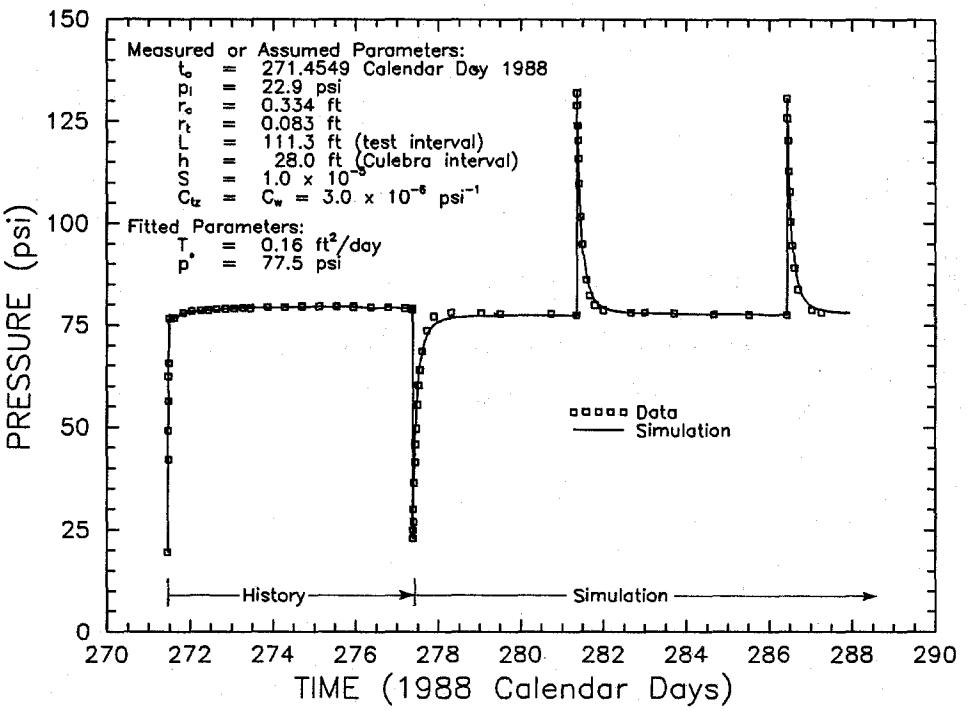


Figure 5-7 Linear-Linear Plot of GTFM Simulation of the Slug Tests of the Culebra Dolomite at Well AEC-7

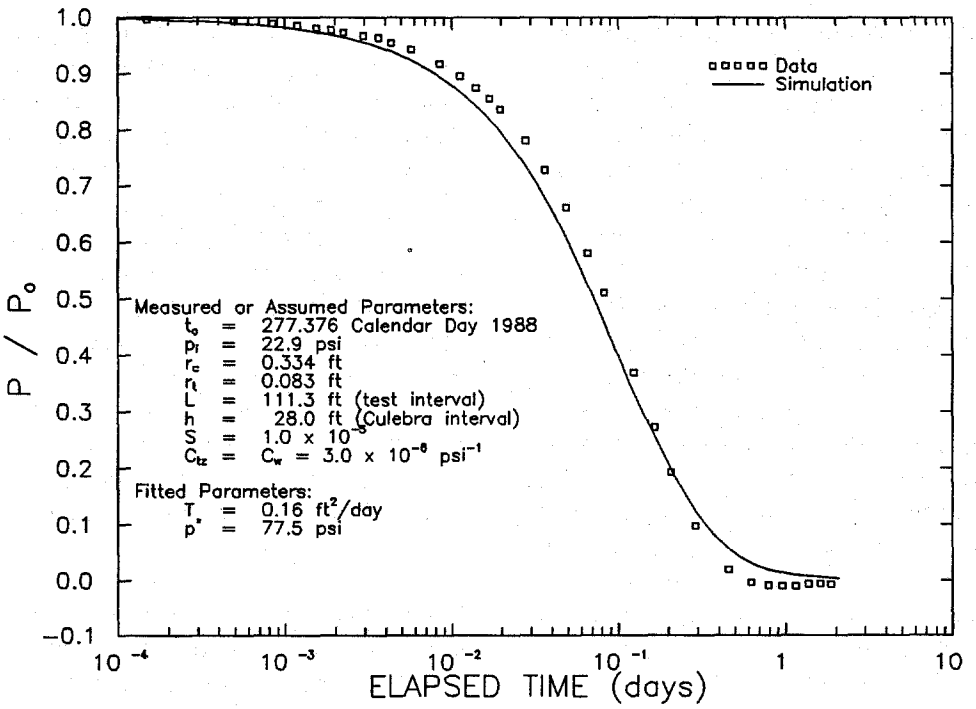


Figure 5-8 Semilog Plot of GTFM Simulation of the Slug-Withdrawal Test of the Culebra Dolomite at Well AEC-7

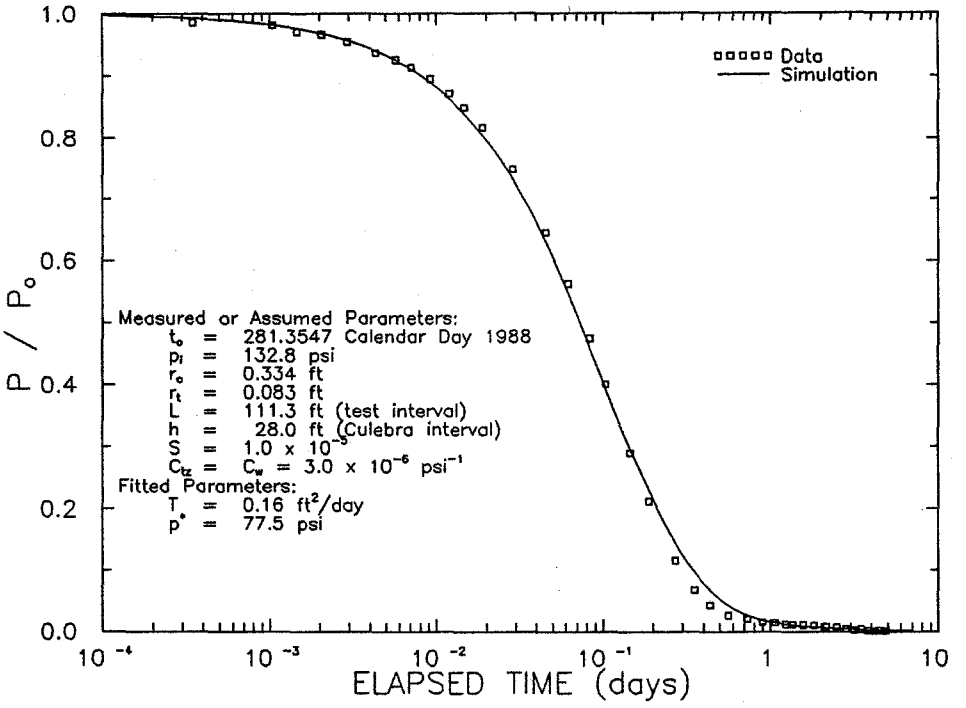


Figure 5-9 Semilog Plot of GTFM Simulation of the First Slug-Injection Test of the Culebra Dolomite at Well AEC-7

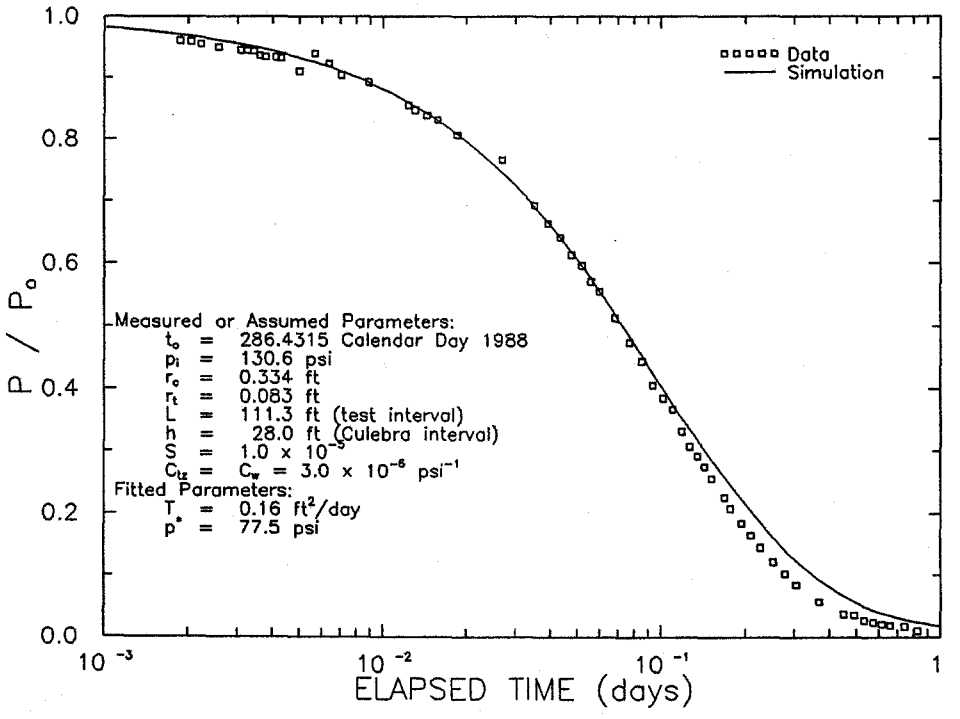


Figure 5-10 Semilog Plot of GTFM Simulation of the Second Slug-Injection Test of the Culebra Dolomite at Well AEC-7

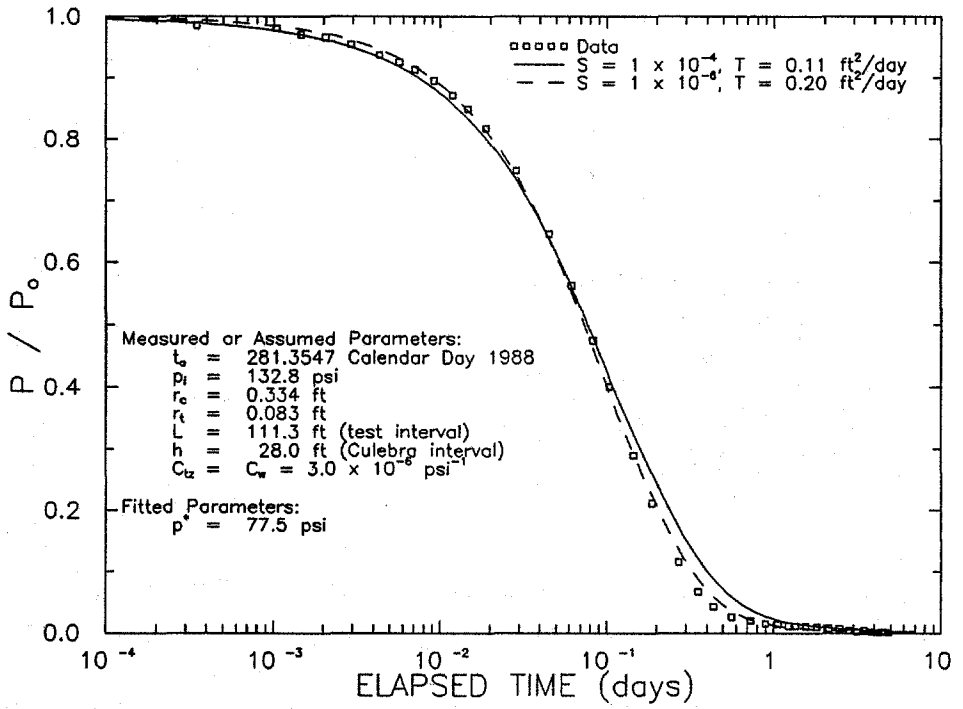


Figure 5-11 Semilog Plot of GTFM Simulations of the First Slug-Injection Test of the Culebra Dolomite at Well AEC-7 Using Different Values for Storativity

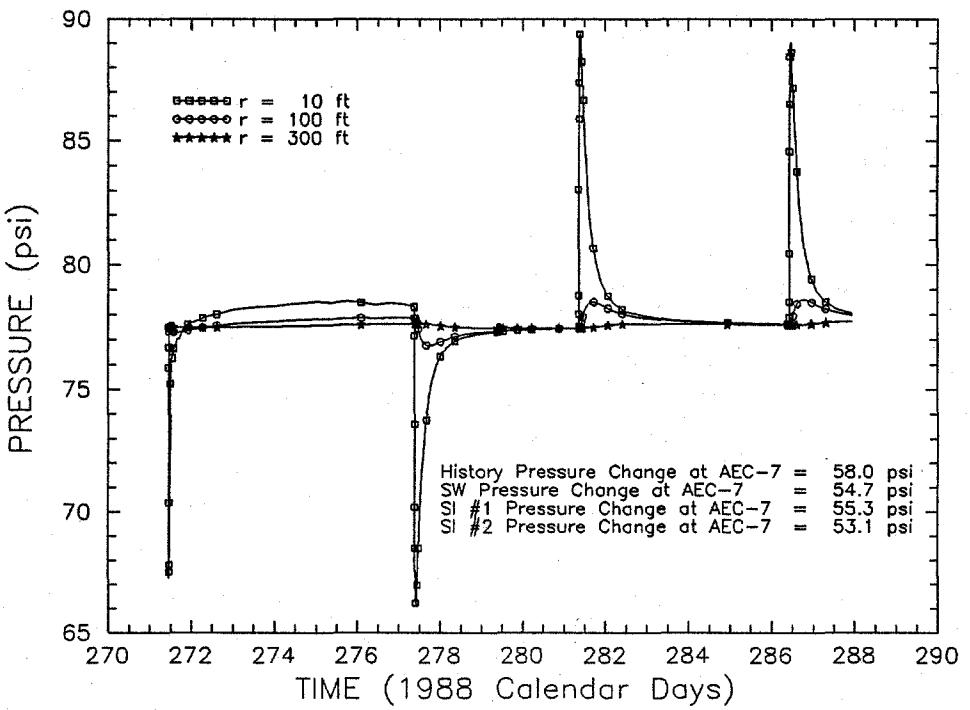


Figure 5-12 Simulated Pore Pressures at Selected Radial Distances from Well AEC-7 During the Slug Tests of the Culebra Dolomite

near static levels between successive tests at all radii examined. Additional GTFM simulations show that the maximum drawdowns occurring at radial distances of 10, 100, and 300 ft from AEC-7 assuming a storativity of $1 \times 10^{-5}$ would occur at radial distances of 4, 33, and 100 ft if the storativity were $1 \times 10^{-4}$, and at 25, 300, and 900 ft if the storativity were $1 \times 10^{-6}$.

Analyses of the slug-withdrawal test and the first slug-injection test were also performed using the same analytical type-curve-matching procedure employed by Mercer et al. (1981), Dennehy and Mercer (1982), Dennehy (1982), and Beauheim (1986, 1987c, 1989) to interpret other slug tests performed at the WIPP site. The fits between the observed data and the type curves are presented in Figures 5-13 and 5-14 for the slug-withdrawal test and the first slug-injection test, respectively. For the slug-withdrawal test, a transmissivity of 0.24 $ft^2$/day was determined. For the first slug-injection test, a transmissivity of 0.27 $ft^2$/day was determined. The transmissivities obtained using GTFM and the analytical type curves are reasonably consistent (Table 5-2). The GTFM analysis is considered more reliable, however, because it represents an integrated, consistent analysis of all three slug tests, while the type-curve solutions treat each test independently.

No indication of double-porosity behavior was evident in the hydraulic responses of the Culebra to the AEC-7 testing. Grader and Ramey (1988) showed that data from a slug test in a double-porosity medium should fit a single-porosity type curve representative of fracture properties at early time, and then deviate towards recovery more rapid than that predicted by the continuation of the curve as the matrix begins to respond. Both single-porosity GTFM simulations and single-porosity analytical solutions fit the observed data adequately, indicating either that double-porosity conditions are absent or that the permeability contrast between the fractures and matrix is too small to produce a distinguishable double-porosity response on a semilog plot. The transmissivity of the Culebra at AEC-7 is consistent with that observed at other wells on the eastern side of the WIPP site, such as H-5b (0.2 $ft^2$/day; Dennehy and Mercer, 1982) and H-15 (0.10 to 0.15 $ft^2$/day; Beauheim, 1987c).

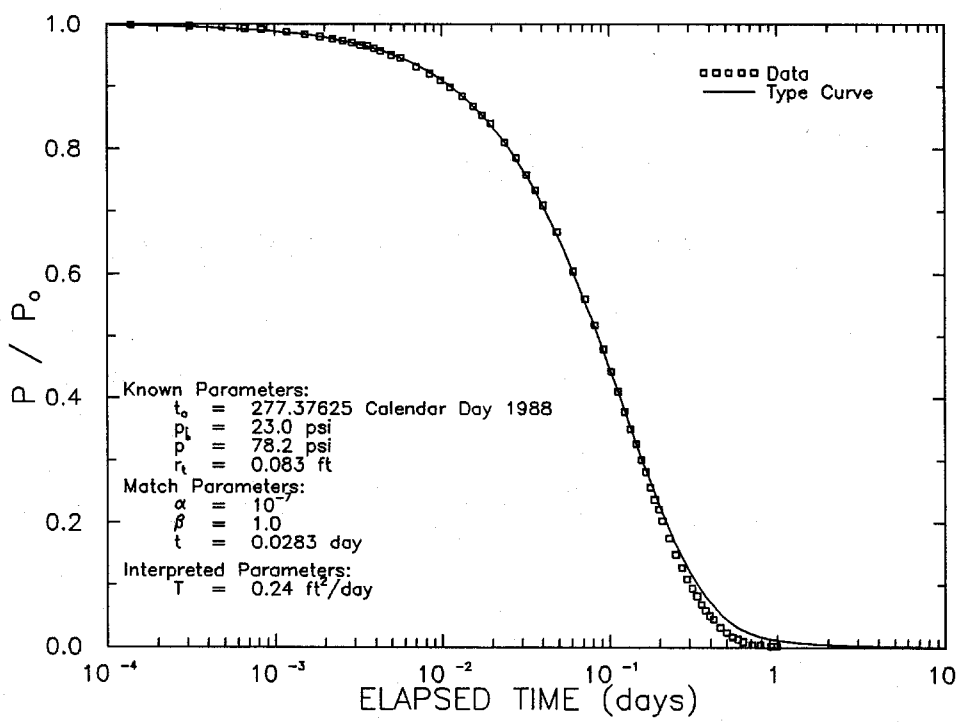


Figure 5-13 Semilog Analytical-Solution Type-Curve Match to the Slug-Wighdrawal Test of the Culebra Dolomite at Well AEC-7

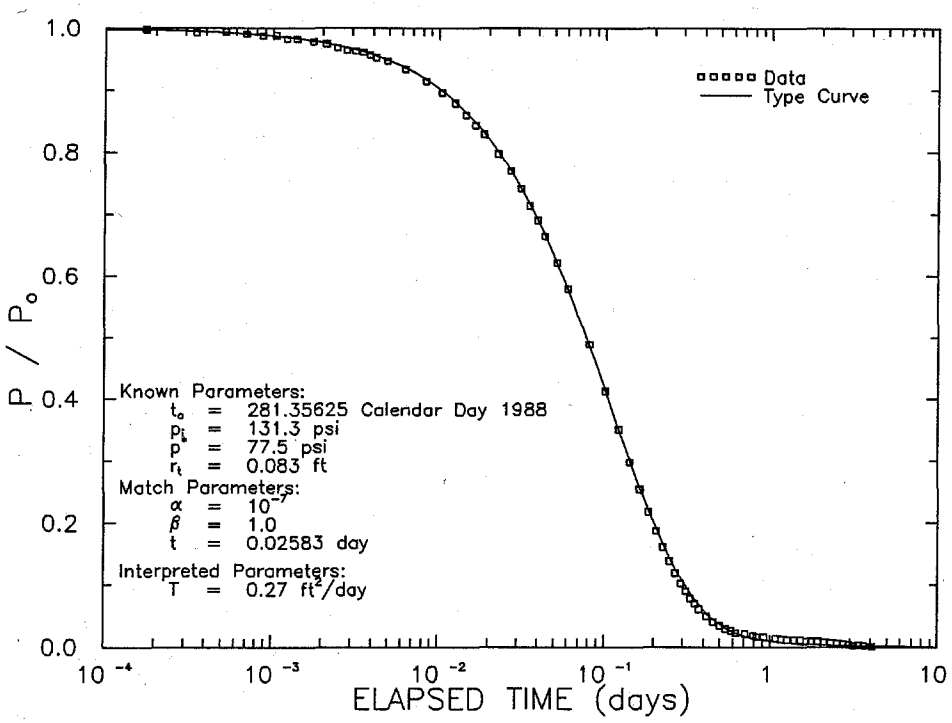


Figure 5-14 Semilog Analytical-Solution Type-Curve Match to the First Slug-Injection Test of the Culebra Dolomite at Well AEC-7

**Table 5-2**

**Comparison of Analytical and GTFM Results**

| | | | TRANSMISSIVITY ($ft^2$/day) | |
|---|---|---|---|---|
| WELL | ZONE NAME | TEST | ANALYTICAL SOLUTION | GTFM SIMULATION |
| AEC-7 | Culebra dolomite | Slug withdrawal | 0.24 | 0.16-0.20 |
| | | Slug injection #1 | 0.27 | 0.16-0.20 |
| D-268 | Culebra dolomite | Slug injection #1 | 1.9 | 1.9-2.5 |

**5.2.2 Well D-268.** Two slug-injection tests were conducted on the Culebra dolomite at well D-268 from December 7 to December 12, 1988 (Calendar Days 342 to 347). Well D-268 is cased to a depth of 528 ft. The casing is perforated between 368 and 398 ft deep to provide hydraulic connection with the Culebra, which lies between 369 and 392 ft deep (see Figure 3-2). The testing at D-268 consisted of an initial shut-in period to raise the pressure to near the static formation pressure followed by two slug-injection tests. Descriptions of the testing instrumentation and the raw test data are contained in Stensrud et al. (1990).

On day 342, well D-268 was shut-in and the pressure was allowed to build to near static formation pressure (Figure 5-15). The pressure reached 20.0 psi before the first slug-injection test started on day 343. The pressure recovered from the slug injection to 20.2 psi within one day of the start of the test. The second slug-injection test was initiated on day 344 with the pressure also recovering back to approximately static formation pressure within one day. The final pressure reading of 20.2 psi was obtained on day 347.

Figure 5-16 shows the best-fit GTFM simulation for the combined pressure-history period and the two slug-injection tests. The simulation was generated using a transmissivity of 2.0 $ft^2$/day and a static formation pressure (at the depth of the transducer) of 20.2 psi. The test data and simulation results for the two slug-injection tests are presented as semilog plots of normalized pressure versus elapsed time in Figures 5-17 and 5-18. Both linear-linear and semilog plots show reasonable comparisons between observed and simulated pressures during the two slug-injection tests. However, the simulation of the first slug test lags behind the data slightly (Figure 5-17), indicating the transmissivity should be slightly higher, whereas the simulation of the second slug test leads the data slightly (Figure 5-18), indicating the transmissivity should be slightly lower. Additional simulations show that the first slug test is best matched by a simulation using a transmissivity of 2.1 $ft^2$/day (Figure 5-17), and the second slug test is best matched using a transmissivity of 1.9 $ft^2$/day (Figure 5-18). This difference is not considered to be significant.

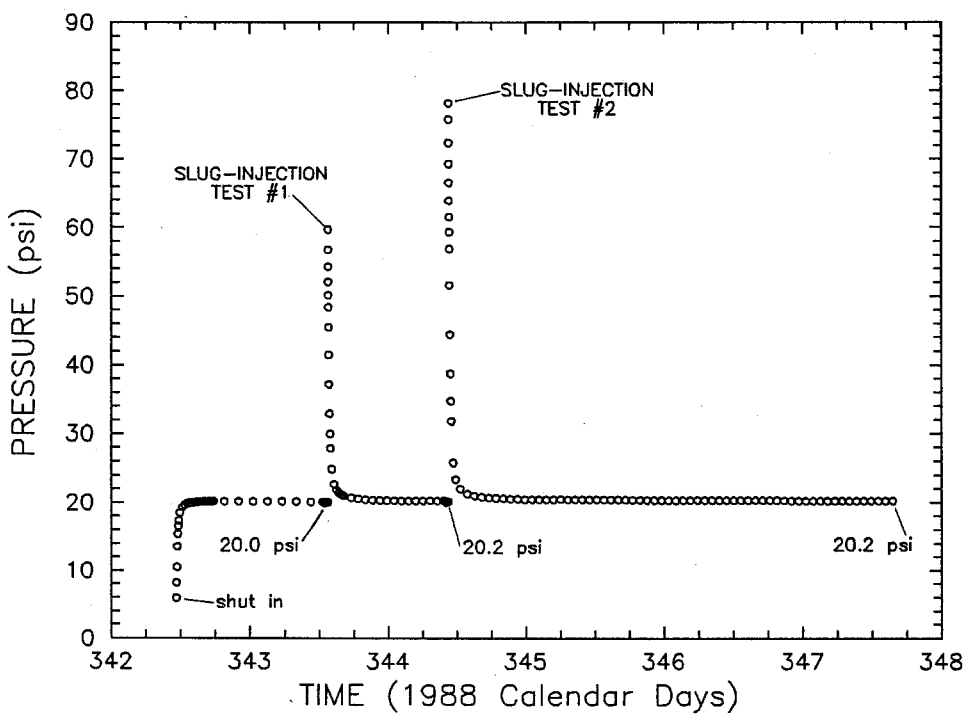


Figure 5-15 Linear-Linear Sequence Plot of Pressure Data from the Slug Tests of the Culebra Dolomite at Well D-268

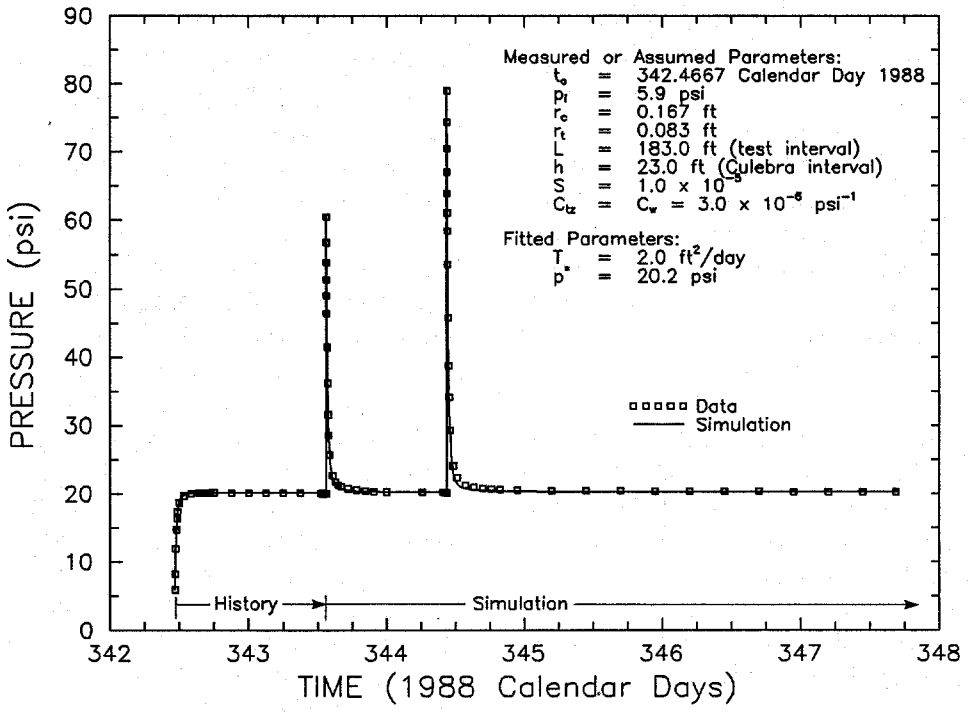


Figure 5-16 Linear-Linear Plot of GTFM Simulation of the Slug Tests of the Culebra Dolomite at Well D-268

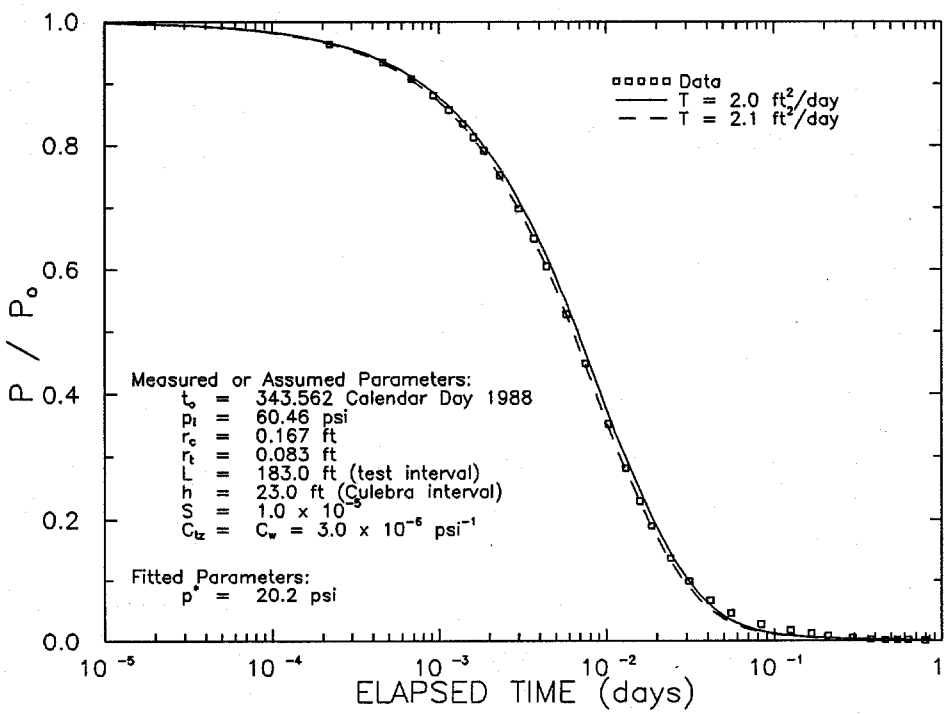


Figure 5-17 Semilog Plot of GTFM Simulations of the First Slug-Injection Test of the Culebra Dolomite at Well D-268

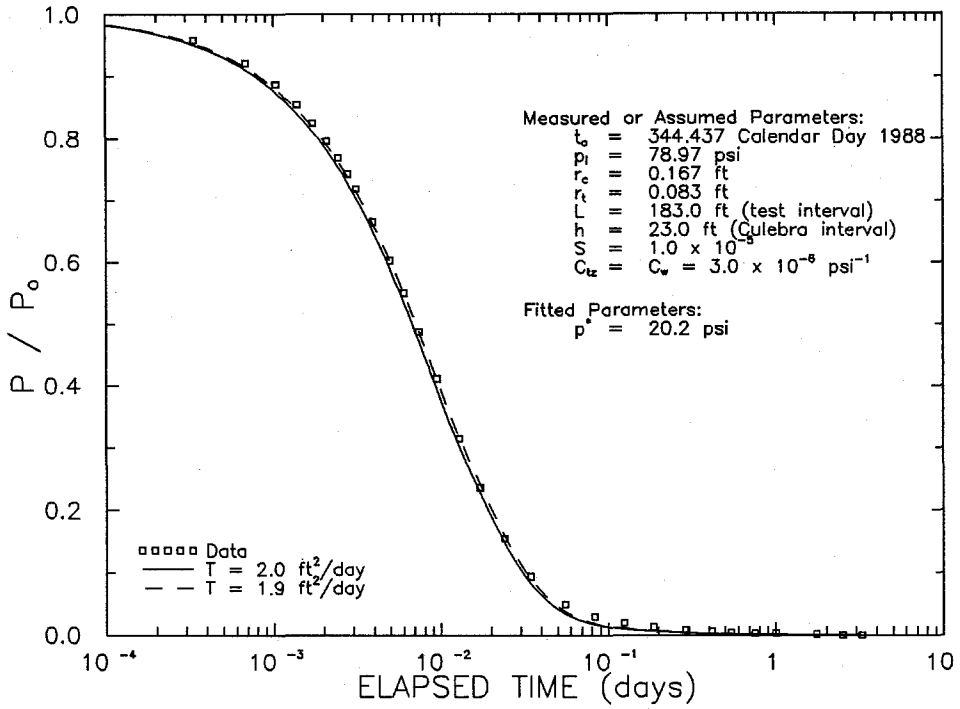


Figure 5-18 Semilog Plot of GTFM Simulations of the Second Slug-Injection Test of the Culebra Dolomite at Well D-268

To evaluate the sensitivity of the interpreted transmissivity to the assumed value of storativity of 1 x $10^{-5}$, simulations were fit to the observed data from the second slug-injection test using storativity values an order of magnitude higher and lower. These simulations are shown in semilog format in Figure 5-19. The best-fit simulation obtained assuming a storativity of 1 x $10^{-4}$ used a transmissivity of 1.4 $ft^2$/day. The best-fit simulation obtained assuming a storativity of 1 x $10^{-6}$ used a transmissivity of 2.3 $ft^2$/day. Similar results were obtained by fitting the first slug test using different values of storativity. With a storativity of 1 x $10^{-4}$, the best-fit transmissivity was 1.6 $ft^2$/day, and with a storativity of 1 x $10^{-6}$, the best-fit transmissivity was 2.5 $ft^2$/day. For both slug tests, the simulations with storativities of 1 x $10^{-6}$ and 1 x $10^{-5}$ match the observed data well over the first 80+ percent of recovery, with the 1 x $10^{-6}$ storativity perhaps providing a slightly better match. The simulations with a storativity of 1 x $10^{-4}$ fit the data the worst of the three simulations. Therefore, the storativity of the Culebra at D-268 is probably less than 1 x $10^{-5}$, and the transmissivity is probably between 1.9 and 2.5 $ft^2$/day (Table 5-1).

The propagation of the pressure transients created within the Culebra dolomite during the pretest history and testing periods was simulated by GTFM. Figure 5-20 presents the pressure responses calculated at radial distances of 10, 100, and 300 ft from D-268 assuming a storativity of 1 x $10^{-5}$. Pressure changes on the order of a few tenths of a psi are calculated to have occurred at a radial distance of 300 ft in response to the testing at D-268. The pressure recovered to near static levels between successive tests at all radii examined. Additional GTFM simulations show that the maximum drawdowns occurring at radial distances of 10, 100, and 300 ft from D-268 assuming a storativity of 1 x $10^{-5}$ would occur at radial distances of 4, 33, and 100 ft if the storativity were 1 x $10^{-4}$, and at 25, 300, and 900 ft if the storativity were 1 x $10^{-6}$.

Analysis of the first slug-injection test was also performed using an analytical type-curve-matching procedure. The fit between the observed data and the type curve is shown in Figure 5-21. A transmissivity of 1.9 $ft^2$/day was obtained from the interpretation. This transmissivity value is in excellent agreement with the values obtained from the GTFM simulations (Table 5-2).

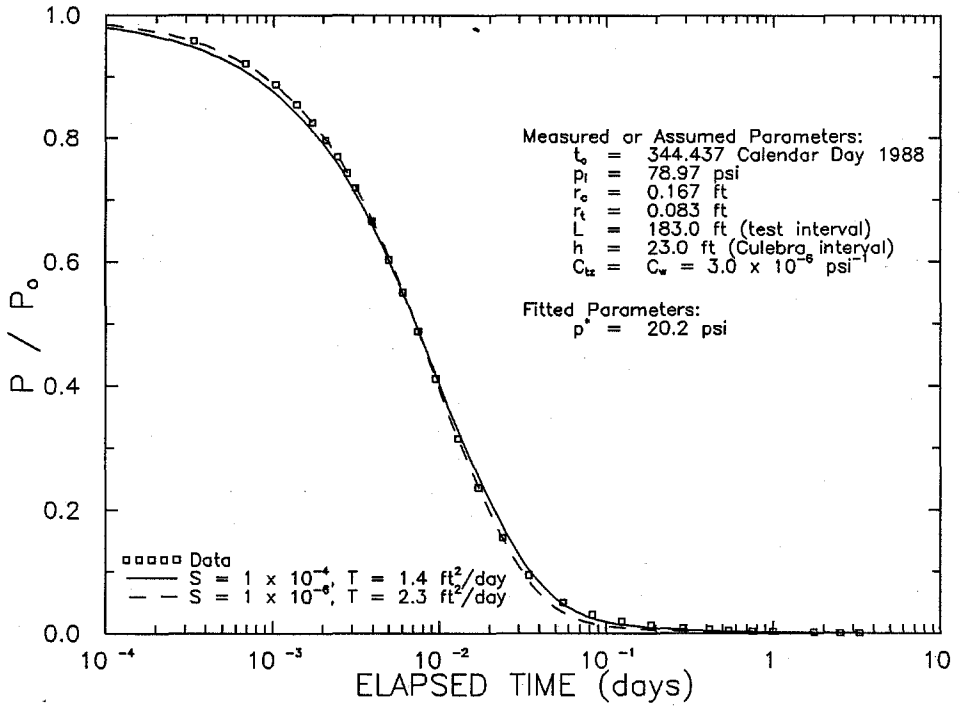


Figure 5-19 Semilog Plot of GTFM Simulations of the Second Slug-Injection Test of the Culebra Dolomite at Well D-268 Using Different Values for Storativity

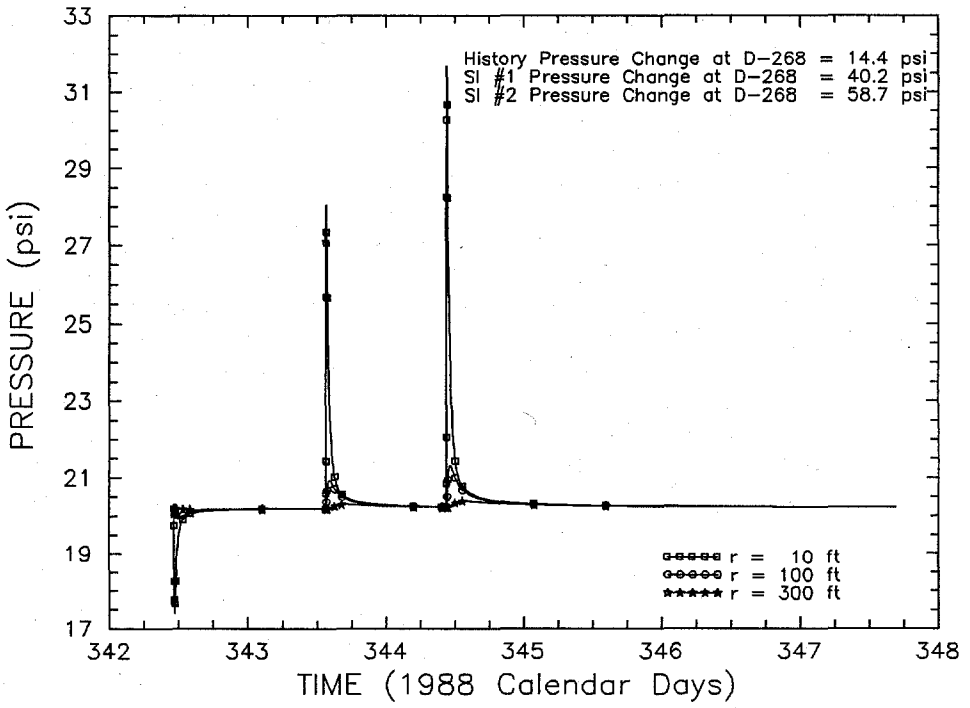


Figure 5-20 Simulated Pore Pressures at Selected Radial Distances from Well D-268 During the Slug Tests of the Culebra Dolomite

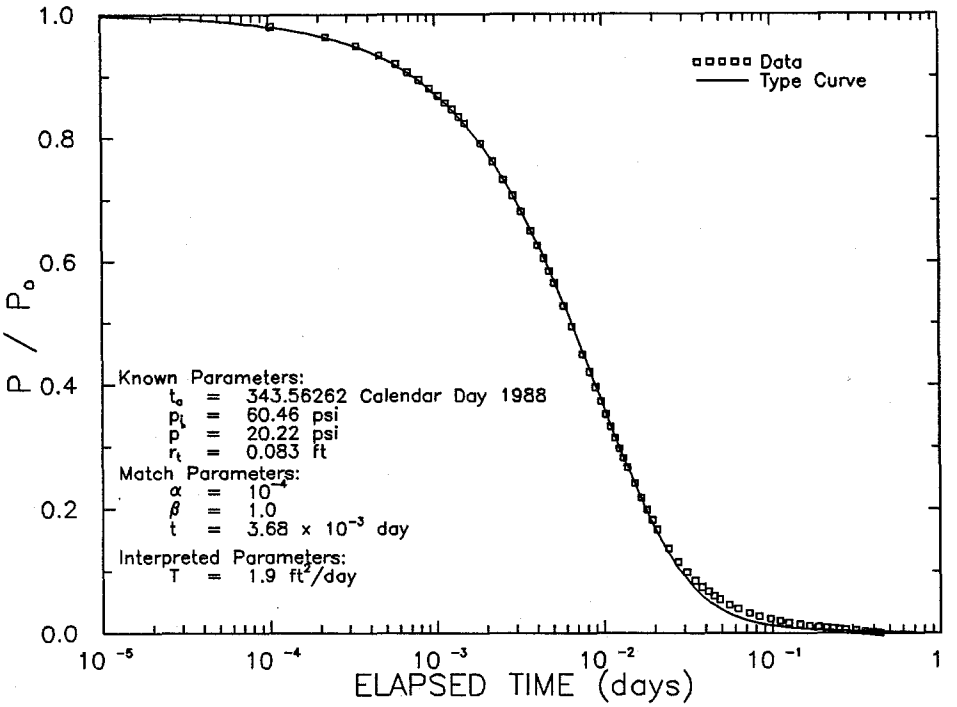


Figure 5-21 Semilog Analytical-Solution Type-Curve Match to the First Slug-Injection Test of the Culebra Dolomite at Well D-268

The slug tests did not provide any evidence that the cement lost in D-268 in 1984 (see Section 3.2) had in any way affected the transmissivity of the Culebra. If cement had partially plugged the Culebra around D-268, we should have observed hydraulic behavior typical of a relatively low transmissivity region surrounded by a relatively high transmissivity region. This could appear as either a highly positive skin on the well, or as a constant-pressure boundary near to the well. Neither of these features was needed to obtain good GTFM simulations of the tests. The analytical-solution type curve fit to the data in Figure 5-21 is also not indicative of a highly positive skin (Ramey et al., 1975). The fate of the cement lost in D-268, therefore, remains unresolved.

No indication of double-porosity behavior was evident in the hydraulic responses observed during slug testing. Both single-porosity GTFM simulations and single-porosity analytical solutions fit the observed data adequately over the entire testing period.

**5.2.3 Well H-18.** Beauheim (1987c) reported on drillstem and slug tests performed at H-18 in October 1987 that provided transmissivity estimates for the Culebra ranging from 1.7 to 2.2 $ft^2$/day. Double-porosity hydraulic behavior has been observed at the H-3 hydropad, where the transmissivity of the Culebra was reported as 1.7 to 2.9 $ft^2$/day (Beauheim, 1987a). To evaluate whether or not the Culebra behaves as a double-porosity system at H-18, a 72-hour pumping test was performed from March 11 to March 14, 1988 (Calendar Days 71 to 74). The interval open to testing was uncased and extended from 683 to 766 ft below ground surface with the Culebra located between 688.6 and 712.8 ft. Descriptions of the testing instrumentation and the raw test data are presented in Stensrud et al. (1988).

The pumping rate over the first day of the test fluctuated between 0.75 and 1.27 gpm, but it remained nearly constant over the remaining two days at about 0.95 gpm (Figure 5-22). The pump was shut off on day 74 and the pressure-recovery response was monitored for almost five days. Figure 5-23 shows the pressures observed in H-18 during the pumping and recovery periods. When pumping began, the pressure was still recovering slowly from well-development pumping performed earlier in the month (Stensrud et el., 1988). At the time the pump was turned on, the pressure was 136.05 psi. When recovery monitoring was terminated 116.5 hr after the end of pumping, the pressure was 136.94 psi and still rising at an ever-decreasing rate.

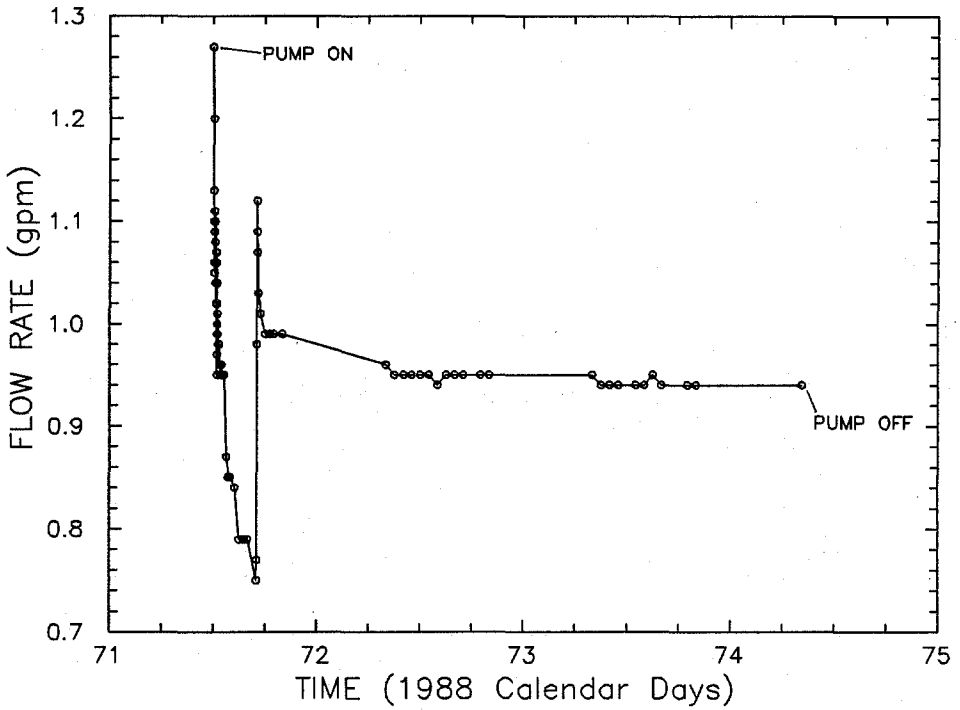


Figure 5-22 Flow Rates During the Pumping Test of the Culebra Dolomite at Well H-18

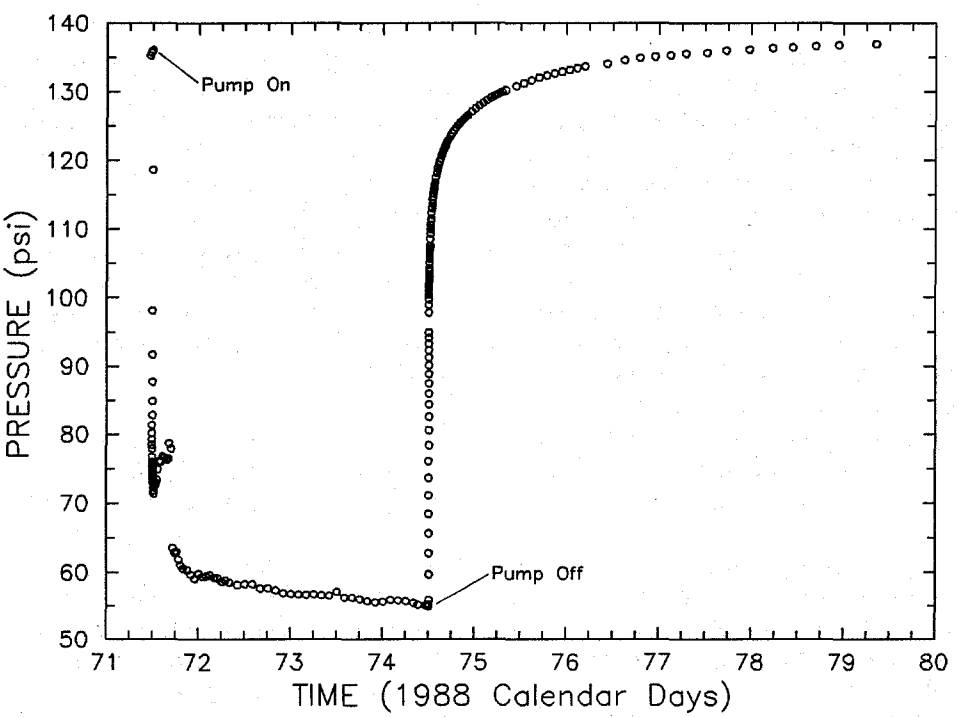


Figure 5-23 Linear-Linear Sequence Plot of Pressure Data from the Pumping Test of the Culebra Dolomite at Well H-18

The H-18 pumping test was analyzed using the Interpret/2 well-test-interpretation code. When using Interpret/2, the pressure derivative (derivative of the pressure change with respect to log time) serves as a diagnostic tool to evaluate the nature (single- or double-porosity, infinite or bounded, etc.) of the system tested (Bourdet et al., 1989). In the case of the H-18 pumping test, the pressure derivative reached a minimum value during the first hour of recovery, after which it rose and stabilized. A minimum in the pressure derivative can be caused by either double-porosity conditions or by a no-flow boundary. Accordingly, attempts were made to interpret the test using both a double-porosity model and a single-porosity model with a no-flow boundary.

The variations observed in the pumping rate during the drawdown portion of the pumping test precluded analysis of the drawdown data with Interpret/2. To maximize analytical accuracy for the recovery data, the pumping period was divided into 51 periods with different durations and pumping rates.

Figure 5-24 shows a log-log plot of the H-18 recovery data along with the best-fit Interpret/2 simulation obtained using a single-porosity model with a no-flow boundary. The observed data and the simulation are in close agreement. The simulation parameters include a transmissivity of 2.0 $ft^2$/day, a well skin factor (s) of about 3.3, a wellbore-storage coefficient (C) of 2.1 x $10^{-2}$ gal/psi, and a distance to the no-flow boundary (d) of 58 ft. The positive skin factor indicates that the well is not in perfect hydraulic communication with the Culebra.

A Horner plot is the petroleum-industry equivalent of the semilog Theis recovery plot used in groundwater hydrology (Earlougher, 1977). Horner plots show pressure recovery versus a logarithmic superposition function. The superposition function represents a superposition of responses to each individual pumping period and rate during a multirate test. A Horner plot of the H-18 recovery data and simulation is shown in Figure 5-25. As with the log-log plot (Figure 5-24), a good match between the data and simulation is evident. Extrapolation of the data to infinite recovery time (superposition function equal to zero) on the Horner plot indicates a final formation pressure of 140.0 psi.

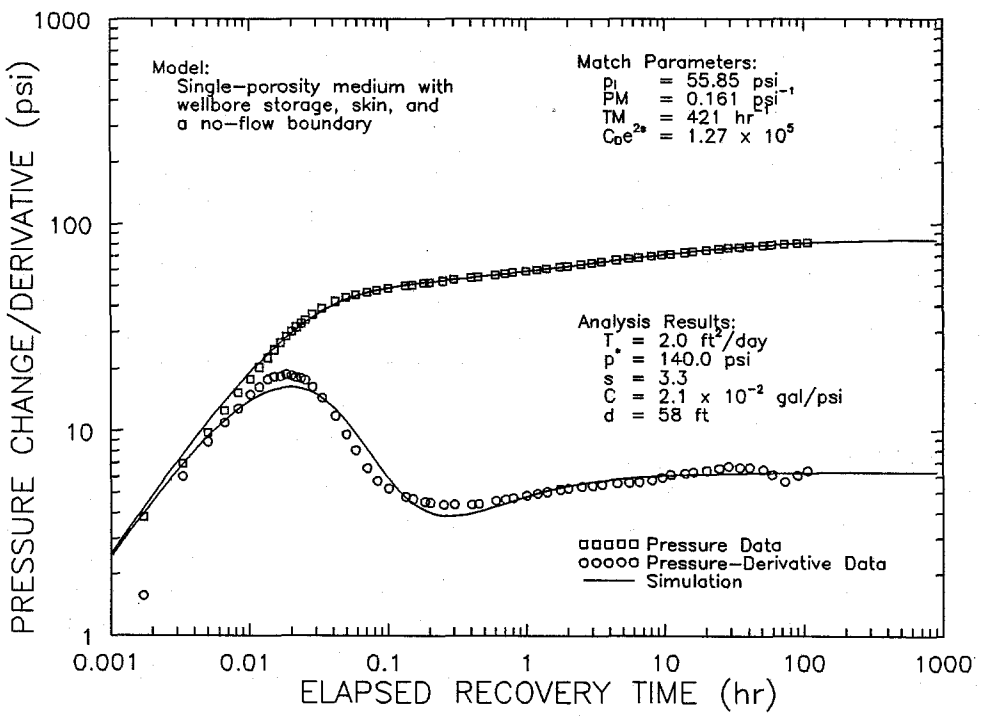


Figure 5-24 Log-Log Plot of Interpret/2 Simulation of the Recovery from the Pumping Test of the Culebra Dolomite at Well H-18 Assuming Bounded Single-Porosity Conditions

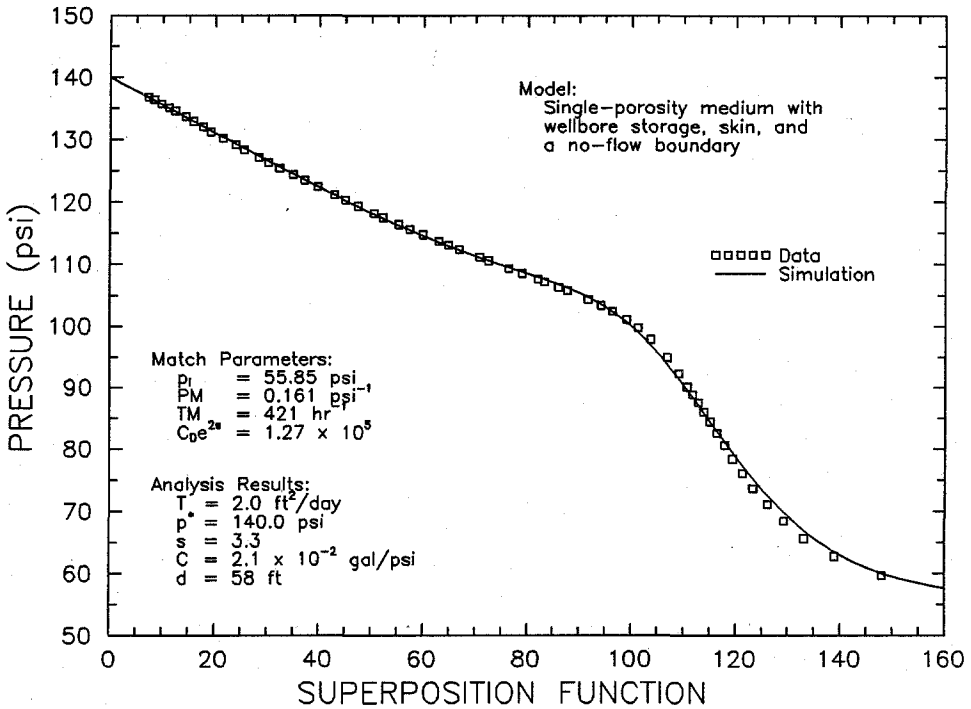


Figure 5-25 Horner Plot of Interpret/2 Simulation of the Recovery from the Pumping Test of the Culebra Dolomite at Well H-18 Assuming Bounded Single-Porosity Conditions

A formation pressure of 140.0 psi is also indicated by the linear-linear simulation of the H-18 pumping test shown in Figure 5-26. While the agreement between the simulation and the observed data is excellent throughout the recovery period, the simulation does not fit the data well during the pumping period. Two factors are likely responsible for this deviation. First, the simulation assumed that the initial pressure was stabilized at 140.0 psi rather than rising from 136.05 psi when pumping began. Consequently, the early simulated responses are offset by about 4 psi. The simulation more nearly approximates the observed data later in the pumping period (Figure 5-26) when more of the recovery from the earlier well-development pumping should have occurred. Second, the specific gravity of the fluid pumped from H-18 was not constant during the test, but instead decreased from 1.06 to 1.03 (Stensrud et al., 1988). Accordingly, pumping a unit volume of fluid from the well early in the test caused a slightly larger pressure change than the removal of a similar volume later in the test. The simulation makes no allowance for this difference.

A log-log plot of the H-18 recovery data along with the best-fit Interpret/2 simulation obtained using a double-porosity model is shown in Figure 5-27. The observed data and the double-porosity simulation are in equally good agreement as the data and the bounded single-porosity simulation (Figure 5-24). The double-porosity model used assumes unrestricted (transient) inter-porosity flow and spherical matrix blocks. The double-porosity simulation parameters include a transmissivity of 1.0 $ft^2$/day, a well skin factor (s) of about -0.9, a wellbore-storage coefficient (C) of 2.1 x $10^{-2}$ gal/psi, a storativity ratio ($\omega$) of 0.01, and an interporosity-flow coefficient ($\lambda$) of 3.1 x $10^{-5}$. The negative skin factor indicates that the well is connected to the Culebra by fractures. The storativity ratio shows that greater than 99 percent of the water produced during the test came from storage in the matrix rather than from storage in the fractures.

Horner and linear-linear plots of the data and double-porosity simulations are shown in Figures 5-28 and 5-29. Again, the double-porosity simulations fit the data as well as the bounded single-porosity simulations (Figures 5-25 and 5-26). Both the Horner and linear-linear double-porosity simulations indicate the same formation pressure of 140.0 psi as the bounded single-porosity simulations.

Neither the bounded single-porosity simulation nor the double-porosity simulation appear to match the H-18 pumping-test data appreciably better than the other. The transmissivity derived from the bounded single-porosity simulation, 2.0 $ft^2$/day, agrees more closely

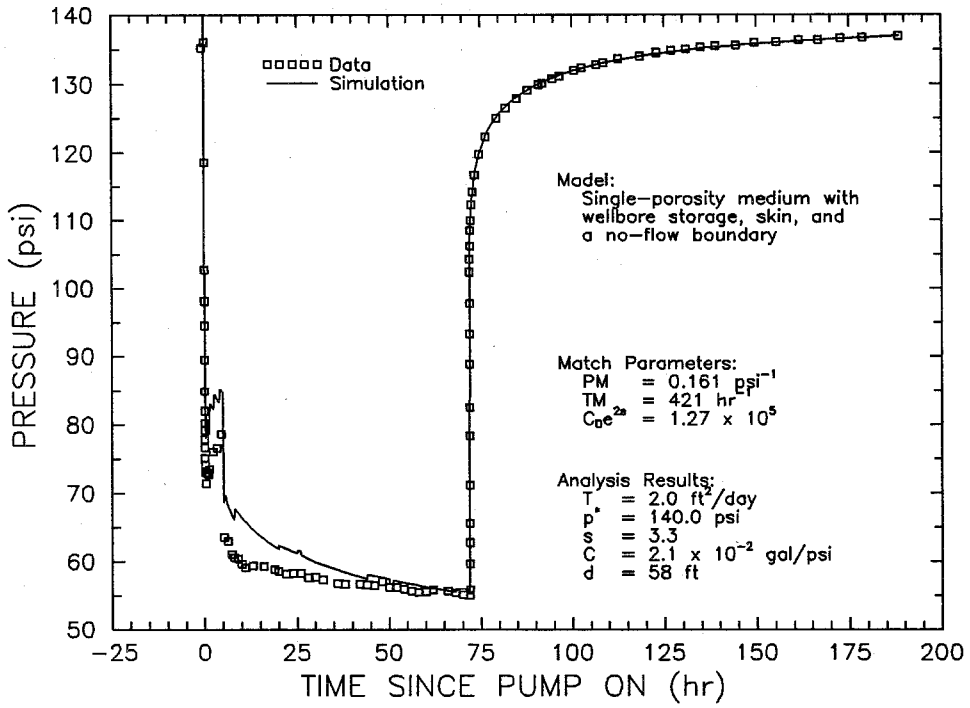


Figure 5-26 Linear-Linear Plot of Interpret/2 Simulation of the Pumping Test of the Culebra Dolomite at Well H-18 Assuming Bounded Single-Porosity Conditions

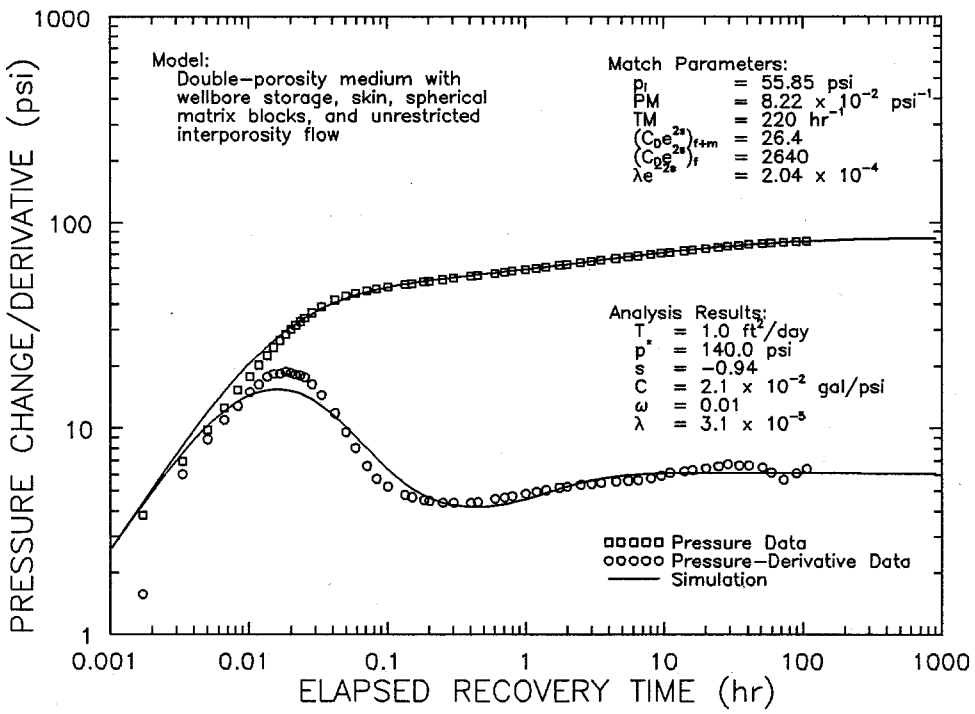


Figure 5-27 Log-Log Plot of Interpret/2 Simulation of the Recovery from the Pumping Test of the Culebra Dolomite at Well H-18 Assuming Double-Porosity Conditions

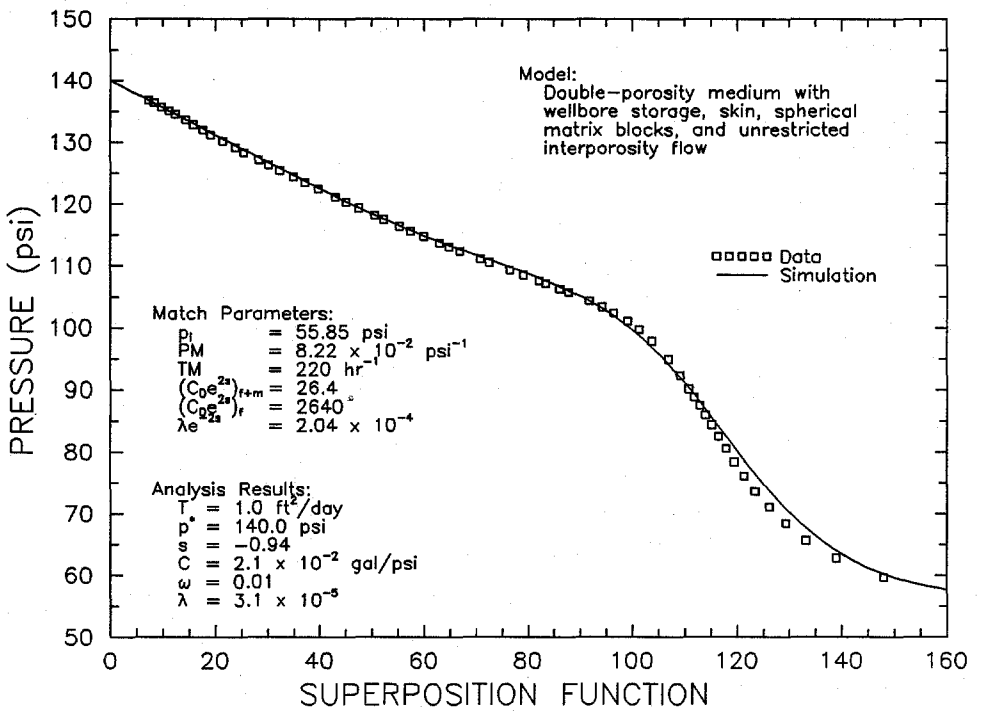


Figure 5-28 Horner Plot of Interpret/2 Simulation of the Recovery from the Pumping Test of the Culebra Dolomite at Well H-18 Assuming Double-Porosity Conditions

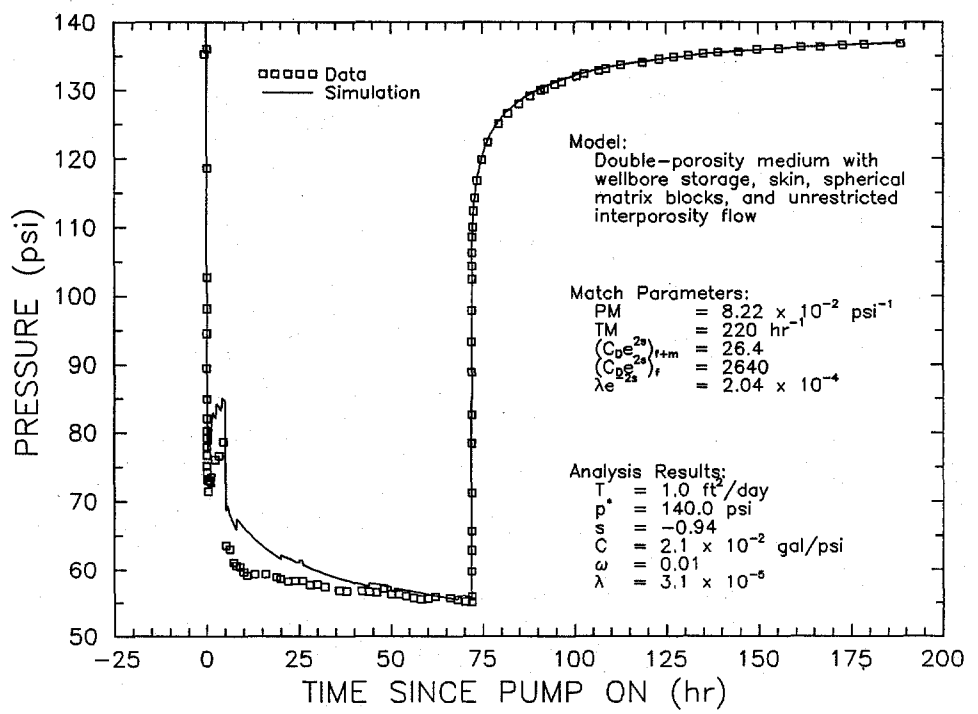


Figure 5-29 Linear-Linear Plot of Interpret/2 Simulation of the Pumping Test of the Culebra Dolomite at Well H-18 Assuming Double-Porosity Conditions

with the transmissivity values reported by Beauheim (1987c), but the interpretation of a no-flow boundary only 58 ft from H-18 is problematic. No geologic reason for the existence of such a boundary in the vicinity of H-18 is known. H-18 lies in a region where weak double-porosity hydraulic behavior might be expected. Clear indications of double-porosity conditions have been observed to the north and northeast of H-18 at WIPP-13 (Beauheim, 1987b) and DOE-2 (Beauheim, 1986), whereas only single-porosity behavior is observed south and east of H-18 at wells such as H-16 and WIPP-12 (Beauheim, 1987c). The match between the observed H-18 recovery data and the double-porosity simulation cannot, however, be considered definitive.

The only conclusion that can be drawn from the H-18 pumping test is that the Culebra has a transmissivity between 1.0 and 2.0 $ft^2$/day at that location (Table 5-1). Fractures were observed in the Culebra core from H-18, but they were largely filled with selenite (Mercer and Snyder, 1990b) and appear to have little effect on hydraulic behavior. Single- and double-porosity models fit the observed test responses equally well. Whether or not a no-flow boundary exists in the Culebra near H-18 remains unresolved.

## 5.3 Magenta Dolomite Member

The Magenta Dolomite Member of the Rustler Formation was tested in wells H-2b1 and H-3b1. The objective of testing the Magenta was to confirm earlier estimations of transmissivity made by the USGS at the H-2 and H-3 hydropads (Mercer, 1983) that lacked complete documentation. For the test interpretations, the Magenta was initially assumed to have a storativity of $1.0 \times 10^{-5}$ in order to maintain consistency with previous work reported by Avis and Saulnier (1990).

**5.3.1 Well H-2b1.** Mercer (1983) reported a transmissivity for the Magenta dolomite at well H-2a, 50 ft from well H-2b1, of 0.01 $ft^2$/day. To confirm this value, hydraulic testing of the Magenta was performed at H-2b1 from April 25 to July 13, 1989 (Calendar Days 115 to 194). The casing is perforated from 510 to 538 ft below ground surface to provide hydraulic communication with the Magenta, which lies between 515 and 540 ft deep (Figure 3-3). The lower 2 ft of the Magenta are not, therefore, directly connected to the well.

The testing at well H-2b1 consisted of a slug-withdrawal test, a pulse-injection test, and a slug-injection test. On day 115, the tubing attached to the PIP set above the Magenta (Figure 3-3) was bailed to create a low-pressure condition in the well. A minipacker was installed in the tubing below the lowered water level, and inflated to allow the pressure beneath to build up to near static formation pressure before the slug-withdrawal test began. The slug-withdrawal test was started on day 121 by deflating the minipacker, and continued until day 132, when the well was shut-in. At that time, the pressure had recovered approximately 80 percent of the slug-induced differential. The remainder of the differential was recovered over the next 12 days while the well was shut-in. On day 144, water was added to the tubing and the minipacker was deflated briefly to initiate the pulse-injection test. After six days of recovery from the pulse injection, a slug-injection test was initiated on day 150 by deflating the minipacker and removing it from the well. The pressure-versus-time data measured using a microcomputer-controlled data-acquisition system for the slug-withdrawal and pulse-injection tests are presented in Figure 5-30. The depth-to-water-versus-time data measured using a water-level sounder for the slug-injection test are presented in Figure 5-31. Descriptions of the test instrumentation and the raw data are contained in Stensrud et al. (1990).

The continued presence of transient pressure conditions caused by the pretest well-reconfiguration and development activities is apparent in the data shown in Figure 5-30. During the initial pretest shut-in period, the pressure recovered to a high of 97.7 psi before declining to a pressure of 96.9 psi before the start of the slug-withdrawal test. The pressure at the start of the pulse-injection test was 94.5 psi. During the pulse-injection test, the pressure recovered to a low of 93.0 psi before increasing to a pressure of 94.4 psi at the start of the slug-injection test. Thus, the pressure was never fully stabilized before any of the individual tests were initiated.

The pressure data from the slug-withdrawal test, the shut-in period, and the pulse-injection test were combined in a single simulation for analysis. The pretest pressure buildup from day 115 through day 121 was also included in the simulation as specified pressure history. Figure 5-32 shows the best-fit GTFM simulation for the combined test data. The best-fit simulation was generated using a transmissivity of $2.6 \times 10^{-3}$ $ft^2$/day and a static formation pressure (at the depth of the transducer) of 96.0 psi. The static formation pressure of 96.0 psi is a best-fit estimate for the combined test sequence of slug-withdrawal test, shut-in period, and pulse-injection test.

The GTFM simulation shown in Figure 5-32 was selected as the best fit that could be obtained for the slug-withdrawal portion of the test data. The simulation did not compare as well with the data collected during the shut-in period, or with the data

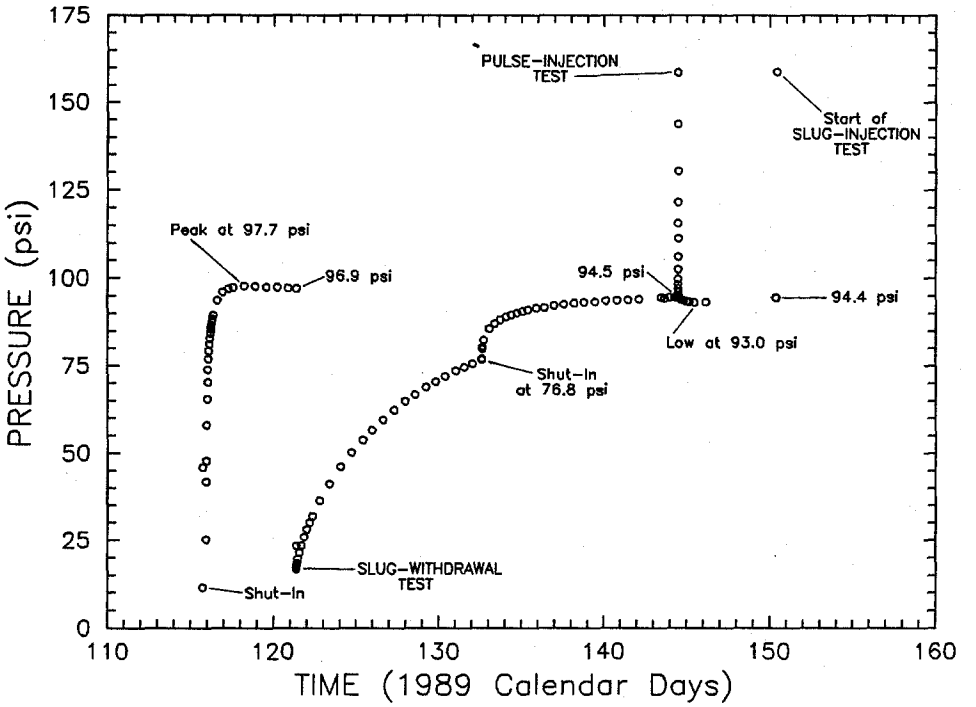


Figure 5-30 Linear-Linear Sequence Plot of Pressure Data from the Slug-Withdrawal and Pulse-Injection Tests of the Magenta Dolomite at Well H-2b1

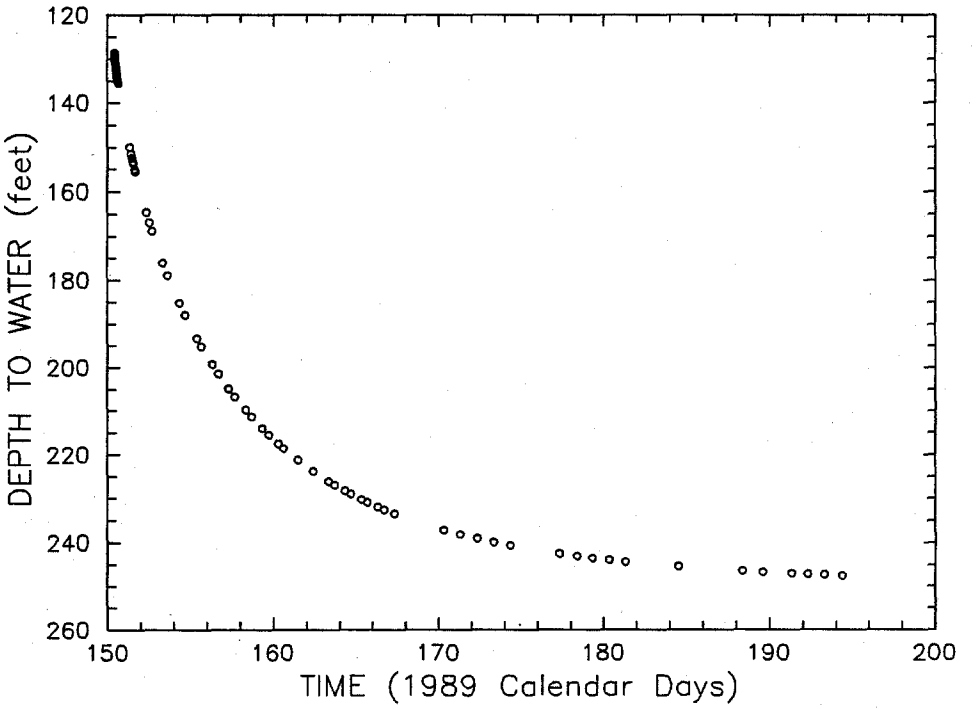


Figure 5-31 Linear-Linear Sequence Plot of Water-Level Data from the Slug-Injection Test of the Magenta Dolomite at Well H-2b1

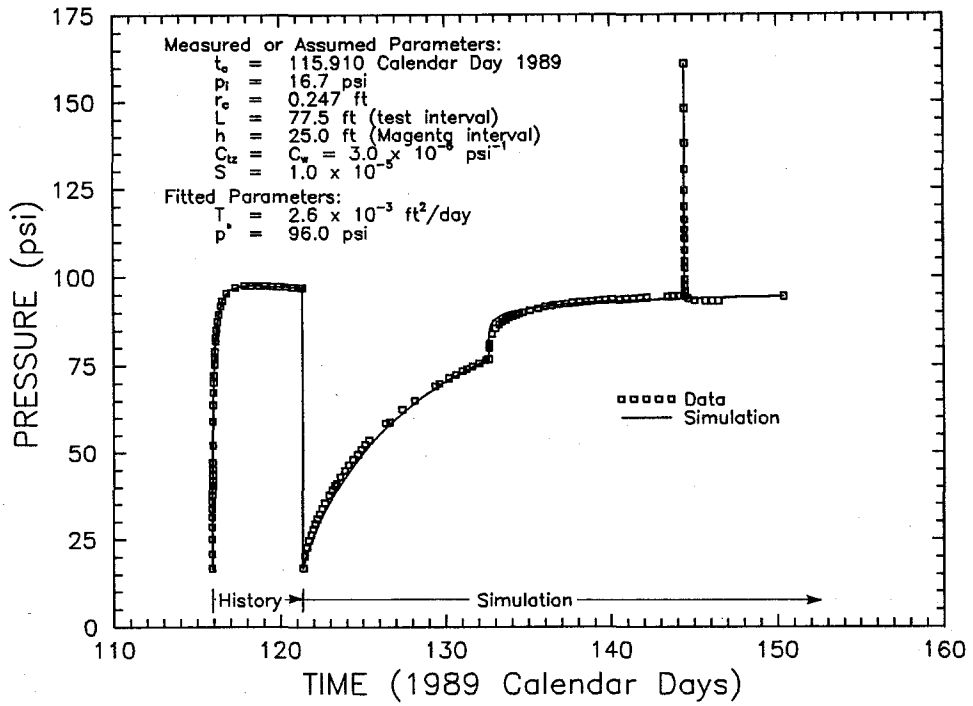


Figure 5-32 Linear-Linear Plot of GTFM Simulation of the Slug-Withdrawal and Pulse-Injection Tests of the Magenta Dolomite at Well H-2b1

from the pulse-injection test. A semilog plot of the slug-withdrawal data (normalized pressure versus elapsed time) and the GTFM simulation is presented in Figure 5-33. The simulation and the measured data compare well on the figure. Figure 5-34 shows a semilog plot of normalized pressure during the pulse-injection test versus elapsed time with the GTFM simulation. The simulation approximates the observed data reasonably well after the first one or two minutes of the test.

The slug-injection test was initiated by deflating the minipacker in the tubing, allowing communication between the water in the tubing and the Magenta. The minipacker was then removed from the tubing, and water levels were measured with an electric water-level sounder for the duration of the test. The first water-level measurement was not made until 20 minutes after the minipacker had been deflated. Therefore, the water level at the start of the test had to be estimated. Based on the water-level change observed over the second 20 minutes of the test, the initial water level was estimated to be about 128 ft.

Figure 5-35 shows the best-fit GTFM simulation of the slug-injection test conducted at H-2b1. The best-fit simulation was generated using a transmissivity of 2.7 x $10^{-3}$ $ft^2$/day and a static water level located at 251.0 ft. Figure 5-36 shows a semilog plot of normalized head versus elapsed time for the data and simulation. The simulation is in excellent agreement with the observed data when plotted in both linear-linear and semilog format. The initial-water-level estimate of 128 ft appears to be reasonably accurate.

The sensitivity of the interpreted transmissivity to the assumed value of storativity of 1 x $10^{-5}$ was evaluated by fitting simulations of the observed data from the slug-injection test using storativity values an order of magnitude higher and lower. A semilog plot of these simulations is shown in Figure 5-37. The best-fit simulation obtained assuming a storativity of 1 x $10^{-4}$ used a transmissivity of 2.1 x $10^{-3}$ $ft^2$/day. The best-fit simulation obtained assuming a storativity of 1 x $10^{-6}$ used a transmissivity of 3.3 x $10^{-3}$ $ft^2$/day. The simulation assuming a storativity of 1 x $10^{-4}$ fits the observed data better than either of the other two simulations until about the last 20 percent of recovery, when the simulation with the base-case value of storativity fits the data best. The simulation with the lower value of storativity provides the worst overall match to the observed data. Thus, the actual storativity of the Magenta dolomite around H-2b1 probably lies between 1 x $10^{-4}$ and 1 x $10^{-5}$, while the transmissivity is between 2.1 x $10^{-3}$ and 2.7 x $10^{-3}$ $ft^2$/day (Table 5-1).

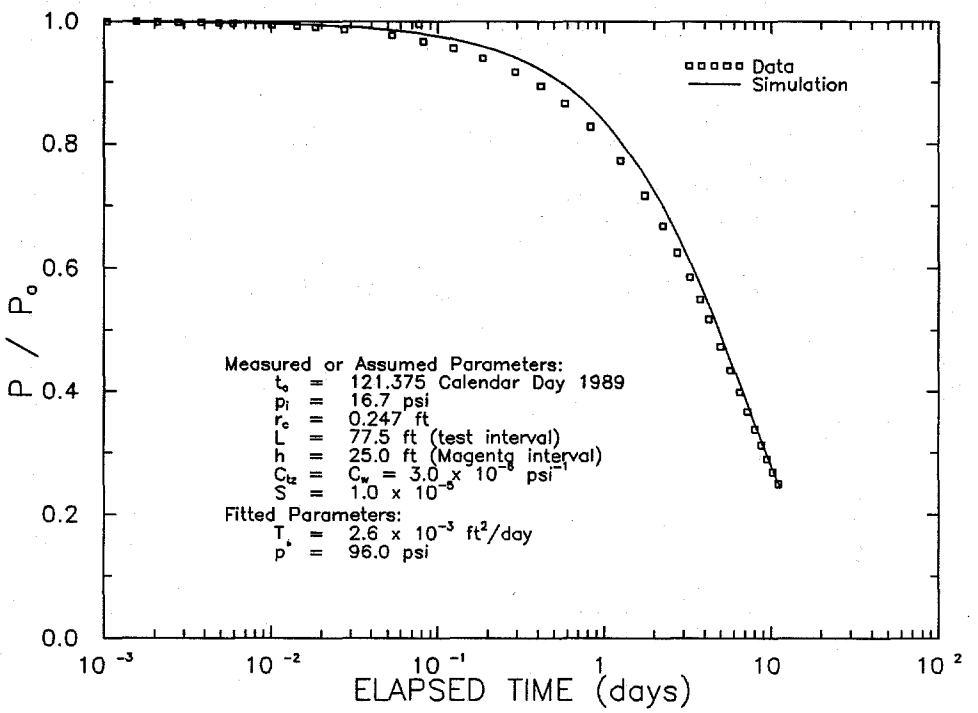


Figure 5-33 Semilog Plot of GTFM Simulation of the Slug-Withdrawal Test of the Magenta Dolomite at Well H-2b1

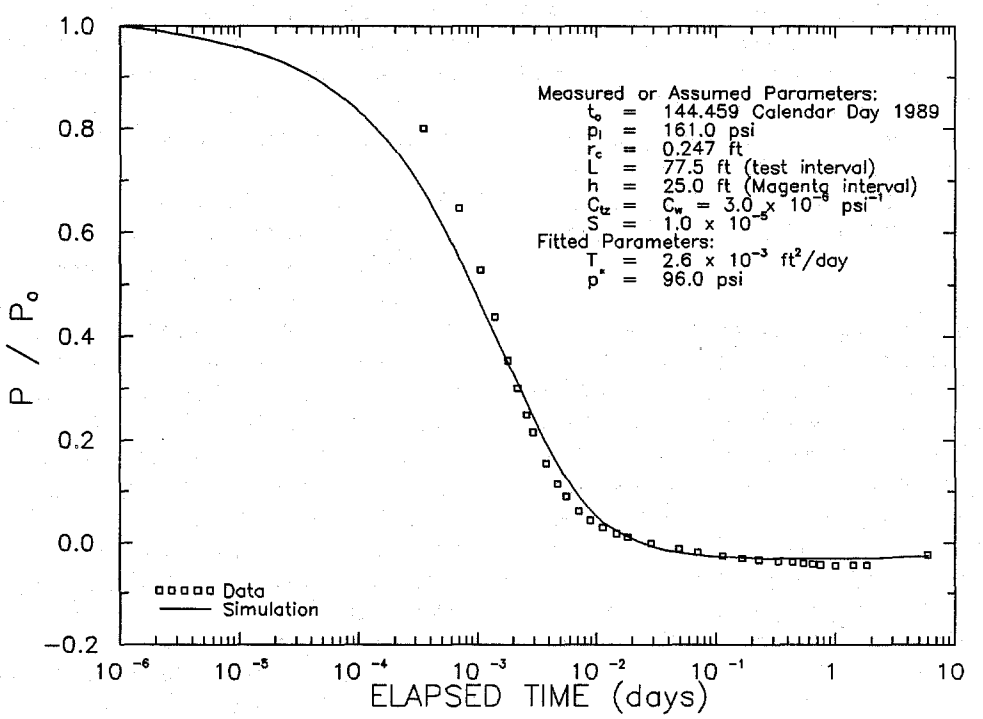


Figure 5-34 Semilog Plot of GTFM Simulation of the Pulse-Injection Test of the Magenta Dolomite at Well H-2b1

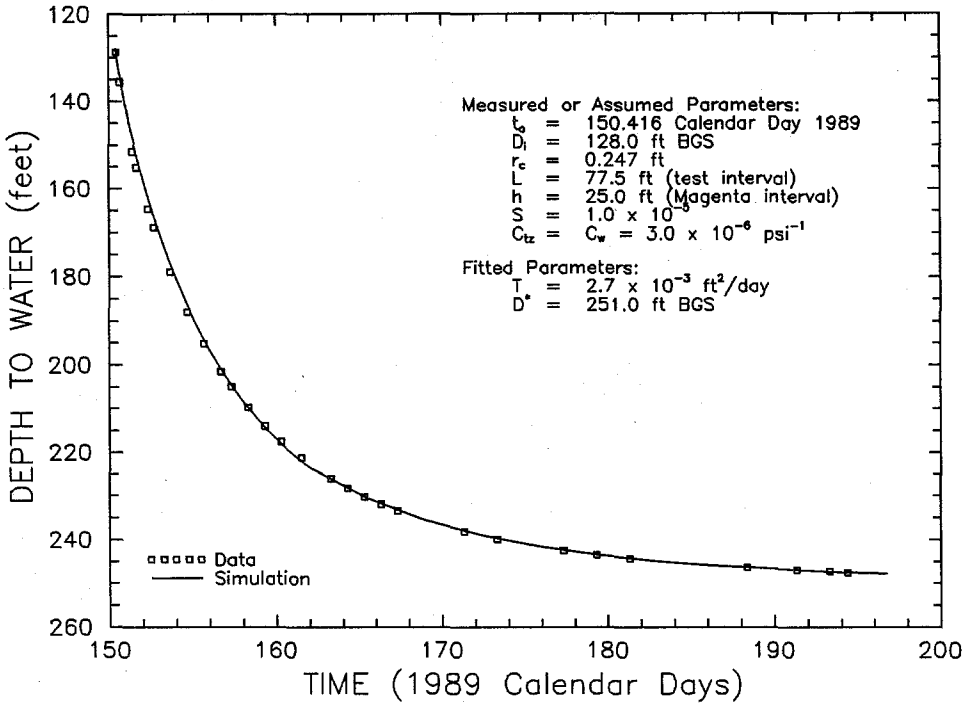


Figure 5-35 Linear-Linear Plot of GTFM Simulation of the Slug-Injection Test of the Magenta Dolomite at Well H-2b1

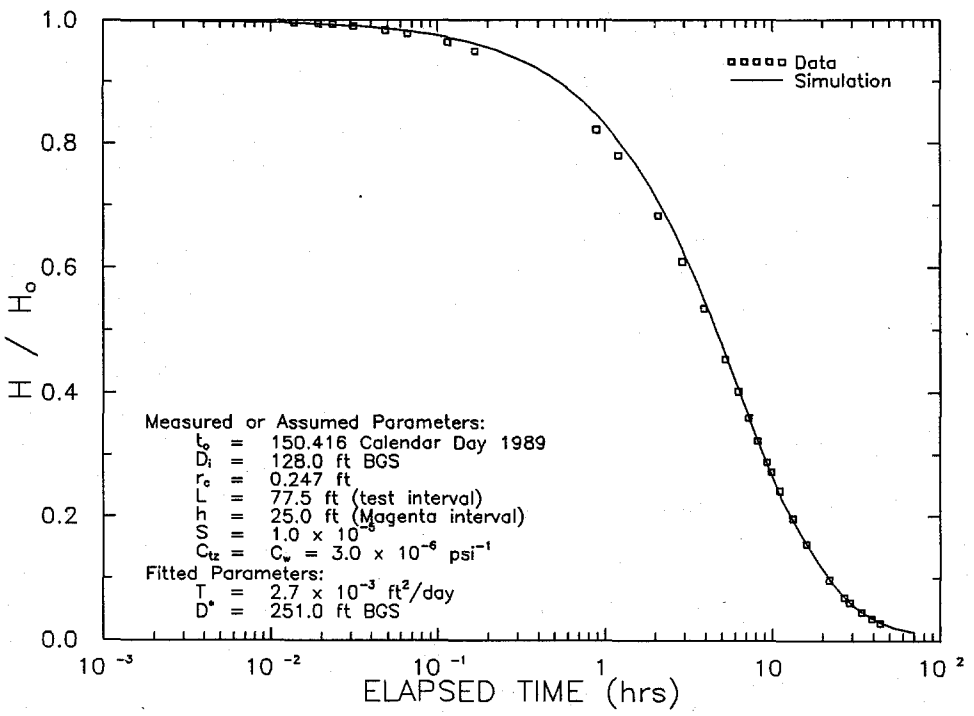


Figure 5-36 Semilog Plot of GTFM Simulation of the Slug-Injection Test of the Magenta Dolomite at Well H-2b1

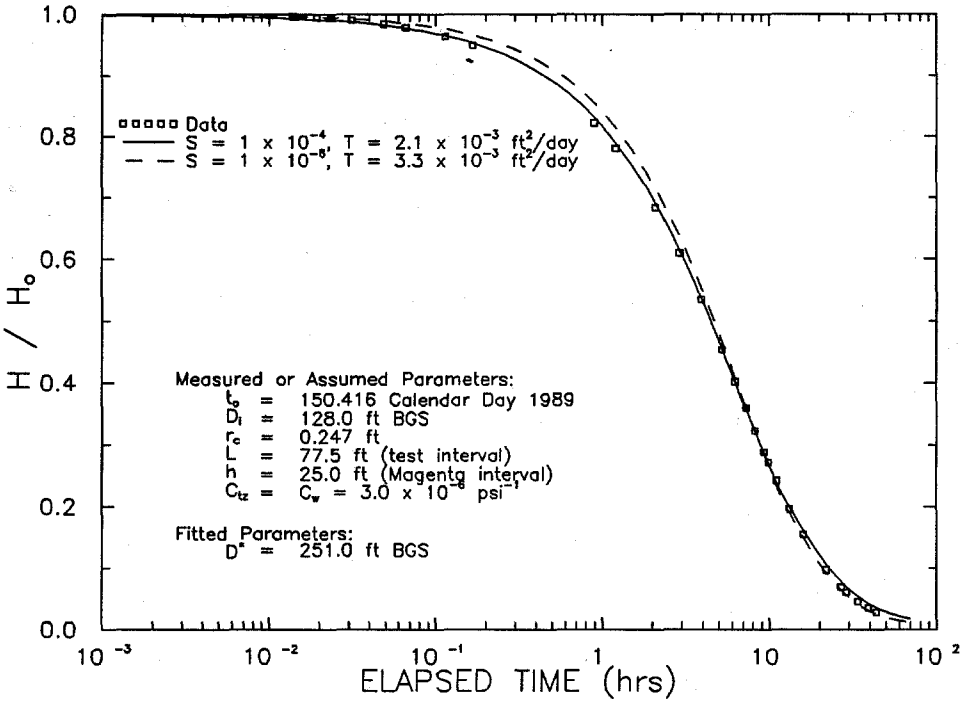


Figure 5-37 Semilog Plot of GTFM Simulations of the Slug-Injection Test of the Magenta Dolomite at Well H-2b1 Using Different Values for Storativity

The propagation of the pressure transients created within the Magenta dolomite during the testing periods was simulated by GTFM. The calculated pressure responses to the pretest history period, slug-withdrawal test, buildup period, and pulse-injection test at radii of 1, 10, and 100 ft from H-2b1 assuming a storativity of $1 \times 10^{-5}$ are shown in Figure 5-38. Pressure changes on the order of 1 psi are calculated to have occurred at a radial distance of 100 ft in response to the testing at H-2b1. The pressure recovered to within about 2 psi of the static level between successive tests at all radii examined. The calculated hydraulic-head responses to the slug-injection test at radii of 1, 10, 100, and 200 ft from H-2b1, again assuming a storativity of $1 \times 10^{-5}$, are shown in Figure 5-39. The maximum hydraulic-head change at a radial distance of 200 ft was about 0.7 ft (about 0.3 psi). Additional GTFM simulations show that the maximum head changes occurring at radial distances of 1, 10, 100, and 200 ft from H-2b1 during the slug-injection test assuming a storativity of $1 \times 10^{-5}$ would occur at radial distances of 0.65, 4.1, 33, and 60 ft if the storativity were $1 \times 10^{-4}$, and at 1.5, 25, 300, and 600 ft if the storativity were $1 \times 10^{-6}$.

In summary, interpretation of the slug and pulse tests at H-2b1 indicates that the transmissivity of the Magenta is between $2.1 \times 10^{-3}$ and $2.7 \times 10^{-3}$ ft$^2$/day. These estimates are a factor of four to five lower than the $1 \times 10^{-2}$ ft$^2$/day reported by Mercer (1983) from testing performed at well H-2a. The difference in the transmissivity estimates from H-2b1 and H-2a could be caused by heterogeneity within the Magenta, or by analytical uncertainty with respect to the interpretation of the H-2a test(s).

**5.3.2 Well H-3b1.** Mercer (1983) reported a transmissivity for the Magenta dolomite at well H-3 (now H-3b1) of 0.1 ft$^2$/day. To confirm this value, the Magenta dolomite was tested at well H-3b1 from July 17 to August 4, 1989 (Calendar Days 198 to 216). At H-3b1, the Magenta dolomite lies between 560 and 584 ft below ground surface. The well is hydraulically connected to the Magenta through casing perforations from 564 to 592 ft deep. The upper 4 ft of the Magenta are not, therefore, directly connected to the well. Descriptions of the testing instrumentation and the raw test data are given in Stensrud et al. (1990).

The testing at well H-3b1 consisted of a pulse-withdrawal test, a slug-withdrawal test, and a slug-injection test. On day 198, the tubing attached to the PIP set above the Magenta (Figure 3-4) was bailed to create a low-pressure condition in the well. A mini-

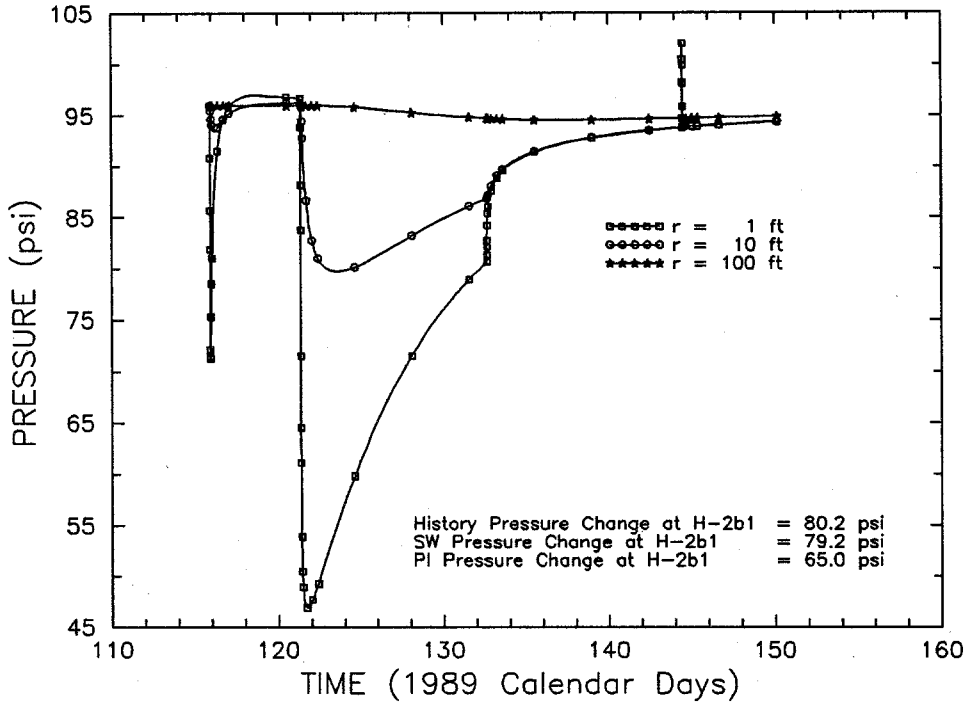


Figure 5-38 Simulated Pore Pressures at Selected Radial Distances from Well H-2b1 During the Slug-Withdrawal and Pulse-Injection Tests of the Magenta Dolomite

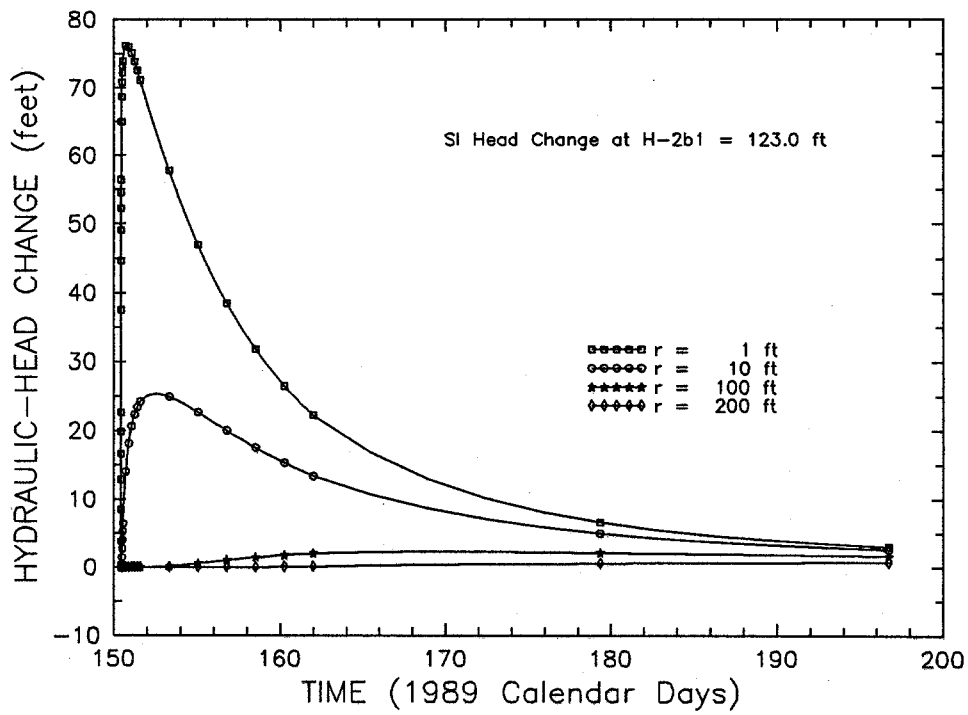


Figure 5-39 Simulated Hydraulic-Head Changes at Selected Radial Distances from Well H-2b1 During the Slug-Injection Test of the Magenta Dolomite

packer was installed in the tubing below the lowered water level, and inflated to allow the pressure beneath to build up to near static formation pressure before the pulse-withdrawal test began (Figure 5-40). When the minipacker was briefly deflated on day 200 to start the pulse-withdrawal test, the pressure had recovered to 117.4 psi. Five days after the initiation of the pulse-withdrawal test, the pressure stabilized at 118.1 psi. The slug-withdrawal test was initiated on day 205 by deflating the minipacker. The well was shut-in at a pressure of 117.9 psi after approximately four days (day 209) of recovery. Over the next four days, the pressure stabilized at about 118.0 psi. Water was added to the tubing above the minipacker, and the minipacker was deflated to initiate a slug-injection test on day 213. The slug-injection test lasted for approximately three days, with a final pressure reading of 118.4 psi measured on day 216.

The initial shut-in response before the pulse-withdrawal test was included as history and combined with the pulse and slug tests to form one continuous test sequence for simulation. Figure 5-41 shows the best-fit GTFM curve generated using a transmissivity of 0.16 $ft^2$/day and a static formation pressure (at the depth of the transducer) of 118.1 psi. The pulse-withdrawal, slug-withdrawal, and slug-injection tests are separated and presented in semilog format as normalized pressure versus elapsed time in Figures 5-42, 5-43, and 5-44, respectively. The simulated and observed data for the slug and pulse tests show excellent agreement on the semilog plots.

The sensitivity of the interpreted transmissivity to the assumed value of storativity of $1 \times 10^{-5}$ was evaluated by fitting simulations of the observed data from the slug-injection test using storativity values an order of magnitude higher and lower. A semilog plot of these simulations is shown in Figure 5-45. The best-fit simulation obtained assuming a storativity of $1 \times 10^{-4}$ used a transmissivity of 0.12 $ft^2$/day. The best-fit simulation obtained assuming a storativity of $1 \times 10^{-6}$ used a transmissivity of 0.20 $ft^2$/day. The simulation assuming a storativity of $1 \times 10^{-5}$ (Figure 5-44) appears to match the observed data slightly better than either of the other two simulations, although all three simulations are similar. Thus, the actual storativity of the Magenta dolomite around H-3b1 is probably about $1 \times 10^{-5}$ plus or minus about half an order of magnitude, while the transmissivity is about 0.14 to 0.18 $ft^2$/day (Table 5-1).

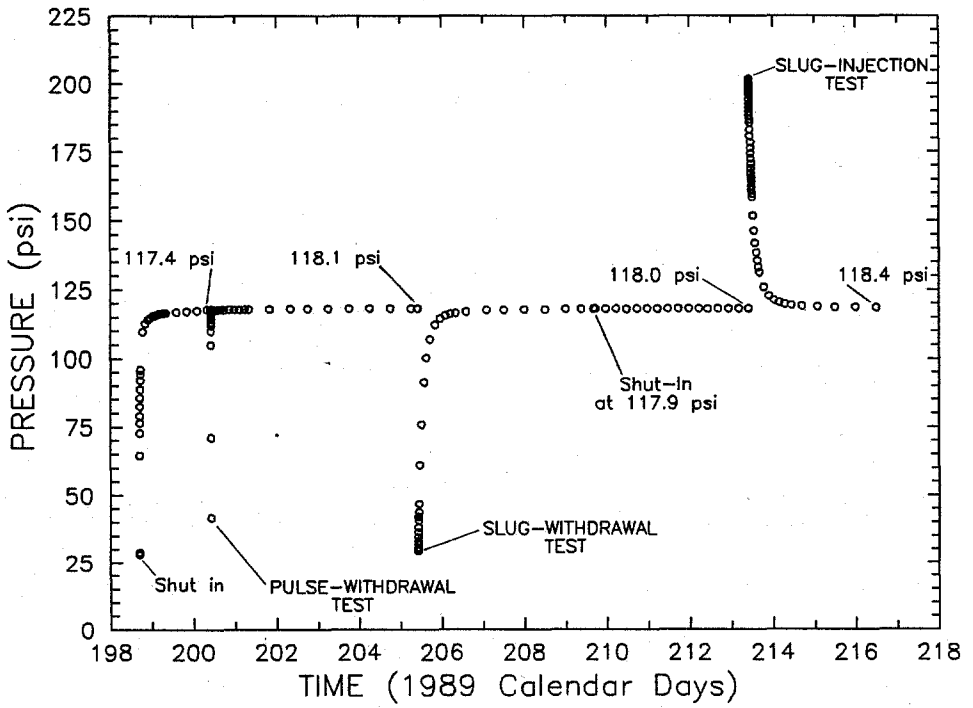


Figure 5-40 Linear-Linear Sequence Plot of Pressure Data from the Pulse and Slug Tests of the Magenta Dolomite at Well H-3b1

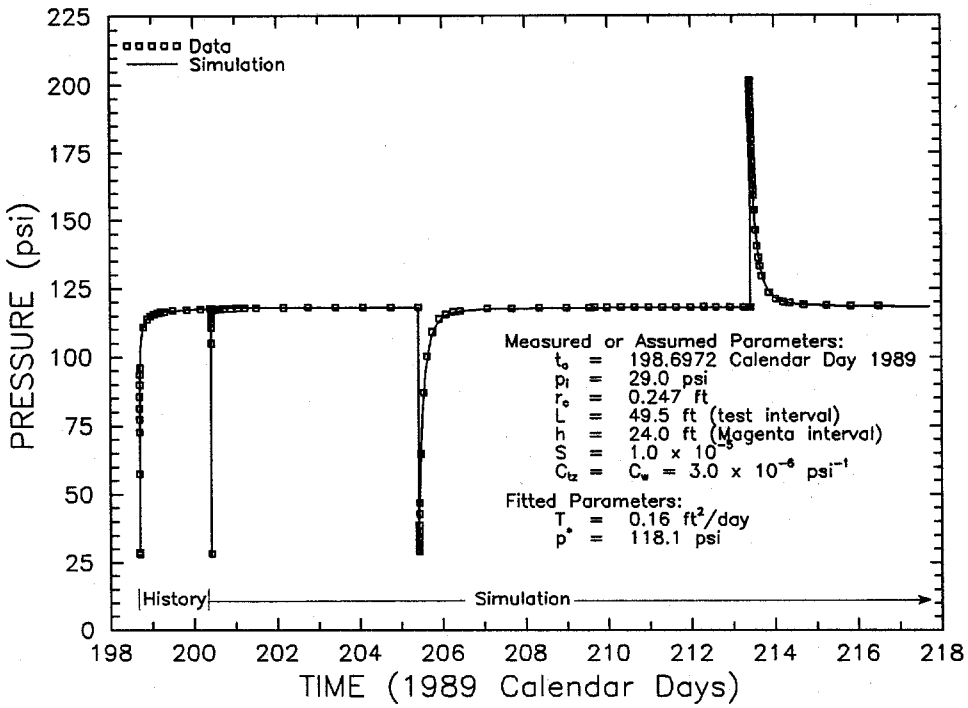


Figure 5-41 Linear-Linear Plot of GTFM Simulation of the Pulse and Slug Tests of the Magenta Dolomite at Well H-3b1

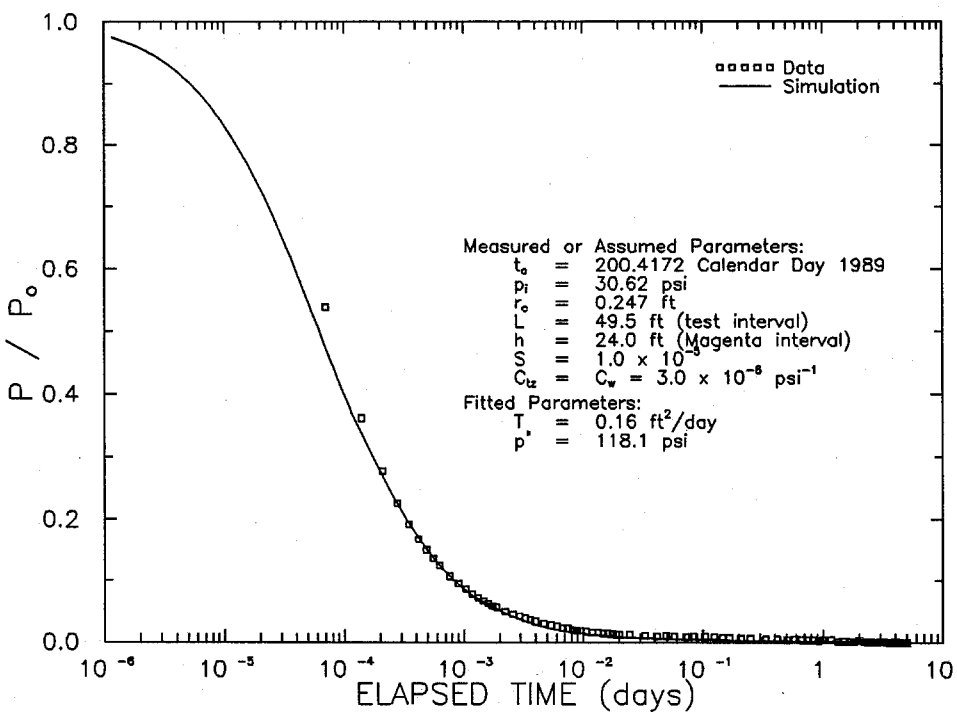


Figure 5-42 Semilog Plot of GTFM Simulation of the Pulse-Withdrawal Test of the Magenta Dolomite at Well H-3b1

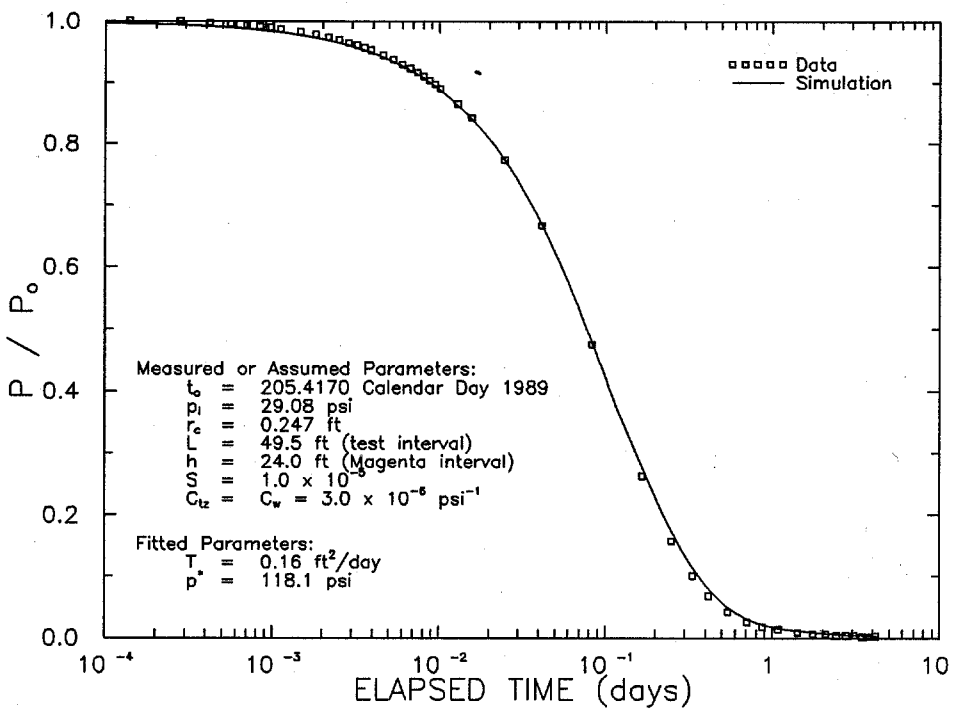


Figure 5-43 Semilog Plot of GTFM Simulation of the Slug-Withdrawal Test of the Magenta Dolomite at Well H-3b1

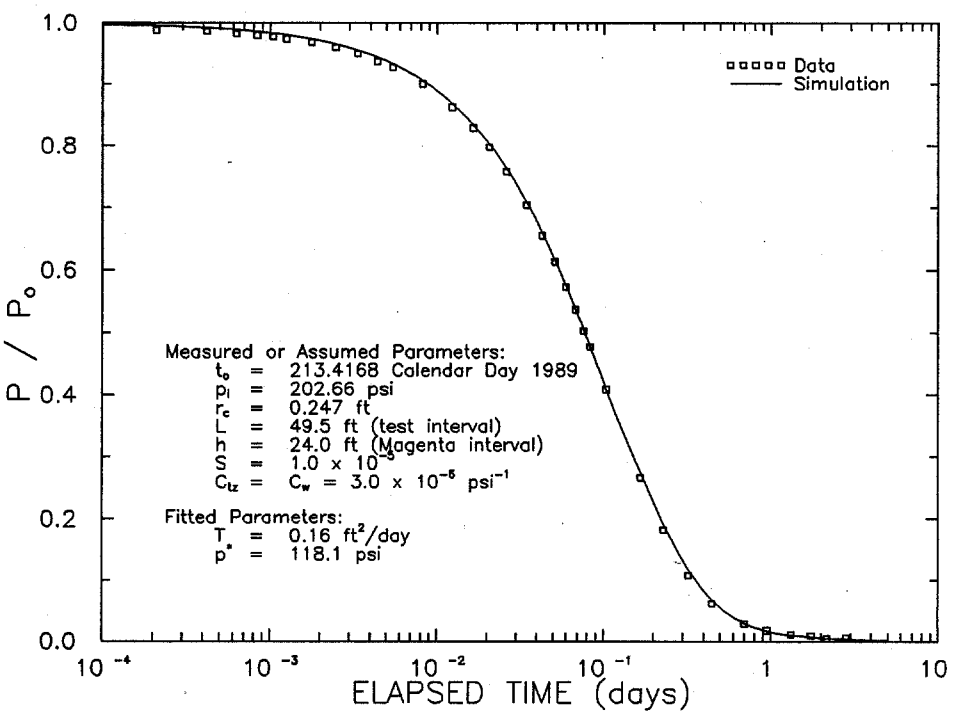


Figure 5-44 Semilog Plot of GTFM Simulation of the Slug-Injection Test of the Magenta Dolomite at Well H-3b1

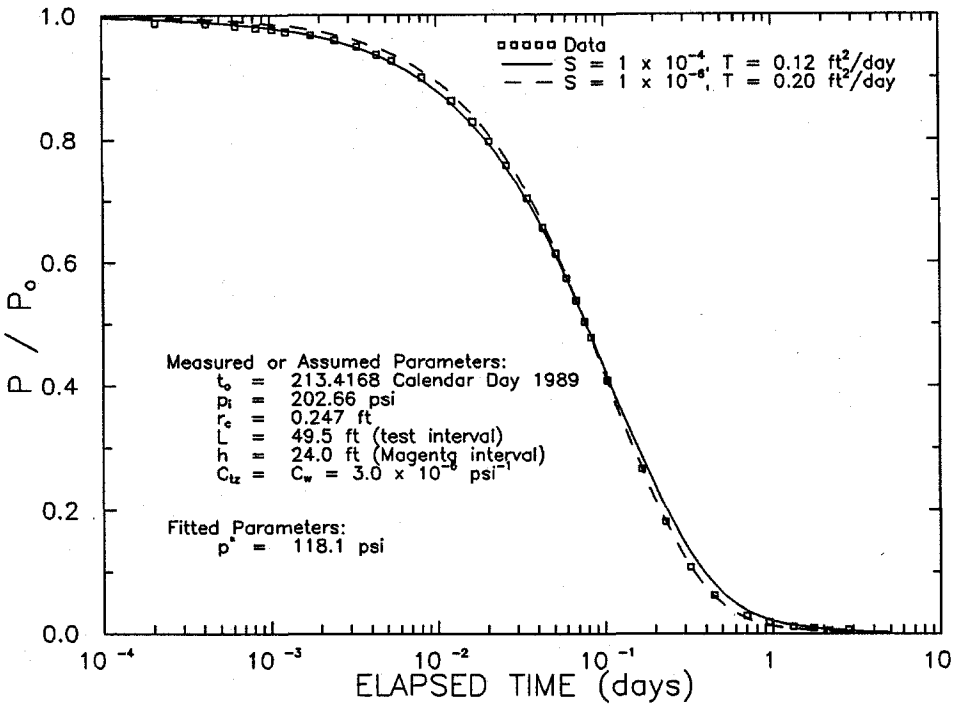


Figure 5-45 Semilog Plot of GTFM Simulations of the Slug-Injection Test of the Magenta Dolomite at Well H-3b1 Using Different Values for Storativity

The propagation of the pressure transients created within the Magenta dolomite during the testing periods was also simulated using GTFM. The calculated pressure responses to the pretest history period, pulse-withdrawal test, slug-withdrawal test, and slug-injection test at radial distances of 1, 10, 100, and 200 ft from H-3b1 assuming a storativity of $1 \times 10^{-5}$ are shown in Figure 5-46. Pressure changes on the order of 0.6 psi are calculated to have occurred at a radial distance of 200 ft in response to the testing at H-3b1. The pressure recovered to its static level between successive tests at all radii examined. Additional GTFM simulations show that the maximum pressure changes occurring at radial distances of 1, 10, 100, and 200 ft from H-3b1 during the slug-injection test assuming a storativity of $1 \times 10^{-5}$ would occur at radial distances of 0.65, 4.1, 33, and 64 ft if the storativity were $1 \times 10^{-4}$, and at 1.5, 25, 310, and 630 ft if the storativity were $1 \times 10^{-6}$.

In summary, interpretation of the slug and pulse tests of the Magenta at H-3b1 provided a transmissivity estimate of 0.14 to 0.18 $ft^2$/day. This range of values is higher than the value of 0.1 $ft^2$/day reported by Mercer (1983), but the difference is not significant from the standpoint of regional-scale modeling of groundwater flow.

## 5.4 Forty-niner Member at Well H-3d

Hydraulic testing of the Forty-niner Member of the Rustler Formation was performed in well H-3d. The Forty-niner Member is composed of two anhydrite/gypsum units separated by a claystone layer. The test interval in H-3d included the full thickness of the claystone between 536 and 546 ft deep, 18 ft of overlying anhydrite/gypsum, and 8 ft of underlying anhydrite/gypsum (Figure 3-5). From previous testing at H-14, the anhydrite/gypsum units have been shown to not contribute significantly to the fluid-pressure responses observed during testing of the Forty-niner (Beauheim, 1987c). Consequently, the responses observed during the testing in H-3d are assumed to be representative only of the Forty-niner claystone. For the test interpretations, a storativity of $1.0 \times 10^{-5}$, consistent with that used by Beauheim (1987c), was initially assumed for the Forty-niner claystone.

The Forty-niner claystone was tested during the period of June 21 to October 3, 1989 (Calendar Days 172 to 276). The testing consisted of a pulse-withdrawal test, a pulse-injection test, and a slug-withdrawal test. On day 172, the tubing attached to the PIP set in the upper Forty-niner anhydrite (Figure 3-5) was bailed to create a low-pressure condition in the well. A minipacker was installed in the tubing below the

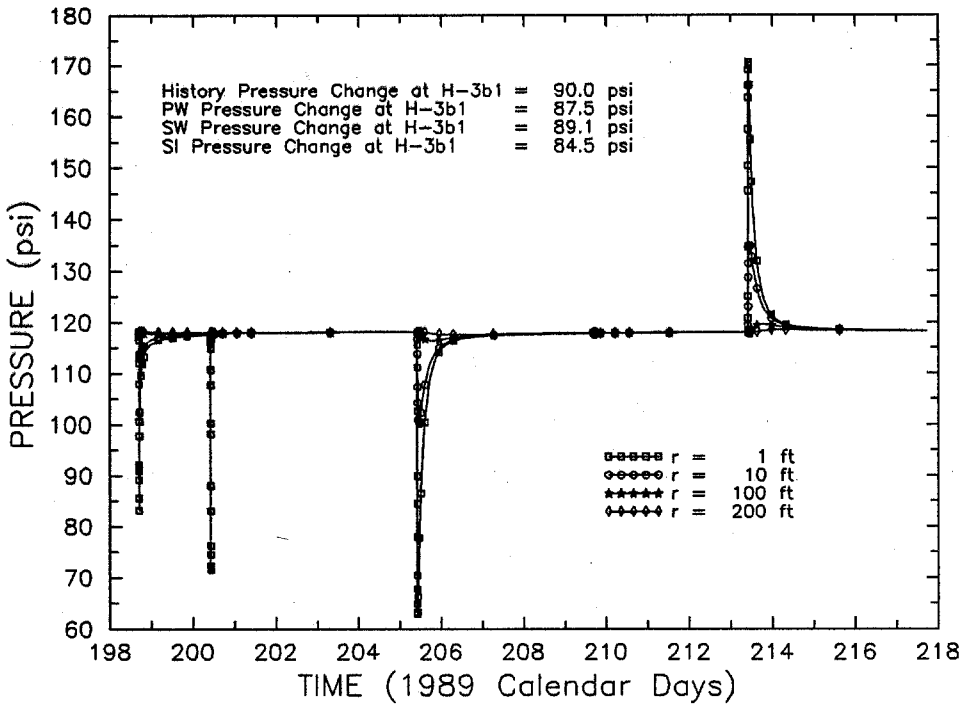


Figure 5-46 Simulated Pore Pressures at Selected Radial Distances from Well H-3b1 During the Pulse and Slug Tests of the Magenta Dolomite

lowered water level, and inflated to allow the pressure beneath to build up to near static formation pressure. A pulse-withdrawal test was initiated on day 177 by deflating the minipacker for about one minute. On day 180, fluid was added to the tubing above the minipacker, and the minipacker was deflated briefly to initiate a pulse-injection test. The early data from the pulse-injection test (Figure 5-47) indicated that the packer may have repositioned during reinflation, causing the pressure to recover too quickly. Therefore, the test was terminated on day 181. The pulse-injection test is not considered to be a valid test (Stensrud et al., 1990) and was not analyzed.

On day 188, the minipacker was deflated and removed, the tubing was bailed, and the minipacker reinstalled and inflated in preparation for the slug-withdrawal test. However, due to a faulty transducer the minipacker had to be removed. A new transducer was installed with the minipacker on day 194. After a pressure build-up of approximately four days, the minipacker was deflated and removed to initiate the slug-withdrawal test on day 198. The pressure-versus-time data measured using a microcomputer-controlled data-acquisition system for the pulse-withdrawal and pulse-injection tests are presented in Figure 5-47. The depth-to-water-versus-time data measured using a water-level sounder for the slug-withdrawal test are presented in Figure 5-48. Descriptions of the testing instrumentation and the raw test data are contained in Stensrud et al. (1990).

The best-fit GTFM simulation of the slug-withdrawal test is shown in Figure 5-49. This simulation was generated using a transmissivity of $4.0 \times 10^{-3}$ $ft^2$/day and a static water level located at a depth of 314 ft. Figure 5-50 presents a semilog plot of normalized hydraulic head versus elapsed time for the slug-withdrawal simulation. The simulated response and observed data show excellent agreement in both the linear-linear and semilog plots.

The sensitivity of the interpreted transmissivity to the assumed value of storativity of $1 \times 10^{-5}$ was evaluated by fitting simulations of the observed data from the slug-withdrawal test using storativity values an order of magnitude higher and lower. A semilog plot of these simulations is shown in Figure 5-51. The best-fit simulation obtained assuming a storativity of $1 \times 10^{-4}$ used a transmissivity of $3.0 \times 10^{-3}$ $ft^2$/day. The best-fit simulation obtained assuming a storativity of $1 \times 10^{-6}$ used a transmissivity of $5.0 \times 10^{-3}$ $ft^2$/day. The simulation assuming a storativity of $1 \times 10^{-5}$ (Figure 5-50) fits the observed data better than either of the

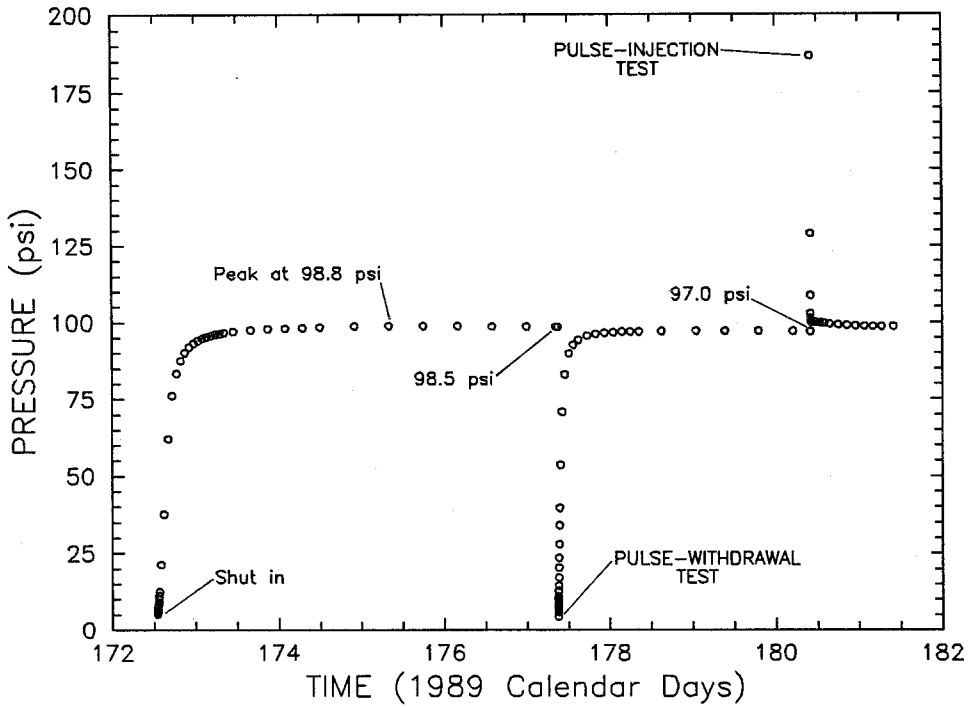


Figure 5-47 Linear-Linear Sequence Plot of Pressure Data from the Pulse Tests of the Forty-niner Claystone at Well H-3d

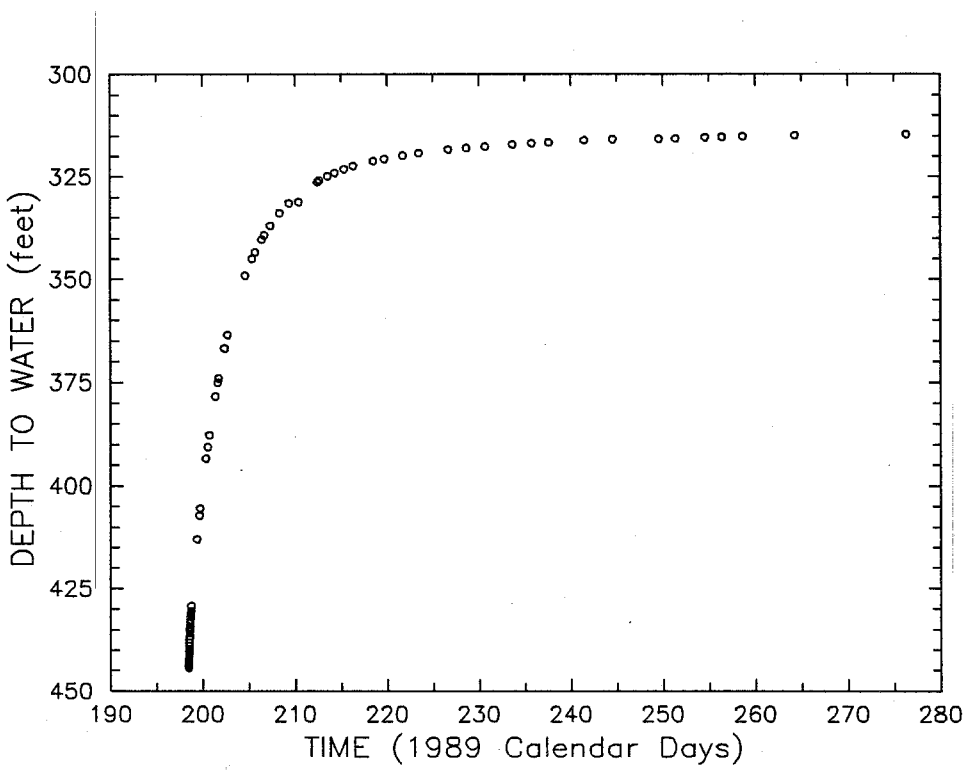


Figure 5-48 Linear-Linear Sequence Plot of Water-Level Data from the Slug-Withdrawal Test of the Forty-niner Claystone at Well H-3d

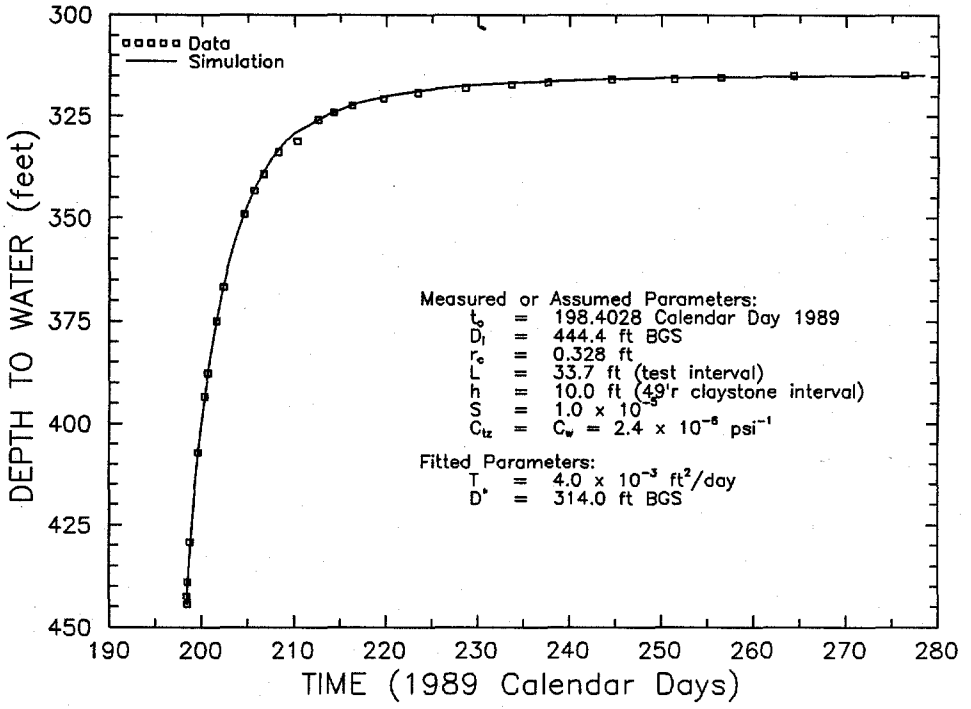


Figure 5-49 Linear-Linear Plot of GTFM Simulation of the Slug-Withdrawal Test of the Forty-niner Claystone at Well H-3d

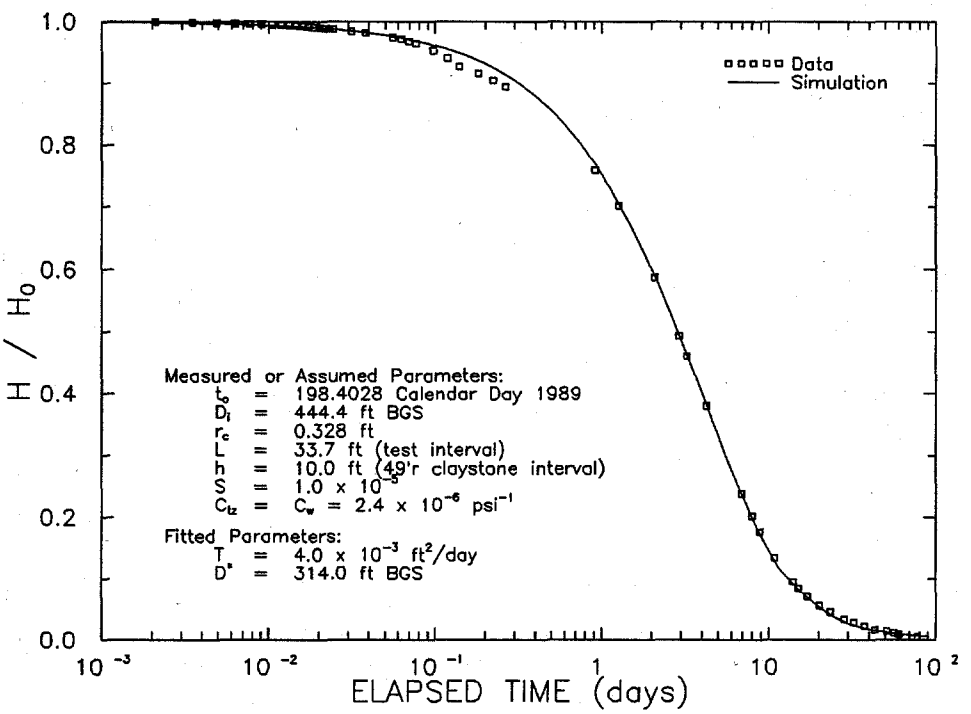


Figure 5-50 Semilog Plot of GTFM Simulation of the Slug-Withdrawal Test of the Forty-niner Claystone at Well H-3d

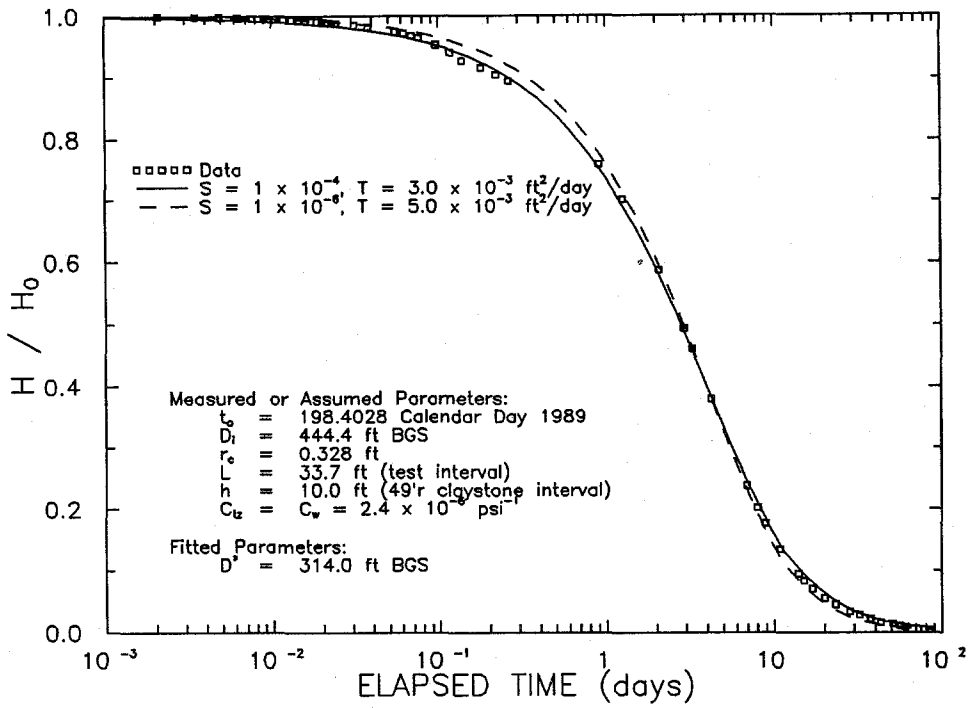


Figure 5-51 Semilog Plot of GTFM Simulations of the Slug-Withdrawal Test of the Forty-niner Claystone at Well H-3d Using Different Values for Storativity

other two simulations. Thus, the actual storativity of the Forty-niner claystone around H-3d is probably about 1 x $10^{-5}$ plus or minus perhaps half an order of magnitude, while the transmissivity is about 3.5 x $10^{-3}$ to 4.5 x $10^{-3}$ $ft^2$/day (Table 5-1).

Figures 5-52 and 5-53 show simulations of the pulse-withdrawal test in linear-linear and semilog format using the transmissivity derived from the slug-test analysis and a static formation pressure of 97.5 psi. The solid lines on the figures represent a simulation using the same storativity (1 x $10^{-5}$) and test-zone compressibility (2.4 x $10^{-6}$ $psi^{-1}$) as were used in the slug-test interpretation. This simulation shows recovery occurring much faster than was actually observed. The semilog plot (Figure 5-53) in particular shows that the simulation does not match the data very well.

The pulse-withdrawal test occurred with the well shut in. Pressure responses under shut-in conditions are highly sensitive to test-zone compressibility. With a perfectly rigid packer system, the compressibility of the test zone would simply be the compressibility of the water in the well. Packer systems are never perfectly rigid, however. They typically deform slightly in response to external pressure changes, a process referred to as compliance. Neuzil (1982) and Hsieh et al. (1983) reported test-zone compressibilities five to six times greater than that of water during pressure-pulse testing, and attributed these high compressibilities to test-tool compliance.

By increasing the test-zone compressibility by a factor of 18 from that estimated for the water (brine) in the well, and decreasing the formation storativity by an order of magnitude, while maintaining the same transmissivity and static formation pressure, a better fit between the pulse-test data and a GTFM simulation (dashed lines on Figures 5-52 and 5-53) was obtained. Storativity could be as low as the value of 1.0 x $10^{-6}$ used in the simulation, but the indicated test-zone compressibility appears to be unreasonably high. Without a high test-zone compressibility, however, no simulation of the pulse test fit the observed data well. The pulse-test interpretation remains problematic.

The propagation of the pressure transients created within the Forty-niner claystone during the slug-withdrawal test was simulated by GTFM. The calculated changes in hydraulic head at radial distances of 1, 10, 30, and 150 ft from H-3d assuming a storativity of 1 x $10^{-5}$ are shown in Figure 5-54. The maximum calculated hydraulic-head change at a radial

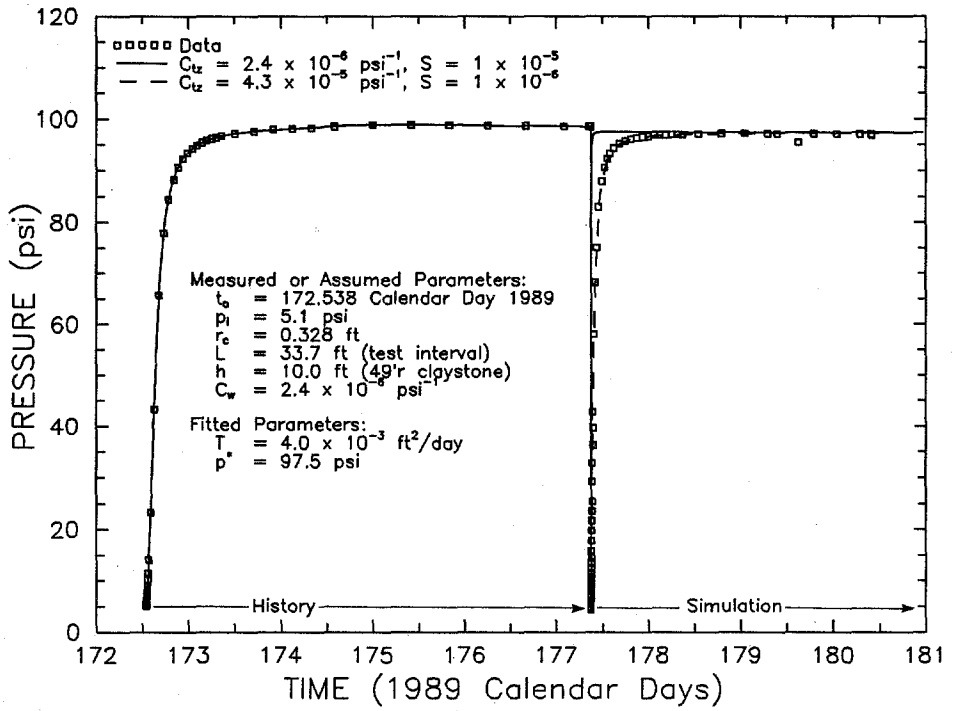


Figure 5-52 Linear-Linear Plot of GTFM Simulations of the Pulse-Withdrawal Test of the Forty-niner Claystone at Well H-3d

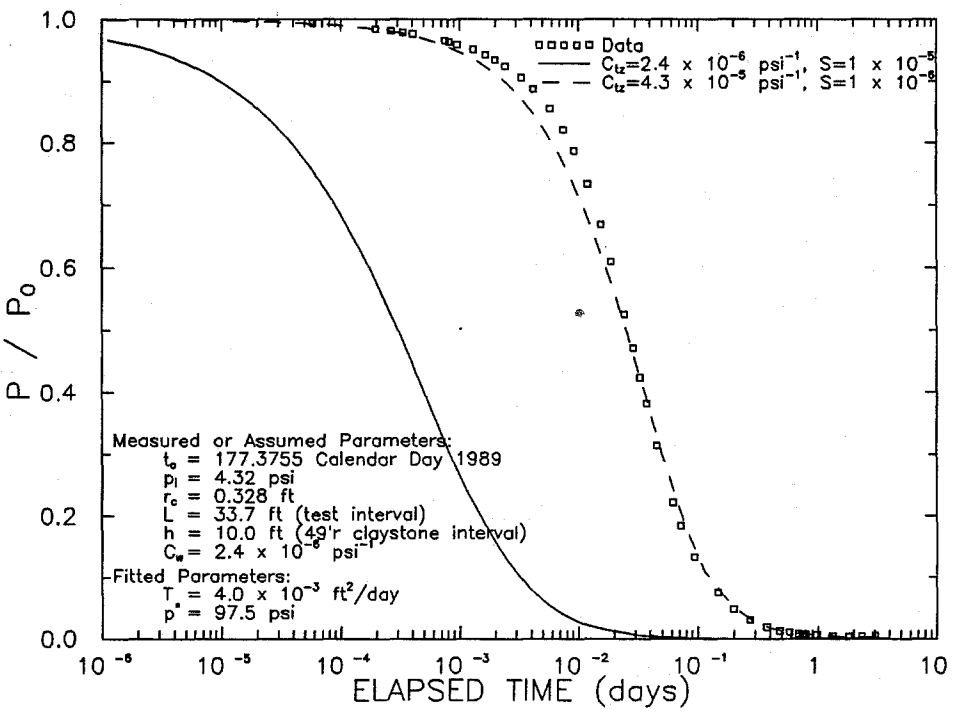


Figure 5-53 Semilog Plot of GTFM Simulations of the Pulse-Withdrawal Test of the Forty-niner Claystone at Well H-3d

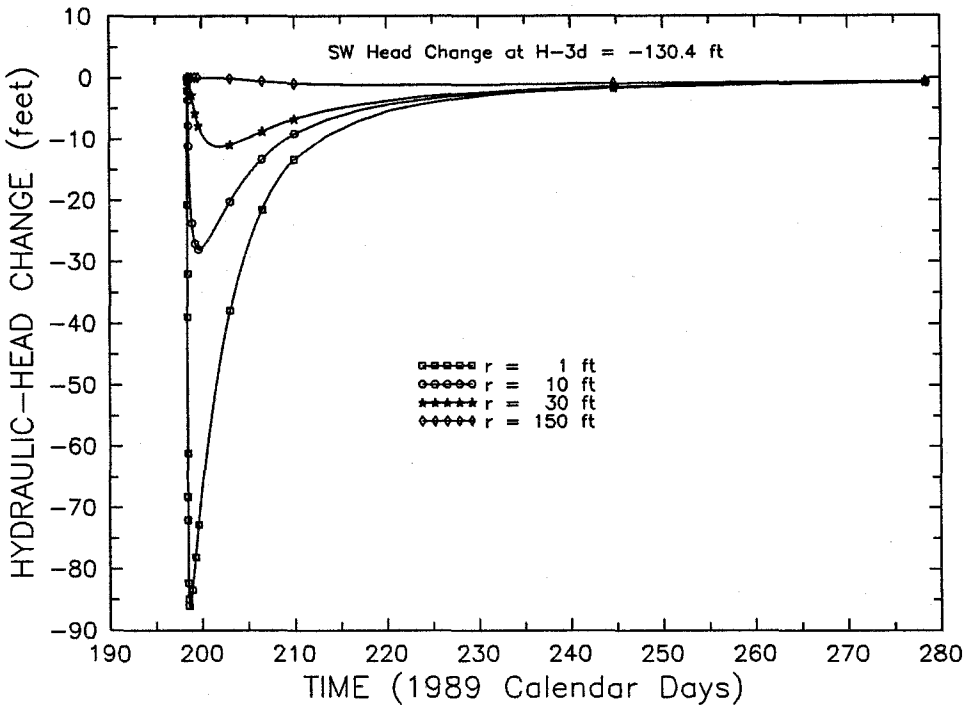


Figure 5-54 Simulated Hydraulic-Head Changes at Selected Radial Distances from Well H-3d During the Slug-Withdrawal Test of the Forty-niner Claystone

distance of 150 ft was about 1.2 ft (about 0.6 psi). Additional GTFM simulations show that the maximum drawdowns occurring at radial distances of 1, 10, 30, and 150 ft from H-3d during the slug-withdrawal test assuming a storativity of $1 \times 10^{-5}$ would occur at radial distances of 0.7, 4.1, 10.8, and 50 ft if the storativity were $1 \times 10^{-4}$, and at 1.5, 24, 85, and 450 ft if the storativity were $1 \times 10^{-6}$.

In summary, interpretation of the slug test of the Forty-niner claystone at well H-3d provided a transmissivity estimate of $3.5 \times 10^{-3}$ to $4.5 \times 10^{-3}$ $ft^2$/day. The interpretation of the pulse test at H-3d was inconclusive.

# 6. SUMMARY AND CONCLUSIONS

In 1988 and 1989, hydraulic tests of four members of the Rustler Formation were conducted in seven wells. The tests were intended to provide data on the transmissivities of the Rustler members for use in regional-scale modeling of groundwater flow through the Rustler. The types of tests performed included pressure-pulse (both injection and withdrawal), slug (both injection and withdrawal), and pumping tests.

The computer code GTFM was used to simulate the tests performed in six of the wells. The GTFM simulations of the slug-withdrawal test at well H-16 provided a transmissivity estimate between $2.1 \times 10^{-4}$ and $3.0 \times 10^{-4}$ $ft^2$/day for the unnamed lower member siltstone. Simulations of the slug tests of the Culebra dolomite provided transmissivity estimates between 0.16 and 0.20 $ft^2$/day at well AEC-7, and between 1.9 and 2.5 $ft^2$/day at well D-268. Simulations of the slug and pressure-pulse tests of the Magenta dolomite at wells H-2b1 and H-3b1 provided transmissivity estimates of $2.1 \times 10^{-3}$ to $2.7 \times 10^{-3}$ $ft^2$/day and 0.14 to 0.18 $ft^2$/day, respectively. GTFM simulations of the slug and pressure-pulse tests of the Forty-niner claystone at well H-3d provided an estimated transmissivity of $3.5 \times 10^{-3}$ to $4.5 \times 10^{-3}$ $ft^2$/day. The radii of influence of the tests, as simulated by GTFM, ranged from about 50 to 300 ft.

Two of the AEC-7 slug tests and one of the D-268 slug tests were also interpreted using a type-curve-matching procedure based on the analytical solution of Cooper et al. (1967). This type-curve-matching procedure had previously been used by Mercer et al. (1981), Dennehy (1982), Dennehy and Mercer (1982), and Beauheim (1986, 1987c, 1989) to interpret other slug tests performed at the WIPP site. The transmissivities interpreted from the AEC-7 tests using type curves were 20 to 35 percent higher than the maximum transmissivity determined using GTFM. The transmissivity interpreted from the D-268 test using a type curve was within the uncertainty bounds of the GTFM transmissivity determination.

The computer code Interpret/2 was used to analyze a pumping test of the Culebra dolomite performed at well H-18. The results of the analysis are ambiguous in that the test responses are equally representative of a single-porosity medium having a transmissivity of 2.0 $ft^2$/day and a no-flow boundary 58 ft from H-18, and of a double-porosity medium with a transmissivity of 1.0 $ft^2$/day and no apparent boundaries.

The pressure-pulse tests considered in this report proved to be difficult to interpret. The technique employed to perform the tests involved briefly deflating and then reinflating a small-diameter minipacker suspended on a wireline inside well tubing to transmit a pressure pulse to the test interval. This technique did not allow measurement of the amount of water that moved into or out of the test interval in association with the pulse, precluding calculation of the compressibility of the test interval. Error in the value of test-interval compressibility used in pulse-test analysis results in linearly proportional error in transmissivity (Neuzil, 1982). Anomalous pressure responses observed during some of the pulse tests also indicated a potential problem with the minipacker repositioning between deflation and reinflation, resulting in movement of the transducer monitoring pressures. If additional pressure-pulse tests of Rustler members were to be performed, testing equipment and procedures would need to be modified to correct these problems.

# NOTATION

| | |
|---|---|
| $d$ | distance to a boundary |
| $h$ | thickness of tested unit |
| $p^*$ | static formation pore pressure |
| $p_i$ | initial pressure for a test period |
| $r$ | radial distance from well |
| $r_c$ | radius of casing |
| $r_t$ | radius of tubing |
| $s$ | wellbore skin |
| $t$ | time match for slug-test type curve |
| $t_0$ | start time for a test period |
| BGS | below ground surface |
| $C$ | wellbore-storage coefficent |
| $C_D$ | dimensionless wellbore-storage coefficient |
| $C_De^{2s}$ | pumping-test type-curve parameter |
| $C_{tz}$ | test-zone compressibility |
| $C_w$ | compressibility of water |
| $D^*$ | static depth to water |
| $D_i$ | initial depth to water for a test period |
| $H$ | head difference |
| $H_0$ | head difference at the start of a slug test |
| $L$ | length of tested interval |
| $P$ | pressure difference |
| PI | pulse injection |
| PM | pressure match |
| PW | pulse withdrawal |
| $P_0$ | pressure difference at the start of a slug or pulse test |
| $S$ | storativity |
| SI | slug injection |
| SW | slug withdrawal |
| $T$ | transmissivity |
| TM | time match |
| $\alpha$ | $r_c^2S/r_t^2$ (slug-test type-curve parameter) |
| $\beta$ | $Tt/r_t^2$ (slug-test type-curve parameter) |
| $\lambda$ | interporosity flow coefficient |
| $\omega$ | storativity ratio |

Subscripts:

| | |
|---|---|
| f | fractures |
| m | matrix |

# REFERENCES


Avis, J.D., and Saulnier, G.J., Jr. 1990. *Analysis of the Fluid-Pressure Responses of the Rustler Formation at H-16 to the Construction of the Air-Intake Shaft at the Waste Isolation Pilot Plant (WIPP) Site*, SAND89-7067 (Albuquerque, NM: Sandia National Laboratories).

Beauheim, R.L. 1986. *Hydraulic-Test Interpretations for Well DOE-2 at the Waste Isolation Pilot Plant (WIPP) Site*, SAND86-1364 (Albuquerque, NM: Sandia National Laboratories), 89 p.

Beauheim, R.L. 1987a. *Analysis of Pumping Tests of the Culebra Dolomite Conducted at the H-3 Hydropad at the Waste Isolation Pilot Plant (WIPP) Site*, SAND86-2311 (Albuquerque, NM: Sandia National Laboratories), 154 p.

Beauheim, R.L. 1987b. *Interpretation of the WIPP-13 Multipad Pumping Test of the Culebra Dolomite at the Waste Isolation Pilot Plant (WIPP) Site*, SAND87-2456 (Albuquerque, NM: Sandia National Laboratories), 171 p.

Beauheim, R.L. 1987c. *Interpretations of Single-Well Hydraulic Tests Conducted At and Near the Waste Isolation Pilot Plant (WIPP) Site, 1983-1987*, SAND87-0039 (Albuquerque, NM: Sandia National Laboratories), 169 p.

Beauheim, R.L. 1989. *Interpretation of H-11b4 Hydraulic Tests and the H-11 Multipad Pumping Test of the Culebra Dolomite at the Waste Isolation Pilot Plant (WIPP) Site*, SAND89-0536 (Albuquerque, NM: Sandia National Laboratories), 197 p.

Bourdet, D.; Ayoub, J.A.; and Pirard, Y.M. 1989. "Use of Pressure Derivative in Well-Test Interpretation," *SPE Formation Evaluation* 4(2):293-302.

Bredehoeft, J.D., and Papadopulos, S.S. 1980. "A Method for Determining the Hydraulic Properties of Tight Formations," *Water Resources Research* 16(1):233-238.

Christensen, C.L., and Peterson, E.W. 1981. *The Bell Canyon Test Summary Report*, SAND80-1375 (Albuquerque, NM: Sandia National Laboratories), 53 p.

Cooper, H.H., Jr.; Bredehoeft, J.D.; and Papadopulos, I.S. 1967. "Response of a Finite-Diameter Well to an Instantaneous Charge of Water," *Water Resources Research* 3(1):263-269.

Dennehy, K.F. 1982. *Results of Hydrologic Tests and Water-Chemistry Analyses, Wells H-6A, H-6B, and H-6C at the Proposed Waste Isolation Pilot Plant Site, Southeastern New Mexico*, USGS Water-Resources Investigations 82-8 (Albuquerque, NM: US Geological Survey), 68 p.

Dennehy, K.F., and Mercer, J.W. 1982. *Results of Hydrologic Tests and Water-Chemistry Analyses, Wells H-5A, H-5B, and H-5C at the Proposed Waste Isolation Pilot Plant Site, Southeastern New Mexico*, USGS Water-Resources Investigations 82-19 (Albuquerque, NM: US Geological Survey), 83 p.

Earlougher, R.C., Jr. 1977. *Advances in Well Test Analysis*. Monograph Volume 5 (Dallas, TX: Soc Pet Eng of AIME), 264 p.

Gonzalez, D.D. 1983. *Groundwater Flow in the Rustler Formation, Waste Isolation Pilot Plant (WIPP), Southeast New Mexico (SENM): Interim Report*, SAND82-1012 (Albuquerque, NM: Sandia National Laboratories), 39 p.

Grader, A.S., and Ramey, H.J., Jr. 1988. "Slug-Test Analysis in Double-Porosity Reservoirs," *SPE Formation Evaluation* 3(2):329-339.

Hsieh, P.A.; Neuman, S.P.; and Simpson, E.S. 1983. *Pressure Testing of Fractured Rocks -- A Methodology Employing Three-Dimensional Cross-Hole Tests*, NUREG/CR-3213 (Washington, DC: US NRC).

Mercer, J.W. 1983. *Geohydrology of the Proposed Waste Isolation Pilot Plant Site, Los Medanos Area, Southeastern New Mexico*, USGS Water-Resources Investigations Rpt 83-4016 (Albuquerque, NM: US Geological Survey), 113 p.

Mercer, J.W.; Davis, P.; Dennehy, K.F.; and Goetz, C.L. 1981. *Results of Hydrologic Tests and Water-Chemistry Analyses, Wells H-4A, H-4B, and H-4C at the Proposed Waste Isolation Pilot Plant Site, Southeastern New Mexico*, USGS Water-Resources Investigations 81-36 (Albuquerque, NM: US Geological Survey), 92 p.

Mercer, J.W., and Orr, B.R. 1979. *Interim Data Report on the Geohydrology of the Proposed Waste Isolation Pilot Plant Site, Southeast New Mexico*, USGS Water-Resources Investigations 79-98 (Albuquerque, NM: US Geological Survey), 178 p.

Mercer, J.W., and Snyder, R.P. 1990a. *Basic Data Report for Drillhole H-16 (Waste Isolation Pilot Plant - WIPP)*, SAND89-0203 (Albuquerque, NM: Sandia National Laboratories).

Mercer, J.W., and Snyder, R.P. 1990b. *Basic Data Report for Drillholes H-17 and H-18 (Waste Isolation Pilot Plant - WIPP)*, SAND89-0204 (Albuquerque, NM: Sandia National Laboratories).

Neuzil, C.E. 1982. "On Conducting the Modified 'Slug' Test in Tight Formations," *Water Resources Research* 18(2):439-441.

Pickens, J.F.; Grisak, G.E.; Avis, J.D.; Belanger, D.W.; and Thury, M. 1987. "Analysis and Interpretation of Borehole Hydraulic Tests in Deep Boreholes: Principles, Model Development, and Applications," *Water Resources Research* 23(7):1341-1375.

Ramey, H.J., Jr.; Agarwal, R.G.; and Martin, I. 1975. "Analysis of 'Slug Test' or DST Flow Period Data," *J. Can. Pet. Tech.* 14(3):37-47.

Robinson, T.W., and Lang, W.B. 1938. "Geology and Ground-Water Conditions of the Pecos River Valley in the Vicinity of Laguna Grande de la Sal, New Mexico," *12th and 13th Biennial Reports: New Mexico State Engineer*, pp. 77-100.

Sandia National Laboratories and D'Appolonia Consulting Engineers. 1983. *Basic Data Report for Drillhole AEC 7 (Waste Isolation Pilot Plant - WIPP)*, SAND79-0268 (Albuquerque, NM: Sandia National Laboratories).

Stensrud, W.A.; Bame, M.A.; Lantz, K.D.; Palmer, J.B.; and Saulnier, G.J., Jr. 1988. *WIPP Hydrology Program, Waste Isolation Pilot Plant, Southeastern New Mexico, Hydrologic Data Report #7*, SAND88-7014 (Albuquerque, NM: Sandia National Laboratories).

Stensrud, W.A.; Bame, M.A.; Lantz, K.D.; Palmer, J.B.; and Saulnier, G.J., Jr. 1990. *WIPP Hydrology Program, Waste Isolation Pilot Plant, Southeastern New Mexico, Hydrologic Data Report #8*, SAND89-7056 (Albuquerque, NM: Sandia National Laboratories).

# APPENDIX A

# ANALYSIS AND INTERPRETATION OF HYDRAULIC-TEST DATA USING THE WELL-TEST-SIMULATION MODEL GTFM

Interpretation of the single-well hydraulic tests presented in this report utilized the well-test-simulation model GTFM. The GTFM model was developed based on graph-theoretical-field-modeling techniques. Detailed documentation on the governing equations, theoretical development, and verification is presented in Grisak et al. (1985) and Pickens et al. (1987). A brief explanation of model discretization, implementation, and boundary conditions is presented below.

## A.1 Model Description

The Graph-Theoretic Field Model (GTFM) constitutes a generalized methodology for modeling the behavior of field- or continuum-type problems. GTFM is based upon linear graph theory, continuum mechanics, and a spatial discretization procedure. Savage and Kesavan (1979) present generalized descriptions of the methodology.

GTFM is a numerical model that simulates the hydraulic response of a single-phase, one-dimensional, radial-flow regime to boundary conditions applied at a borehole located at the center of the modeled flow system. The problem domain is discretized by dividing the radial-flow system into a series of concentric rings centered on the borehole, with each ring represented by a node. A constant multiplicative factor is used to increase the spacing between nodes with increasing distance from the origin (borehole). The model assumes that the formation has a constant thickness with vertically homogeneous hydraulic properties. Formations may be single or double porosity, and may include a single radially centered heterogeneity to simulate the presence of a "skin" zone adjacent to the borehole. The skin zone may have properties different from those of the remainder of the formation.

The GTFM model can be used with assigned conditions of either fixed pressure or zero flow at the external boundary of the model. Selection between the two boundary conditions is made on a test-specific basis, depending on whether or not the test data show boundary effects. If no boundary effects are indicated by the test data, a fixed-pressure boundary condition is specified at a distance from the borehole such that the type of boundary has no effect on the calculated fluid-pressure or water-level response in the borehole. The adequacy of the specified distance is verified by ensuring that the pressure in the portion of the simulated formation adjacent to the boundary does not change over the duration of the test-interpretation simulation. In cases where boundary effects are indicated, the type of, and distance to, the boundary are parameters selected and fitted as part of the test interpretation.

The model has wellbore boundary conditions which can be used to simulate pulse-injection/withdrawal tests, specified borehole-pressure conditions, specified formation-flow rates, and slug-injection/withdrawal tests. The effects of consecutive tests are incorporated in the simulations. The model can also incorporate test-zone pressure changes resulting from temperature variations in the test zone as well as test-equipment- and/or formation-induced changes in the test-zone volume. The model output consists of simulated fluid-pressure responses in the borehole and at selected radial distances from the borehole. The model can also calculate formation-flow rates and cumulative production based on the formation's estimated hydraulic properties.

The individual testing periods for each borehole are subdivided into discrete time intervals, called sequences. Sequences are differentiated by the wellbore boundary conditions in effect during these time periods. History sequences are used to represent the test interval's pretest borehole-pressure history during the open-borehole period between drilling and initial shut-in of the test zone, and also to represent time periods when non-ideal behavior characterized

the fluid-pressure responses. Under these conditions, the pressure conditions in the isolated test intervals are specified directly using the fluid pressures recorded by the data-acquisition instrumentation. Pulse sequences are used to simulate the fluid-pressure buildups observed after shutting in the test zones and also the fluid-pressure-recovery responses to individual pulse-injection and pulse-withdrawal tests.

## A.2 Verification

GTFM has been verified by comparing its results to analytical solutions for constant-flow-rate pumping tests, slug tests, and pulse tests. Verification was achieved through graphical comparison of simulation results to those generated by the analytical solutions. The GTFM and analytical-solution results showed excellent agreement for all cases (Grisak et al., 1985, and Pickens et al., 1987).

**A.2.1 Pumping-Test Sequence.** Correct simulation of pumping-test sequences was verified by comparing observation files produced by GTFM to data computed using the analytical solution published by Theis (1935). The solution allows calculation of hydraulic head at a fixed radius and varying times or at a fixed time and varying radii for a line-source well with a constant-flow-rate boundary condition at the well. The line-source well was simulated by GTFM as a well of radius 0.01 m. Observation files were generated at a distance of 10.0 m. This was felt to be sufficiently distant from the well to avoid any boundary effects introduced by the finite-radius well.

Simulations were performed for two transmissivity (T) and three storativity (S) values in order to provide results for a range of conditions. Figure A-1 shows the comparison between the simulated and analytical results.

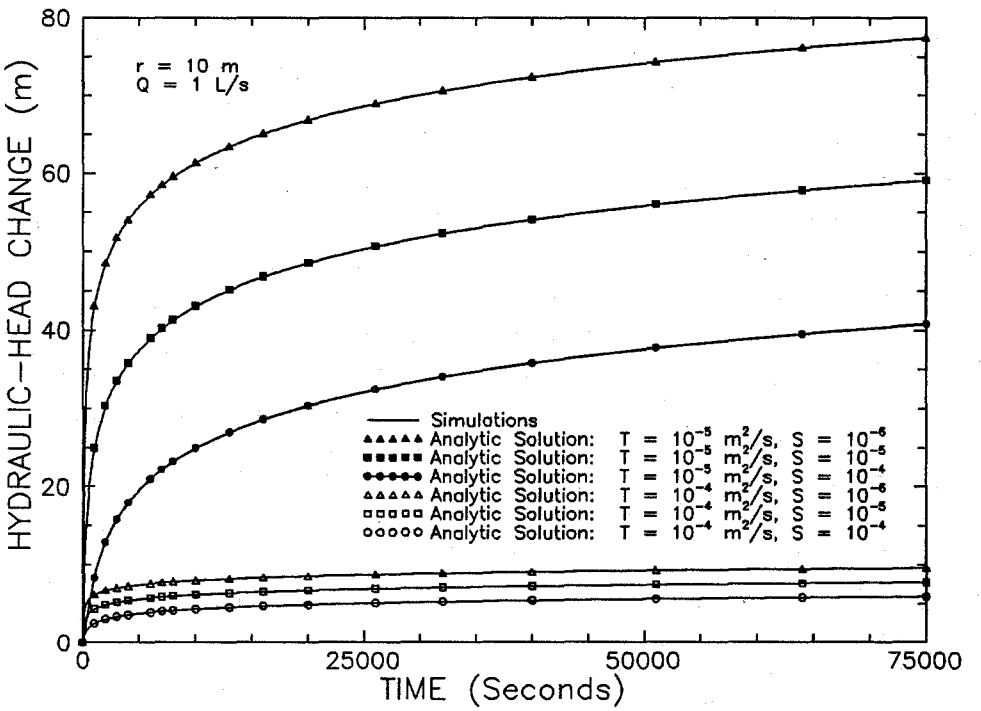


Figure A-1 Verification of GTFM by Comparison to Theis (1935) Analytic Solution for Pumping Tests

**A.2.2 Slug-Test Sequence.** Verification of a slug-test-sequence simulation was accomplished by comparing wellbore sequence files produced by GTFM to data computed using the analytical solution published by Cooper et al. (1967). The solution calculates pressure in a well subjected to a slug stimulus.

A total of six simulations were performed for combinations of three transmissivities and two storativities. Results of the comparison are given in Figure A-2.

**A.2.3 Pulse-Test Sequence.** Pulse-test-sequence simulation verification was accomplished by comparing GTFM results to data computed using the analytical solution published by Bredehoeft and Papadopulos (1980). The solution calculates pressure in an isolated test section subjected to a pulse stimulus.

Two values of storativity and three transmissivities were simulated. Figure A-3 gives the results of the comparison. Slight anomalies in the analytic-solution results for $T = 10^{-12}$ $m^2/s$ with $S = 10^{-6}$ and for $T = 10^{-11}$ $m^2/s$ with $S = 10^{-6}$ are due to minor oscillations in the Laplace inversion routine used in the numerical implementation of the analytical solution of Bredehoeft and Papadopulos (1980).

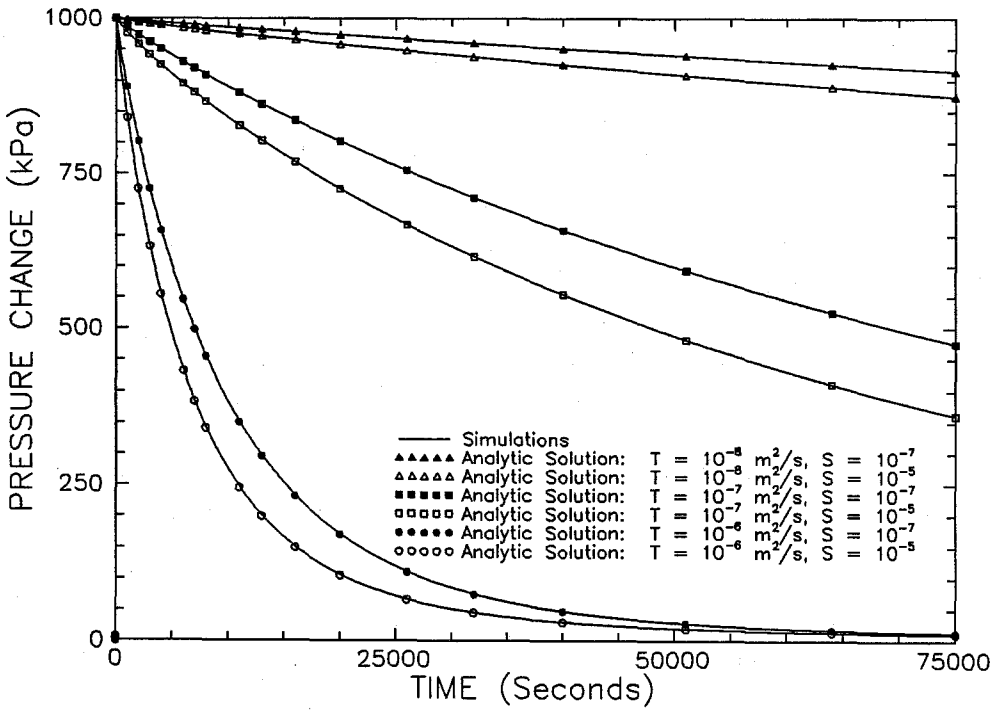


Figure A-2 Verification of GTFM by Comparison to Cooper et al. (1967) Analytic Solution for Slug Tests

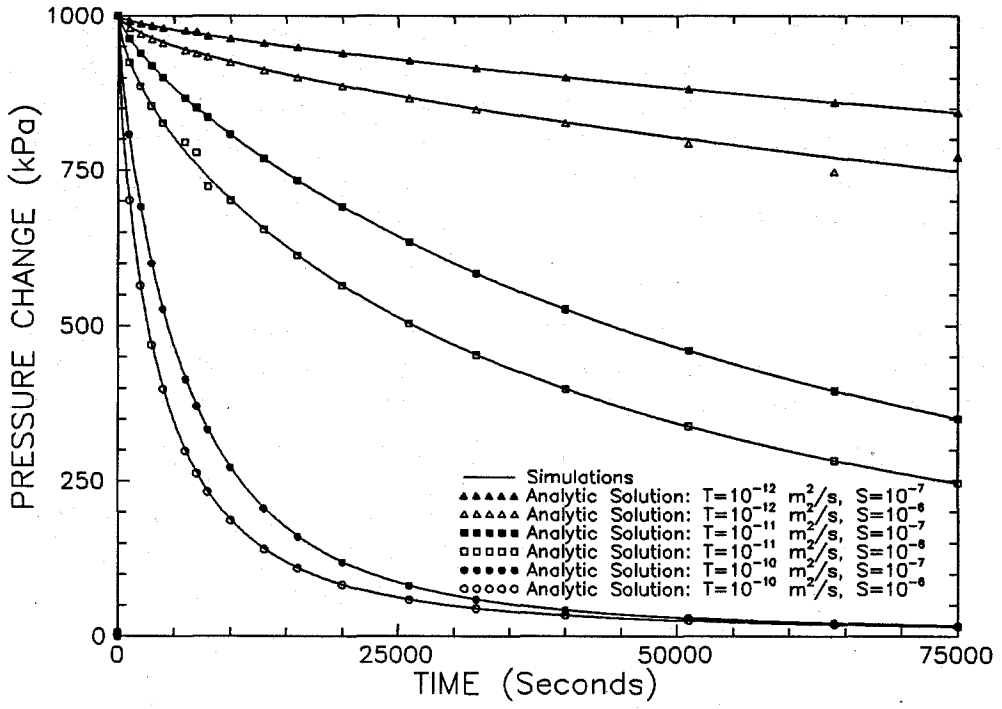


Figure A-3 Verification of GTFM by Comparison to Bredehoeft and Papadopulos (1980) Analytic Solution for Pulse Tests

## REFERENCES


Bredehoeft, J.D., and Papadopulos, S.S. 1980. "A Method for Determining the Hydraulic Properties of Tight Formations," *Water Resources Research* 16(1):233-238.

Cooper, H.H., Jr.; Bredehoeft, J.D.; and Papadopulos, I.S. 1967. "Response of a Finite-Diameter Well to an Instantaneous Charge of Water," *Water Resources Research* 3(1):263-269.

Grisak, G.E.; Pickens, J.F.; Belanger, D.W.; and Avis, J.D. 1985. *Hydrogeologic Testing of Crystalline Rocks During the Nagra Deep Drilling Program,* Technischer Bericht 85-08 (Baden, Switzerland: Nationale Genossenschaft für die Lagerung radioaktiver Abfälle), 194 p.

Pickens, J.F.; Grisak, G.E.; Avis, J.D.; Belanger, D.W.; and Thury, M. 1987. "Analysis and Interpretation of Borehole Hydraulic Tests in Deep Boreholes: Principles, Model Development, and Applications," *Water Resources Research* 23(7):1341-1375.

Savage, G.J., and Kesavan, H.K. 1979. "The Graphic Theoretic Field Model, 1. Modeling and Formulations," *J. Franklin Inst.* 307:107-147.

Theis, C.V. 1935. "The Relation Between the Lowering of the Piezometric Surface and the Rate and Duration of Discharge of a Well Using Ground-Water Storage," *Trans AGU* 2:519-524.

# DISTRIBUTION

## Federal Agencies

U.S. Department of Energy (5)
Office of Civilian Radioactive Waste Management
Office of Geological Repositories
Forrestal Building
Washington, DC 20585
Deputy Director, RW-2
Associate Director, RW-10
Office of Program Administration and Resources Management
Associate Director, RW-20
Office of Facilities Siting and Development
Associate Director, RW-30
Office of Systems Integration and Regulations
Associate Director, RW-40
Office of External Relations and Policy

U.S. Department of Energy (4)
WIPP Project Integration Office
P.O. Box 5400
Albuquerque, NM 87115-5400
W.J. Arthur III
L.W. Gage
P.J. Higgins
D.A. Olona

U.S. Department of Energy/AL
P.O. Box 5400
Albuquerque, NM 87185-5400
National Atomic Museum Librarian

U.S. Department of Energy (6)
WIPP Project Site Office (Carlsbad)
P.O. Box 3090
Carlsbad, NM 88221
V. Daub
R. Batra
R. Becker
D. Blackstone
J. Lippis
J. Mewhinney

U.S. Department of Energy
Research & Waste Management Division
P.O. Box E
Oak Ridge, TN 37831
W. R. Bibb, Director

U.S. Department of Energy
Richland Operations Office
Waste Management Division
P.O. Box 550
Richland, WA 99352
R. F. Guercia

U.S. Department of Energy
Room E-178
GAO/RCED/GTN
Washington, DC 20545
E. Young

U.S. Department of Energy (6)
Office of Environmental Restoration and Waste Management
Washington, DC 20585
J. Lytle, EM-30
M. Frei, EM-34(3)
M. Duff, EM-34
C. Frank, EM-50
S. Schneider, EM-342

U.S. Department of Energy (3)
Office of Environment, Safety and Health
Washington, DC 20585
R. Pelletier, EH-231
K. Taimi, EH-232
C. Borgstrom, EH-25

U.S. Department of Energy (2)
Idaho Operations Office
Fuel Processing and Waste Management Division
785 DOE Pl.
Idaho Falls, ID 83402

U.S. Department of Energy
Savannah River Operations Office
Defense Waste Processing Facility Project Office
P.O. Box A
Aiken, SC 29802
W. D. Pearson

U.S. Environmental Protection
Agency (2)
Office of Radiation Programs (ANR460)
Washington, DC 20460
R. Guimond

U.S. Geological Survey (2)
Water Resources Division
345 Middlefield Rd.
Menlo Park, CA 94025
P. A. Hsieh
A. F. Moench

U.S. Geological Survey
431 National Center
Reston, VA 22092
C. E. Neuzil

U.S. Geological Survey
Water Resources Division
Suite 200
4501 Indian School, NE
Albuquerque, NM 87110
J. Carr
K. Peters

U.S. Geological Survey
Conservation Division
P.O. Box 1857
Roswell, NM 88201
W. Melton

U.S. Nuclear Regulatory Commission (4)
Division of Waste Management
Mail Stop 623SS
Washington, DC 20555
J. Bunting, HLEN 4H3OWFN
R. Ballard, HLGP 4H3OWFN
J. Philip
NRC Library
H. Marson

## Boards

Defense Nuclear Facilities Safety Board
Suite 700
625 Indiana Ave., NW
Washington, DC 20004
D. Winters

U.S. Department of Energy
Advisory Committee on Nuclear
Facility Safety
Washington, DC 20585
M.E. Langston, AC21

Nuclear Waste Technical Review Board (2)
Suite 910
1100 Wilson Blvd.
Arlington, VA 22209-2297
D.A. Deere
S.J.S. Parry

Advisory Committee on Nuclear Waste
Nuclear Regulatory Commission
7920 Norfolk Avenue
Bethesda, MD 20814
R. Major

## State Agencies

Environmental Evaluation Group (3)
7007 Wyoming Blvd., NE, Suite F-2
Albuquerque, NM 87109
R. H. Neill, Director

Environmental Evaluation Group (3)
Attn: Library
Suite F-2
7007 Wyoming, NE
Albuquerque, NM 98109

NM Department of Energy & Minerals
P.O. Box 2770
Santa Fe, NM 87501
K. LaPlante, Librarian

New Mexico State Engineers Office
District II, 1900 W. Second St.
Roswell, NM 88201-1712
A. Mason

NM Environmental Improvement
Department (5)
1190 St. Francis Dr.
Santa Fe, NM 87503-0968
Deputy Director

New Mexico Bureau of Mines
and Mineral Resources (2)
Socorro, NM 87801
F. E. Kottolowski, Director
J. Hawley

NM Environment Department (2)
WIPP Project Site
P.O. Box 3090
Carlsbad, NM 88221
P. McCausland

NM Environment Department (3)
Secretary of the Environment
1190 St. Francis Drive
Santa Fe, NM 87503-0968
J. Espinosa

## Laboratories/Corporations

Argonne National Laboratory
9700 South Cass Ave.
Argonne, IL 60439
D. Hambeley

Battelle Pacific Northwest
Laboratories (5)
Battelle Blvd.
Richland, WA 99352
D. J. Bradley, K6-24
J. Relyea, H4-54
R. E. Westerman, P8-37
H. C. Burkholder, P7-41
L. Pederson, K6-47

Bechtel Inc. (2)
P.O. Box 3965
45-11-B34
San Francisco, CA 94119
E. Weber
H. Taylor

Brookhaven National Laboratory
Associated Universities, Inc.
Upton, NY 11973
P. W. Levy, Senior Scientist

Southwest Research Institute (4)
Center for Nuclear Waste Regulatory
Analysis
6220 Culebra Rd.
San Antonio, TX 78228-0510
P. K. Nair

L. Lehman and Associates, Inc.
1103 W. Burnsville Pkwy.
Suite 209
Minneapolis, MN 55337
L. Lehman

Los Alamos National Laboratory
P.O. Box 1663
Los Alamos, NM 87544
B. Erdal, CNC-11

National Ground Water
Information Center
6375 Riverside Dr.
Dublin, OH 43017
J. Bix

Savannah River Laboratory (6)
Aiken, SC 29801
N. Bibler
E. L. Albenisius
M. J. Plodinec
G. G. Wicks
C. Jantzen
J. A. Stone

Westinghouse Electric Corporation (11)
P.O. Box 2078
Carlsbad, NM 88221
Library
C. Cox
L. Fitch
A. L. Trego
W. P. Poirer
W. R. Chiquelin
V. F. Likar
D. J. Moak
R. F. Cook
R. Richardson
R. F. Kehrman

INTERA Inc. (12)
6850 Austin Center Blvd., Suite 300
Austin, TX 78731
G. E. Grisak
J. F. Pickens (5)
G. J. Saulnier
J. D. Avis
G. A. Freeze
M. Reeves
T. L. Cauffman
A. Haug
Library

INTERA Inc. (2)
8100 Mountain Rd. Pl., NE
Albuquerque, NM 87110
D. T. Upton
A. M. LaVenue

INTERA Inc. (7)
P.O. Box 2123
Carlsbad, NM 88221
W. A. Stensrud
M. D. Fort
R. A. Roberts
J. B. Palmer
T. F. Dale (3)

IT Corporation (2)
P.O. Box 2078
Carlsbad, NM 88221
D. Deal

IT Corporation (5)
5301 Central Ave., NE
Suite 700
Albuquerque, NM 87108
R. F. McKinney
M. E. Crawley
R. M. Holt
J. Myers
P. Drez

RE/SPEC, Inc. (4)
P.O. Box 725
Rapid City, SD 57709
A. F. Fossum
G. Callahan
J. Pfeifle
J. L. Ratigan

RE/SPEC, Inc. (4)
4775 Indian School Rd., NE
Suite 300
Albuquerque, NM 87110-3927
W. Coons

S-Cubed
P.O. Box 1620
La Jolla, CA 92038
E. Peterson

Tech Reps, Inc. (3)
5000 Marble, NE
Albuquerque, NM 87110
J. Chapman
B. Jones
E. Lorusso

Roy F. Weston Corporation
Suite 1000
5301 Central, NE
Albuquerque, NM 87108
D. Lechel

Savannah River Plant
Building 704-S
Aiken, SC 29808
R. G. Baxter

Arthur D. Little, Inc.
Acorn Park
Cambridge, MA 01240-2390
C. R. Hadlock

Golder Associates (3)
4104 148th Ave., NE
Redmond, WA 98052
T. W. Doe
C. Voss
M. Kenrick

SAIC
10260 Campus Point Dr.
San Diego, CA 92121
H. R. Pratt

SAIC
Suite 1250
160 Spear St.
San Francisco, CA 94105
M. B. Gross

SAIC
101 Convention Center Dr.
Las Vegas, NV 89109
G. Dymmel

S.S. Papadopulos and Associates, Inc.
12596 W. Bayard Ave.
Suite 290
Lakewood, CO 80228
J. W. Anthony

## Universities

University of Arizona
Department of Hydrology
Tucson, AZ 85721
S. P. Neuman

University of Arizona
Department of Nuclear Engineering
Tucson, AZ 85721
J. G. McCray

University of California (3)
Lawrence Berkeley Laboratory
Earth Sciences Division
1 Cyclotron Road
Berkeley, CA 94720
K. Karasaki
C. F. Tsang
J. C. S. Long

Kansas Geological Survey
University of Kansas
1930 Constant Ave., Campus West
Lawrence, KS 66046
J. Butler

University of Wisconsin-Madison
Department of Geology and Geophysics
1215 W. Dayton St.
Madison, WI 53706
H. F. Wang

The Pennsylvania State University
Materials Research Laboratory
University Park, PA 16802
D. Roy

Texas A & M University
Department of Geology
College Station, TX 77843
P. A. Domenico

Texas A & M University
Center of Tectonophysics
College Station, TX 77840
J. Handin

South Dakota School of Mines
Dept. of Geology and Geological
Engineering
Rapid City, SD 57701
W. M. Roggenthen

University of New Mexico (2)
Geology Department
Albuquerque, NM 87131
M. Campana
Library

University of Nevada, Reno
Department of Mining Engineering
Reno, NV 89557-0139
J.J.K. Daemen

University of Washington
College of Ocean
and Fishery Sciences
583 Henderson Hall
Seattle, WA 98195
G. R. Heath

New Mexico Tech (4)
Department of Geoscience
Socorro, NM 87801
J. L. Wilson
F. Phillips
C. S. Chen
R. S. Bowman

## National Academy of Sciences, WIPP Panel:

Dr. Charles Fairhurst, Chairman
Department of Civil and
Mineral Engineering
University of Minnesota
500 Pillsbury Dr., SE
Minneapolis, MN 55455-0220

Dr. John O. Blomeke
3833 Sandy Shore Dr.
Lenoir City, TN 37771-9803

Dr. John D. Bredehoeft
Western Region Hydrologist
Water Resources Division
U.S. Geological Survey (M/S 439)
345 Middlefield Rd.
Menlo Park, CA 94025

Howard Adler
Oak Ridge Associated Universities
Medical Sciences Division
P.O. Box 117
Oak Ridge, TN 37831-0117

Dr. Fred M. Ernsberger
250 Old Mill Rd.
Pittsburgh, PA 15238

Dr. Rodney C. Ewing
Department of Geology
University of New Mexico
200 Yale, NE
Albuquerque, NM 87131

Dr. Leonard F. Konikow
U.S. Geological Survey
431 National Center
Reston, VA 22092

B. John Garrick
Pickard, Lowe & Garrick, Inc.
Suite 400
4590 MacArthur Blvd.
Newport Beach, CA 92660-2027

Jeremiah O'Driscoll
Jody Inc.
505 Valley Hill Dr.
Atlanta, GA 30350

Dr. Christopher G. Whipple
Clement International
Suite 1380
160 Spear St.
San Francisco, CA 94105

Dr. Peter B. Meyers, Staff Director
National Academy of Sciences
Committee on Radioactive Waste
Management
2101 Constitution Ave.
Washington, DC 20418

Dr. Geraldine Grube, Staff Officer
National Academy of Sciences
Board on Radioactive Waste Management
GF456
2101 Constitution Ave.
Washington, DC 20418

## Libraries

Hobbs Public Library
509 N. Ship St.
Hobbs, NM 88248
M. Lewis, Librarian

Government Publications Dept.
General Library
University of New Mexico
Albuquerque, NM 87131

Pannell Library
New Mexico Junior College
Lovington Highway
Hobbs, NM 88240
R. Hill

New Mexico Tech
Martin Speere Memorial Library
Campus St.
Socorro, NM 87810

Roswell Public Library
301 N. Pennsylvania Ave.
Roswell, NM 88201
N. Langston

Southwest Collection
New Mexico State Library
325 Don Gaspar
Santa Fe, NM 87503
N. McCallan

Zimmerman Library
University of New Mexico
Albuquerque, NM 87131
Z. Vivian

WIPP Public Reading Room
Atomic Museum
Kirtland East AFB
Albuquerque, NM 87185-5400
G. Schreiner

WIPP Public Reading Room
Carlsbad Public Library
Attn: Director
101 S. Halagueno St.
Carlsbad, NM 88220

WIPP Public Reading Room
Carlsbad Municipal Library
101 S. Halagueno St.
Carlsbad, NM 88220
L. Hubbard, Head Librarian

Thomas Brannigan Library
106 W. Hadley St.
Las Cruces, NM 88001
D. Dresp, Head Librarian

## The Secretary's Blue Ribbon Panel on WIPP

Dr. Thomas Bahr
New Mexico Water Resources Institute
New Mexico State University
P.O. Box 3167
Las Cruces, NM 88003-3167

Mr. Leonard Slosky
Slosky and Associates
Suite 1400
Bank Western Tower
1675 Broadway
Denver, CO 80202

Mr. Newal Squyres
Holland & Hart
P.O. Box 2527
Boise, ID 83701

Dr. Arthur Kubo
Vice President
BDM International, Inc.
7915 Jones Branch Dr.
McLean, VA 22102

Mr. Robert Bishop
Nuclear Management Resources Council
Suite 300
1776 I Street, NW
Washington, DC 20006-2496

## Foreign Addresses

British Nuclear Fuels, PLC
Risley, Warrington, Cheshire
WA3 6AS 1002607 GREAT BRITAIN
D. R. Knowles

Institut für Tieflagerung (4)
Theodor-Heuss Strasse 4
D-3300 Braunschweig
FEDERAL REPUBLIC OF GERMANY
K. Kuhn

Bundesanstalt für
Geowissenschaften
und Rohstoffe
Postfach 510 153
D-3000 Hannover 51
FEDERAL REPUBLIC OF GERMANY
M. Langer

Hahn-Meitner Institut für
Kernforschung
Glienicker Strasse 100
100 Berlin 39
FEDERAL REPUBLIC OF GERMANY
W. Lutze

Bundesministerium für Forschung
und Technologie
Postfach 200 706
D-5300 Bonn 2
FEDERAL REPUBLIC OF GERMANY
Rolf-Peter Randl

Gesellschaft für Reaktorsicherheit (GRS) (2)
Schwertnergasse 1
D-5000 Cologne
FEDERAL REPUBLIC OF GERMANY
B. Baltes
W. Muller

Universidad Politécnica de Valencia
Departamento de Ingenieria Hidráulica
y Medio Ambiente
46071 Valencia SPAIN
J. Jaime Gómez-Hernández

Colenco Ltd.
Mellingerstrasse 207
CH-5405 Baden, SWITZERLAND
S. Löw

Physikalisch-Technische
Bundesanstalt
Postfach 33 45
D-3300 Braunschweig
FEDERAL REPUBLIC OF GERMANY
P. Brenneke

British Nuclear Fuels, plc
Risley, Warrington, Cheshire WA3 6AS
1002607 UNITED KINGDOM
D.R. Knowles

AEA Technology
D5W/29 Culham Laboratory
Abington, Oxfordshire OX14 3DB
UNITED KINGDOM
J.H. Rees

AEA Technology
O44/A31 Winfrith Technical Centre
Dorchester, Dorset DT2 8DH
UNITED KINGDOM
W.R. Rodwell

AEA Technology
B4244 Harwell Laboratory
Didcot, Oxfordshire OX11 0RA
UNITED KINGDOM
J.E. Tinson

Kernforschung Karlsruhe
Postfach 3640
D-7500 Karlsruhe
FEDERAL REPUBLIC OF GERMANY
K. D. Closs

Japan Atomic Energy Research Institute
Tokai-Mura, Naka-Gun
Ibaraki-Ken 319-11, JAPAN
Shingo Tashiro

Svensk Kärnbränsleforsorjning AB
Project KBS
Karnbranslesakerhet
Box 5864
S-102 48 Stockholm, SWEDEN
F. Karlsson

Svensk Kärnbränslehantering AB
Box 5864
S-102 48 Stockholm, SWEDEN
K.-E. Almén

Atomic Energy of Canada, Ltd. (6)
Whiteshell Nuclear Research
Establishment
Pinewa, Manitoba, CANADA
R0E 1L0
P. Haywood
C. C. Davison
D. Stevenson
B. Goodwin
M. Stevens
D. Wushke

Studiecentrum Voor Kernenergie
Centre D'Energie Nucleaire
SCK/CEN
Boeratang 200
B-2400 Mol, BELGIUM
A. Bonne

Geosigma AB
P.O. Box 894
S-751 08 Uppsala, SWEDEN
P. Andersson

SolExperts Ltd.
Ifangstrasse 12
CH-8603 Schwerzenbach, SWITZERLAND
E. Wyss

Golder Associates Umwelt Technik
Im Werder 4
D-3100 Celle
FEDERAL REPUBLIC OF GERMANY
L. Ostrowski

Agence Nationale pour la Gestion des
Déchets Radioactifs (2)
Route du Panorama Robert Schuman
B.P. 38
92266 Fontenay-aux-Roses
Cedex, FRANCE
L. Dewiere
F. Chenevier

Ontario Hydro Research Lab (2)
800 Kipling Avenue
Toronto, Ontario, CANADA
M8Z 5S4
D. K. Mukerjee
A. T. Jakubick

Centre D'Etudes Nucleaires
De La Vallee Rhone
CEN//VALRHO
S.D.H.A. BP 171
30205 Bagnols-Sur-Ceze, FRANCE
C. Sombret

OECD Nuclear Energy Agency
Division of Radiation Protection
and Waste Management
38, Boulevard Suchet
75016 Paris, FRANCE
J-P Olivier

Netherlands Energy Research
Foundation ECN (3)
3 Westerduinweg
P.O. Box 1
1755 ZG Petten, NETHERLANDS
T. Deboer, Mgr.
L. H. Vons
K. A. Duijves

Nationale Genossenschaft für die
Lagerung Radioaktiver Abfälle (3)
Hardstrasse 73
CH-5430 Wettingen, SWITZERLAND
S. Vomvoris
P. Zuidema
M. Thury

Conterra AB
Krokslätts Fabriker 30
S-413 37 Mölndal, SWEDEN
A. Winberg

Harwell Laboratory
Theoretical Studies Dept.
Radwaste Disposal Division,
Bldg. 424.4
Oxfordshire
Didcot, Oxon
OX11 0RA, UNITED KINGDOM
C. P. Jackson

National Institue of Public Health and Environmental
Protection (2)
Antonie von Leeuwenhoeklaan 9
P.O. Box 1
3720 BA Bilthoven, THE NETHERLANDS
S. M. Hassanizadeh
P. Glasbergen

Environment Canada
National Water Research Institute
Canada Centre for Inland Lakes
867 Lakeshore Road
P.O. Box 5050
Burlington, Ontario
L7R 4A6 CANADA
K. S. Novakowski

Technical Research Center of Finland
Nuclear Engineering Laboratory
P.O. Box 169
SF-00181 Helsinki, FINLAND
V. Taivassalo

Atomic Energy Control Board
Waste Management Division
P.O. Box 1046, Station 'B'
Ottawa, Ontario
K1P 5S9 CANADA
D. Metcalfe

Intera Sciences
Chiltern House
45 Station Road
Henley-on-Thames, Oxfordshire
RG9 1AT, UNITED KINGDOM
M. D. Impey

Golder Associates
Landmere Lane, Edwalton
Nottingham
NG12 4DE, UNITED KINGDOM
J. H. Black

## Individuals

D. W. Powers
Star Route Box 87
Anthony, TX 79821

## Sandia Internal

| | |
|---|---|
| 1510 | J. C. Cummings |
| 1511 | D. F. McTigue |
| 1550 | C. W. Peterson |
| 3141 | S. A. Landenberger (5) |
| 3145 | Document Processing for DOE/OSTI (8) |
| 3151 | G. C. Claycomb (3) |
| 6000 | D. L. Hartley |
| 6232 | W. R. Wawersik |
| 6253 | N. R. Warpinski |
| 6300 | T. O. Hunter |
| 6310 | T. E. Blejwas |
| 6312 | F. W. Bingham |
| 6312 | G. E. Barr |
| 6313 | L. E. Shephard |
| 6314 | L. S. Costin |
| 6315 | F. B. Nimick |
| 6316 | R. P. Sandoval |
| 6340 | W. D. Weart |
| 6340 | S. Y. Pickering |
| 6341 | R. C. Lincoln |
| 6341 | Staff (9) |
| 6341 | Sandia WIPP Central Files (10) |
| 6342 | D. R. Anderson |
| 6342 | Staff (11) |
| 6342 | P. Swift |
| 6342 | M. G. Marietta |
| 6342 | R. P. Rechard |
| 6343 | T. M. Schultheis |
| 6343 | Staff (2) |
| 6344 | E. D. Gorham |
| 6344 | Staff (10) |
| 6344 | R. L. Beauheim (5) |
| 6344 | P. B. Davies |
| 6344 | F. Gelbard |
| 6344 | A. L. Jensen |
| 6344 | T. F. Corbet |
| 6344 | C. F. Novak |
| 6344 | S. W. Webb |
| 6345 | A. R. Lappin |
| 6345 | Staff (9) |
| 6346 | E. H. Ahrens |
| 6346 | J. R. Tillerson |
| 6346 | Staff (7) |
| 6347 | A. L. Stevens |
| 6347 | Staff |
| 8523-2 | Central Technical Files (1) |
| 9300 | J. E. Powell |
| 9310 | J. D. Plimpton |
| 9320 | M. J. Navratil |
| 9325 | L. J. Keck |
| 9333 | J. W. Mercer |



*U.S. GOVERNMENT PRINTING OFFICE 1991-0-673-038/44087

8232-2/920068
00000001 -
8232-2/920068
00000001 -
8232-2/920068
00000001 -

| Org. | Bldg. | Name | Rec'd by | Org. | Bldg. | Name | Rec'd by |
|---|---|---|---|---|---|---|---|
| 8523-2 | | | | | | | |
| | | | | | | | |
| | | | | | | | |
| | | | | | | | |
| | | | | | | | |
| | | | | | | | |
| | | | | | | | |
| | | | | | | | |
| | | | | | | | |
| | | | | | | | |
| | | | | | | | |
| | | | | | | | |
| | | | | | | | |
| | | | | | | | |
| | | | | | | | |

Sandia National Laboratories